A Study of Impact of Thermal Model Resolution and Zone Set Point Profiles on Peak Heating Load and its Calculation

Jennifer Date

A Thesis

In the Department

of

Building, Civil and Environmental Engineering

Presented in Partial Fulfillment of the Requirements

for the Degree of Master of Applied Science (Building Engineering) at

Concordia University

Montréal, Québec, Canada

July 2015

CONCORDIA UNIVERSITY

School of Graduate Studies

This is to certify that this thesis is prepared

By: **Jennifer Date**

Entitled: **A Study of Impact of Thermal Model Resolution and Zone Set Point Profiles on Peak Heating Load and its Calculation**

and submitted in partial fulfillment of the requirements for the degree of

Master of Applied Science (Building Engineering)

complies with the regulations of the University and meets the accepted standards with respect to originality and quality.

Signed by the final examining committee:

Dr. B. Lee — Chair

Dr. M. Paraschivoiu — Examiner

Dr. L. Wang — Examiner

Dr. A. Athienitis — Supervisor

Approved by

Chair of Department or Graduate Program Director

Dean of Faculty

Date

Abstract

A Study of Impact of Thermal Model Resolution and Zone Set Point Profiles on Peak Heating Load and its Calculation

Jennifer Date

This thesis presents an experimental and theoretical study of the dynamic response of convectively heated buildings and their respective space heating peak demands for different room temperature set point profiles and thermal mass levels, with a focus on the impact of thermal model resolution on the peak demand calculation.

Experiments were conducted at two identical and highly instrumented houses. One house is modified with different floor coverings, while the other is kept unchanged and used for reference. Through experimentation and simulation, peak power (due to space heating) reduction strategies are investigated.

Twelve equivalent RC thermal network models of varying model resolution are developed for a north zone of the houses. Modelling approximations including linearization of the heat transfer, spatial and/or temporal discretization and approximations for reduction in model complexity are implemented into the models and their effects are investigated. The focus is on simple and physically meaningful building thermal models suited for model-based control.

The models are used to study the impact of set point ramping lengths and "near-optimal" transition curves between two temperatures on peak demand reductions for a very cold day. Alterations to walls and ceilings in the models were done to hypothetically modify their properties in the zone and the effects in combination with ramping profiles were analyzed. This work can inform the development of new building materials.

A commercial building is also considered and two low order RC thermal network are compared. The first model excludes the mass of the interior partitions, while the second model incorporates them. An advantage of the model with interior partitions is it can be used for retrofit studies.

Acknowledgements

I would like to express my gratitude to my supervisor, Dr. Andreas Athienitis for his full support, expert guidance and understanding throughout my studies and research. I have learned a lot from him throughout the completion of this thesis work.

While realising the following list must be incomplete, I would like to thank all of my colleagues within the Centre for Zero Energy Building Studies, including Edvinas Bigaila, Ali Saberi, Costa Kapsis, Sam Yip, Tingting Yan, Diane Bastien, Colin Beattie, Vasken Dermardiros, Stratos Ru and many others with whom I share an office space. Thank you all for your helpful ideas, enthusiasm and friendship during the last two years. Special thanks to Yuxiang Chen for taking the time to look over my work during my studies and providing me with constructive feedback.

I would like to acknowledge the technical and financial support from the NSERC/Hydro-Québec Industrial Research Chair and the Faculty of Engineering and Computer Science of Concordia University. The use of the Hydro-Québec Experimental Houses for Building Energetics facilities for my experiments is greatly appreciated. Thank you to Michael Fournier and the Hydro-Québec technicians for helping with the experiment design and set-up, and data aquisition and analysis. Thank you also to Karine Lavigne and José Candanedo for sharing your time and expertise.

I am appreciative of the unconditional love and support from my parents, Paul and Kathleen, and my sister Chantal. I know it must be hard not having me close to home. Finally, I would like to express a special thank you to Boris Besner for his endless support and encouragement.

Table of Contents

List of Figures

List of Tables

Nomenclature

Symbols

A_i	Area of surface(s) represented by node i	m^2
A_w	window area	m^2
C_i	thermal capacitance at node i	J/K
c_p	specific heat	J/K
D	diameter of the globe	m
e_i	error between setpoint and air temperature	°C
	at time step i	°C
f_{eff}	ratio of radiating surface of the human body	
	to its total DuBois surface area	
G	solar radiation	W/m^2
GT	globe temperature	°C
h_c	convective heat transfer coefficient	$W/(m^2K)$
h_i	interior film coefficient	$W/(m^2K)$
h_r	radiative heat transfer coefficient	$W/(m^2K)$
h_o	exterior film coefficient	$W/(m^2K)$
k	thermal conductivity	W/mK
K_i	integral control constant	W/(°Cs)
K_p	proportional control constant	W/°C

L	thickness of a surface	m
P	power	W (Js^{-1})
q	heating load	W (Js^{-1})
q_{aux}	auxilliary heating source	W (Js^{-1})
q_i	Source entering node i	W (Js^{-1})
Q_s	Solar gains	W (Js^{-1})
R_i	thermal resistance at node i	K/W
T_a	air temperature	°C
T_{db}	air (dry bulb) temperature	°C
T_{eo}	sol-air temperature	°C
T_i	temperature at node i	°C
T_o	operative temperature	°C
T_{mr}	Mean Radiant Temperature	°C
U_i	thermal conductance at node i	W/K
U_{inf}	Infiltrations conductance	W/K
V_a	air velocity at the level of the globe	m/s

Greek letters

α	Thermal diffusivity, $k/\rho c_p$	m^2/s
α_s	solar absorptance of the wall	
ϵ	emissivity of the globe	
ρ	density	Kg/m^3
σ	Stefan-Boltzmann constant 5.67×10^{-8}	$W/(m^2K^4)$
Δt	simulation time step	s

Abbreviations and Acronyms

ach	air change per hour	
ASHRAE	American Society of Heating, Refrigerating, and Air-Conditioning Engineers	
CFD	computational fluid dynamics	
cfm	cubic feet per minute	ft^3/min
CV-RMSE	coefficient of variation of the root mean squared error	
HVAC	Heating, Ventilation and Air Conditioning	
NMBE	mean biased error	
RSME	root mean squared error	

Chapter 1

Introduction

1.1 Background and Motivation

In the province of Québec, 94% of generated electricity comes from hydroelectric plants (Le Bel & Gelinas, 2012). Due to its cold winter weather, Québec has a high space heating demand. In 2011, the province of Québec's primary electricity generation was 170,260 GWh (Statistics Canada, 2011b), while household energy use of electricity was 56,272 GWh, 33% of total electricity generation. Figure 1.1 shows that 82% of Québec's households reported electricity as their main heating fuel (Statistics Canada, 2011a) and 63% of total household energy use was electricity. Figure 1.2 shows 66% of houses in Québec reported using baseboards as the main heating equipment and 9% electric radiant heating. The shape of the region's demand profile is strongly coincident with the demand profile from these customers. For the commercial and institutional sector (CI), electricity is the main source of energy for space heating for 60% of the utility's customers, of which 75% have baseboards and room thermostats similar to the equipment used in the residential sector.

In the winter, the electricity grid peak demand in Québec occurs on weekday mornings between 6am and 9am and evenings between 4pm and 8pm. During winter peak periods, space heating represents up to 80% of the total demand of the households (Le Bel & Handfield, 2008). It is expected that the installation of electric space heating in Québec will increase over the coming years due to their low initial and operating cost. Electric space heating of residential homes is therefore a relevant load for demand response (DR) in the winter in heating dominated climates such as Québec. In January 2013 there was a peak demand of 39.1 GW reported by Hydro-Québec (Hydro-Québec, 2013). Finding ways to reduce the peak demand and energy consumption of buildings, and consideration of energy efficiency measures in buildings is a necessity.

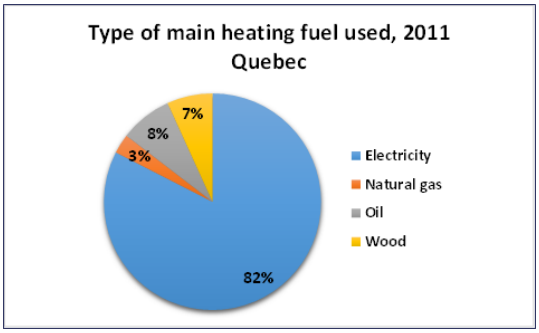

Figure 1.1: Main heating fuel used, 2011 Québec

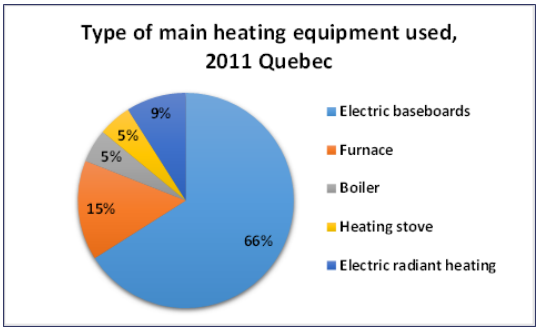

Figure 1.2: Main heating equipment used, 2011 Québec

Control in buildings is usually done by establishing a schedule of set-points for room temperatures and other variables (e.g., humidity, state of charge of a thermal energy storage device). Conventional approaches include maintaining a fixed set-point, or using a different night-time set point. An estimation of future loads could be useful in planning the collection, storage and delivery of energy, as well as in demand response strategies. One way to accomplish this is to use model-based control to investigate control actions that will optimize an objective function (such as energy consumption, peak demand or cost).

Anticipatory or predictive control strategies for buildings, based on weather and load forecasting, have been proposed and studied as a suitable alternative to conventional building control for many decades (Candanedo et al. (2010), Henze et al. (1997, 2005a), Kintner-Meyer & a.F. Emery (1995), Kummert et al. (2006), Winn & Wins (1985)). The availability of accurate live weather forecasts has opened up new possibilities for the use of model based and predictive control strategies in buildings. With accurate forecasts of future conditions, building models can be used to calculate building energy needs over a prediction horizon (of up to a few days) (Candanedo et al., 2013) and this knowledge can then be used to decide on the optimal distribution of resources over time. Model-based predictive control (MPC) is a control approach using optimization algorithms to choose an optimal operation sequence based on a system model and forecast data (Camacho & Bordons, 2004). Despite much research on the application of MPC and other advanced control techniques in buildings, there is still a large gap between the potential of these techniques and current control practices (Cigler et al., 2013). This gap is due to multiple factors: the lack of tools to easily incorporate weather forecasts into building automation systems; the scarcity of user-friendly software to test and develop control strategies in buildings; and the limited familiarity of building professionals with control engineering methods (Candanedo & Athienitis, 2010).

Models with fewer parameters facilitate setting-up initial states, which is a key consideration in controls (Candanedo et al., 2013). A control-oriented model is intended to predict the system response over a short period (e.g., hours), therefore knowing the "starting point" or initial states is important. Sensor measurements such as room air temperature can be used to set the initial conditions of a simplified model. Simpler models also reduce the number of calculations required by the optimization algorithm.

The main motivation of this thesis is to evaluate the benefits of different levels

of modelling resolution for understanding building thermal behavior of buildings and energy management in buildings. The effect of employing different control strategies on building performance can be investigated by using energy models developed for the buildings. Also, well calibrated low-order models are well-suited for the application of model based control in which models can be implemented into the building automation system. Using the developed models, peak demand response strategies are investigated further. The level of thermal mass in a zone and its effect on peak demand reduction strategies is also discussed. MPC gives context to the work to be presented in this thesis, however, implementation of MPC using the developed models is beyond the scope of this work but is a logical next step for future work.

1.2 Research Objectives

The main research objectives of this thesis are:

1. Better understand heat transfer and system dynamics of different types of zones in conventional Québec buildings heated by convection, under Québec winter climatic conditions.

2. Better understand level of modelling detail required to sufficiently capture system phenomena.

    - Adjust model order (using finite difference method)
    - Constant vs. temperature dependent heat transfer coefficients

3. Develop calibrated models that sufficiently represent building thermal response for different types of zones.

4. Explore peak heating demand reduction strategies and impact on model accuracy.

- Temperature set point adjustments
- Varying thermal mass properties

1.3 Scope and Outline of the Thesis

This thesis covers experimental results from experiments conducted at a built environment research facility, which were used to validate thermal models. The theoretical background for the finite difference thermal modelling approach is introduced, and the accuracy achieved for the different levels of resolution of thermal modelling are presented. Results of implementable peak heating power demand reduction strategies are also presented. An occupied small commercial building case study is also presented.

The following list summarizes the content of each chapter in this thesis:

Chapter 1: *Introduction*. Presents the motivation and objectives of the work done as well as the thesis outline.

Chapter 2: *Literature Review*. Presents a review of related literature and previous works in the field of energy modelling, demand response and residential thermostat use.

Chapter 3: *Methodology*. Presents the methodology and steps used for the experimental study and modelling analysis.

Chapter 4: *Experimental Description and Results*. Describes the experimental procedure and presents the results of the experiments conducted at the Experimental Houses for Building Energetics (EHBE) in Shawinigan, Québec.

Chapter 5: *Thermal Modelling Description and Results*. Presents the models developed and compares their accuracy to experimental data using statistical

indices and visual inspection. Also, Chapter 5 presents results of peak power reduction strategy simulations by means of thermostat set point modulation and thermal mass alterations. A commercial building case study is also presented.

Chapter 6: *Conclusions*. Includes conclusions, a summary of main contributions and the recommendations for future work.

Chapter 2

Literature Review

Creating good models is fundamental to engineering research. Models are key tools for engineers as they aid in acquiring a better understanding of the system under investigation. In building engineering, models are used for many things such as: design decision making, reducing operation costs, improving mechanical system performance, reducing the consumption of energy or power demand, or improving building occupant comfort.

This chapter reviews literature related to building thermal modelling and discusses the significance of appropriate modelling resolution. This review will also provide an overview of the research published on the topic of peak power demand response, with specific attention to demand response strategies for the heating season in cold climates. Another topic presented in this review is the effect of thermostat use has on the energy consumption and thermal comfort of dwellings, as a topic to keep in mind for the level of impact controls have on comfort and energy consumption.

Section 2.1 presents the review of buildings thermal modelling approaches.

Section 2.2 discusses residential thermostat use and heating control strategies.

Section 2.3 discusses peak demand and demand response strategies.

2.1 Building Thermal Modelling

Building thermal modelling is most commonly used to study the energy consumption of buildings and different design options. Buildings contribute to roughly 40% of western countries energy consumption (Pérez-Lombard et al., 2008), thus buildings pose as an interesting sector to study the reduction of their energy consumption and their related carbon footprint. To slow energy demand growth and reduce the amount of energy used within buildings, it is important to understand the energy distribution throughout a building, and how building parameters contribute to energy consumption and demand (Langner et al., 2012). Energy consumption analysis of buildings can be a difficult task as it requires detailed knowledge of interactions among the building, the HVAC system and the surroundings or external factors such as weather, as well as obtaining mathematical and physical models that effectively characterize each of those items. The dynamic behaviour of weather conditions, building operation and occupant behaviour, and the presence of multiple variables, requires the use of computer aid in the design and operation of high energy performance buildings. The research field related to building modelling and energy performance prediction is very productive, involving various research domains (Foucquier et al., 2013). Among them one can distinguish physics-related fields, focusing on the resolution of equations simulating building thermal behaviour and mathematical-related ones, consisting in the implementation of prediction model with the use of machine learning techniques. There is a third area where physics based and mathematical based techniques are combined together, commonly referred to as grey-box models.

2.1.1 Physics Based Models

The physical based techniques of building thermal modelling are based on solving of equations describing the physical behaviour of heat transfer. The principal in-coming and out-coming fluxes taking place in the heat transfer are conduction through the walls, convection, long wave and short wave radiation and the ventilation. The corresponding heat exchanges on a wall are shown in Figures 2.1 and 2.2. Three main building models are currently used: CFD (Computational Fluid Dynamics), zonal and lumped parameter thermal network based methods. Each method has its own application and the choice of the physical method depends highly on the problem.

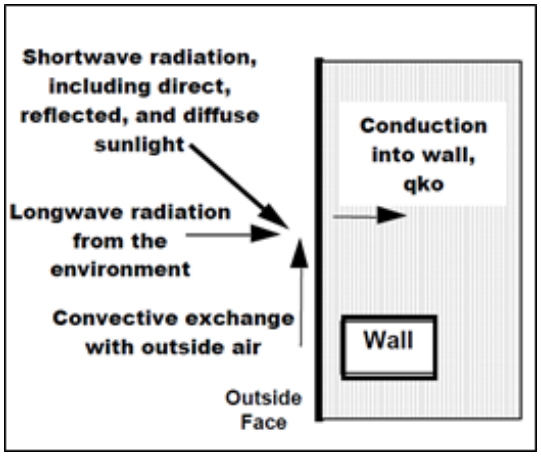

Figure 2.1: Outside Heat Balance Control Volume Diagram (DOE, 2013)

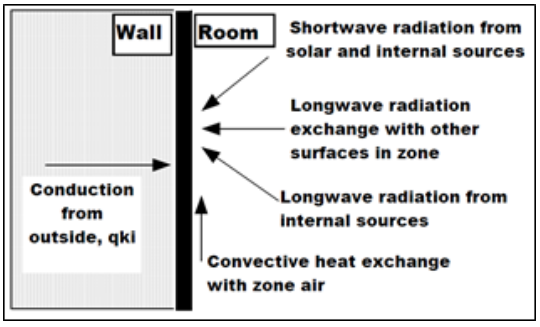

Figure 2.2: Inside Heat Balance Control Volume Diagram (DOE, 2013)

Computation Fluid Dynamics Method

The most detailed approach in thermal building simulation is the CFD (Computational Fluid Dynamics) method. This is a microscopic approach of the thermal transfer modelling allowing to detail the flow field three dimensionally. It generally focuses on heat transfer through convection. It is based on the decomposition of each building zone in a large number of control volumes with a homogeneous or

heterogeneous global mesh. Software using the CFD model are based on the resolution of the Navier–Stokes equation. A number of CFD software are available such as FLUENT (FLUENT, 2015), COMSOL Multiphysics (COMSOL, 2015), etc. Their application fields are large and not always specific to building simulation. The CFD method is mainly used for its ability to produce a detailed description of the different flows inside buildings (airflow, pollutant flow, etc.). The main disadvantage of the CFD approach is its huge computation time (Tan & Glicksman, 2005), due to the fact that a complete detailed 3D-description of the building with a very fine mesh is required. Therefore, though CFD is well adapted to describe flow fields in buildings, the large computation time makes difficult the generalization to all building applications.

Zonal Method

It is not always necessary to give a very fine description and a way to overcome the difficulties of CFD is to model the building behaviour in a simpler form by giving a less detailed description of the interested zone (Abadie et al., 2012). The first simplification of CFD is the zonal technique. It has been introduced by Bouia & Dalicieux (1991) and Wurtz (1995) in the beginning of 1990s. It is a way to obtain a simpler model while maintaining the complexity in 2D. This approach is a fast way to detail the indoor environment and to estimate zone thermal comfort. The zonal approach consists of dividing each building zone into several cells. Each cell corresponds to a small part of a room, making it a two- dimensional approach. This technique requires previous knowledge on the flow profiles, thus the study of pollutant transport remains limited. Wurtz et al. (2006) showed that the zonal simulation is a suitable method for an accurate estimation of the temperature field in a room and of the indoor thermal comfort. Such a detailed behaviour description is once again not always required and although it has been hugely

enhanced with the zonal approach, the computation time can again be reduced by decreasing the complexity of the model.

Lumped Parameter and Thermal Network Based Methods

The simplest and last approach is called the lumped parameter and thermal network based method. It considers the following assumption: each building zone is a homogeneous value characterised by uniform state variables. In the method, one zone is approximated to a node that is described by a unique temperature, pressure, etc. A node generally represents a room, a wall or the exterior of the building and can also represent more specific loads such as internal gains from occupants or equipment. The thermal transfer equations are solved for each node of the system. TRNSYS (TRNSYS, 2015), EnergyPlus (EnergyPlus, 2015), IDA-ICE (IDA, 2015), ESP-r (ESP-r, 2015), Clim2000 (Bonneau et al., 1993), BSim (Rode & Grau, 2011) and BUILDOPT-VIE (BuildOpt-VIE, 2015) are the most popular software using this approach employed for building simulations. The finite difference method is notably employed using a description of the heat transfers from an electrical analogy. It is very useful since it simplifies the physical problem through a linearization of the equations and thus reduces the computation time. The principle of the electrical analogy is to associate a thermal resistance R and a thermal capacity C to a wall. The analogy gives the following equivalence with Ohm's law:

$$U_1 - U_2 = RI \Leftrightarrow \theta_1 - \theta_2 = \frac{e}{\lambda S}\Phi_L \tag{2.1}$$

The temperature θ is equivalent to voltage U, the heat flux Φ_L to current I and the thermal resistance $e/\lambda S$ (L/kA) to electrical resistance R.

The great advantage of this technique is its ability to describe the behaviour of a multiple zone building on a large scale with a small computation time. It is well suited for the estimation of the energy consumption and the evolution of the space-averaged temperature in a room. One disadvantage is it difficult to study thermal comfort and air quality inside, due to simplifications used in the technique.

The following three types of approximations are commonly introduced in mathematical models to facilitate representation of the building thermal behaviour (Athienitis & O'Brien, 2015):

1. *Linearization of heat transfer*: Convective and radiative heat transfer are nonlinear processes and the respective heat transfer coefficients are usually linearized so that the system energy balance equations can be solved by direct linear algebra techniques and, if desired, represented by a linear thermal network. Linearization generally introduces less error for long-wave radiant exchanges between surfaces than convection between surfaces and room air. In some cases heat flow reversal can occur such as between a cold floor and warm air when the convective heat transfer coefficient can be of the order of 1 W/m^2K versus 3 W/m^2K for a heated floor and cold air. A linear lumped parameter system can be represented by a set of ordinary differential equations and thermal networks. An important subset of linear systems are those with time varying coefficients – an important case in building energy analysis, where we can often represent thermal conductances such as a known variable level of natural ventilation or time-varying infiltration.
2. *Spatial and/or temporal discretization*: Transient heat conduction is described by a parabolic, diffusion type partial differential equation. Thus, when using finite difference methods, a conducting medium with significant thermal capacity such as concrete or brick must be discretized into a number of regions, commonly known as control volumes, which may be modelled

by lumped network elements (thermal resistances and capacitances). Also, time domain discretization is required in which an appropriate time step is employed. It should be noted that when thermal storage undergoes phase change (e.g. phase change materials – PCM) a linear approximation may not be possible in some cases and specialized modelling will be required.

3. *Approximations for reduction in model complexity - (establishing appropriate model resolution)*: These approximations are employed in order to reduce the number of simultaneous equations to be solved and the required data input or to enable the derivation of closed form analytical solutions. They are the most important approximations (Athienitis & O'Brien, 2015). Examples include combining radiative and convective heat transfer coefficients, assuming that surfaces are at the same temperature, or considering certain heat exchanges as negligible. These approximations must be carefully selected and applied by considering the expected temperature variations (spatial and temporal) in a zone. As an example, a zone with large windows or floor heating may exhibit large spatial temperature variations, in which case the use of combined film coefficients would results in high errors in room operative temperature or floor heating rate calculations.

Goyal & Barooah (2012) used the electrical analogy to implement a lumped thermal simulation model. It is able to predict the temperature and the humidity in multi-zone buildings from outside temperature and humidity, heat gains from occupants and solar radiation, supply air flow rates and supply air temperatures. Their objective was to decrease the order of this model by testing several reduction methods. Such scientific fields are useful considering some applications such as HVAC control or monitoring. Hazyuk et al. (2012) developed an in-house multi-zone model from the electrical analogy. They proposed a description of the walls and the floor by two identical resistances and one capacity. The thermal mass is characterized by a single capacity and windows by single resistances. Athienitis

et al. (1985) used the nodal approach to model multi-zone passive solar buildings. Fraisse et al. (2002) suggests that a 3 resistance, 4 capacitance model is sufficient to model the conductive transfers within a wall if the temperature distribution within the wall is not necessary.

Frequency Domain Technique

An alternative approach in dynamic thermal modelling involves using frequency domain techniques. Frequency domain approach has been shown to be efficient in building energy analysis in conjunction with network theory (Athienitis et al., 1990). This method can facilitate the integration of design and control (Chen et al., 2013). Shou (1991) stated some potential advantages of frequency domain techniques over time domain techniques:

- More efficient and less expensive solutions than time domain due to the fact that there is no time step involved in calculations in the frequency domain.
- No discretization of elements with thermal mass is needed. Instead, the exact solution obtained from solving the 1-D conduction heat transfer in Laplace domain is used.

The main disadvantage of frequency domain modelling is the difficulty of accommodating non-linearities, such as temperature dependent heat transfer coefficients. However, in practice, linearization of heat transfer phenomena is often an acceptable compromise (Shou, 1991). Athienitis et al. (1986) presented an analytical method to determine room temperature swings in direct gain rooms. Also Athienitis et al. (1987) used discrete frequency domain methodology to determine auxiliary energy load in buildings. Haghighat & Athienitis (1988) compared two computer programs; one in a frequency domain and the other in time domain, and compared their result with the experimental data.

Generally, a main disadvantage of the physical formulation is the fact that it suggests a detailed description of the physical behaviour. Therefore, it requires extensive knowledge on the physical system, especially on the mechanisms occurring inside and outside the building geometry. Unfortunately, this information is not always available. In contrast, the statistical tools (black-box models) have the ability to produce models only from measures using techniques such as machine learning or system identification.

2.1.2 Inverse Models

Inverse models are those for which the identification problem must be solved without any insight into the physical properties or prior knowledge of the process under study. They are data-driven models that mathematically connect the system input(s) to its output(s) without including any physical meaning in the equation parameters. Inverse models are built using data gathered from the system responses to disturbances and/or controlled inputs.

System Identification Technique

The Swedish professor Lienard Ljung, a pioneer in the field of system identification (SI) research describes SI as: "[...] the art and science of building mathematical models of dynamic systems from observed input-output data. It can be seen as the interface between the real world of applications and the mathematical world of control theory and model abstractions." (Ljung, 2010). Åström & Eykhoff (1971), in their early review of system identification developments, identified one root of the human interest for this field of research as the "Definite needs by engineers [...] to obtain a better knowledge about their plants for improved control". Because computational capacities have increased, the possibilities for system identification have grown steadily since the early surveys of Åström & Eykhoff (1971) and Bekey

(1970). Improving controls, design or thermal comfort drive building engineers to make use of, study, and assess system identification techniques.

Artificial Intelligence Building Models

The artificial neural network (ANN) is a non-linear statistical technique principally used for prediction. This artificial intelligence method was inspired by the central nervous system with their neurons, dendrites, axons and synapses. It was first introduced in its mathematical form by McCulloch and Pitts in 1943, with their first works being published in 1959 (Lettvin et al., 1959). An advantage of ANN is its ability to deduce from data the relationships between different variables without any assumptions of a model. It also overcomes the discretization problem and is able to manage data unreliability (Foucquier et al., 2013).

ANNs are limited in that they require a relevant database. It is mandatory to train an ANN with an extensive learning basis with representative and complete samples (for example, samples in different seasons or moments of the day or during weekends and holidays).

In building simulation, artificial neural networks are usually used for the prediction of the energy consumption or the forecasting of energy use as the cooling or heating demand without knowing the geometry or the thermal properties of the building. Different kinds of databases can be considered depending on the time scale as the hour, the month or the year and the nature of the data (real or simulated and instantaneous or time/ space-averaged data). The completeness of the learning data is the one main condition that is absolutely essential for applying the artificial neural network technique.

2.1.3 Grey-box (Hybrid) Models

The complexity of computer aided building modelling tools using complex RC-network models (e.g., EnergyPlus (2015) and TRNSYS (2015)) grows exponentially as the number of building zones increases. A large amount of measurement data is required to identify the parameters used for these complex models, which usually causes data over-fitting problems and high modelling uncertainties (EnergyPlus, 2015). Thus it is necessary to consider reduced models with a simpler structure and fewer parameters for the ease of parameter estimation and data fitting. Second, the model complexity is a major issue for implementing the on-line optimization-based control schemes, e.g. MPC, particularly if the optimization is to be performed with a day-long prediction horizon to take advantage of slow thermal responses of buildings as well as daily variations in environment and energy prices It is essential to develop reduced models to achieve a trade-off between prediction accuracy and model complexity. In practice, one can make a trade-off between the simulation accuracy and computational complexity of the reduced-order model by choosing an appropriate order of reduction.

The principle of grey-box (or hybrid) models is based on the coupling of statistical and physical models. Grey-box modelling is well proven as a comprehensive and accurate method to model dynamical systems and obtain knowledge of the thermal properties of a building (Bacher & Madsen, 2011). One strategy consists of using statistical methods in fields where physical models are not effective or accurate enough. Another application would be to determine the heat behaviour in multiple zone buildings where the thermal properties of some zones are unknown. Some zones would be physically studied while others would need to be described statistically via measurements collected in these zones.

This approach has been introduced at the beginning of the 1990s for a specific application which was the automatic control system. For example, Teeter & Chow

(1998) combined an artificial neural network with a single-zone thermal model to improve the efficiency of the HVAC control by performing HVAC parameters identification. Other more recent examples are the works of Paris et al. (2010) and Paris et al. (2011) who combined the fuzzy logic, a PID controller and a dynamic model describing the thermal behaviour of the building for implementing several heating control schemes.

Bacher & Madsen (2011) developed a procedure for identification of suitable grey-box models for the heat dynamics of a building. Their procedure for identification of the most suitable models for the heat dynamics of a building is based on likelihood-ratio testing combined with forward selection strategy. The proposed models are grey-box models, where a combination of prior physical knowledge and data-driven modelling is utilized. Bacher & Madsen (2011) state a suitable model is a sufficient model which is the smallest model that describes all information embedded in the data.

Applications of this type of grey-box model selection procedure include:

1. Accurate description of energy performance of the building

2. Forecasting of energy consumption for heating

3. Indoor climate control

For grey-box model selection, often a purely algorithmic and exhaustive selection procedure is seldom feasible, hence iterative methods, in which the modeller is partly involved in the selection, are commonly applied.

Deng et al. (2014) proposes an aggregation-based model reduction method for non-linear models of multi-zone building thermal dynamics. The focus is on model reduction of multi-zone building thermal dynamics. An advantage of the proposed method, apart from being applicable to the non-linear thermal models, is that the reduced model obtained has the same structure and physical intuition

as the original model. A recently developed aggregation-based method of Markov chains is employed to aggregate the large state space of the full-order model into a smaller one. Utilization of physical models in supervisory-level control can largely minimize building-wide energy consumption and properly satisfy thermal comfort requirements.

Kummert et al. (2006) also states that parameter identification on a detailed building is a complex problem due to the large number of parameters and to the possibility of achieving the same result through different actions (e.g., increasing the infiltration rate or increasing the thermal conductivity of a low-mass wall or window) . The very large number of parameters in the building model makes parameter identification a complex problem, and the desired level of accuracy is very high—performance differences of less than 10% must be reproduced. They use a simpler model combined with on-line parameter identification for comparisons, combining simulation with experimental results for studying the performance of different controllers in passive solar buildings. Considerable care must be taken when defining the structure of the building model (e.g., include a model of the occupants' reaction rather than its effects) and identifying the parameters to avoid the risk of over fitting. Their study, however, has shown that it can be easier to reach a high level of accuracy with simple models that allow a greater flexibility in parameter identification. Detailed building models that are commonly used to optimize building designs require thousands of parameters, which makes them unsuitable for classical parameter identification techniques.

Models with fewer parameters facilitate setting-up initial states, which is a key consideration in controls (Candanedo et al., 2013). In design simulations, a long "warming up period" is usually applied; and when the main goal is determining the annual energy consumption, initial states are not as important. A control-oriented model is, however, intended to predict the system response over

a short period (e.g., hours), therefore knowing the "starting point" or initial conditions is important. In real control installation, sensor measurements such as air temperature can be used to set the initial conditions of a simplified model. Simpler models also reduce the number of calculations required by the optimization algorithm. Simplified models have been applied to the study of advanced building controls, but a systematic methodology to generate simplified models for control applications is still needed.

2.1.4 Model Calibration

Calibrating a model or simulation is the process of obtaining outputs that are very close to selected measured data, such as energy usage or room temperature for building simulations. Calibration can be done by varying some inputs and observing the changes to the outputs. This method identifies which parameters have a significant impact on the output results and is a way to reduce the difference between measurements and simulation results. Calibration of an energy model implies changing the inputs in a reasonable range to make the simulation results more accurate. For a building model to be accurate, it is important not only to closely match the predicted total energy use to the real energy use, but also to account for all sources and uses of energy.

Generally, calibrating a model implies comparing the simulation results to utility data, but there is no specific method to do so. The most common graphical approaches that have been used in the past are: 1) monthly percent time-series graph, 2) bar charts, and 3) monthly x-y scatter plots. Measurement technology has become increasingly inexpensive and therefore accessible, which allows for measurements of energy usage and environmental data over long periods of time and at sub-hourly intervals. It has become common in the engineering community to compare hourly simulation results to hourly measured data. Newer advanced

methods for comparing the two sets of data include: weather day-type analysis, carpet plots, and comparative 3D time series plots.

The results of the building energy model depend considerably on a number of factors: i) the user's experience with the simulation program, ii) the time allocated for the calibration procedure, iii) the modeling capabilities of the selected software, iv) the user's knowledge of design and operation of the building and HVAC systems.

Many techniques have been explored over the years to calibrate building energy models. Trial and error is a very popular method, but it is time consuming and not always reliable. According to Troncoso (1997), a major problem is that in order to perform model calibration, the analyst has to adjust the input data without sufficient evidence on which data should be modified or to what extent. In general, an energy simulation program will have outputs such as electrical demand and consumption data, which has to be compared to monitored data. If the simulation results and measured data are very different, then the user must adjust inputs and parameters on a trial-and-error basis, until the percent difference is satisfactory. The fact that these parameters are being continuously changed during the model tuning process reduces the liability of the calibrating process. Gathering information about the building can be a tedious and long process, and it is common that the building information is too complex for the model input; therefore the analyst is forced to base himself on his engineering knowledge and experience which leads to user-specific results. Troncoso (1997) presented some steps to perform calibration of building simulation that are based on the definition of the parameters that most affect the main electric end-uses of a building. Calibration methodology is composed of six stages: definition of power and schedule of constant loads, simulation of design days for thermal loads analysis, sensitivity analysis over input parameters related to significant gain/loss, adjustment of input

values of high level of influence and uncertainty, whole year simulation and final results.

The ASHRAE Guideline 14 (Gillespie et al., 2002) contains a methodology for performing calibrated simulation. The following steps are proposed: 1) produce a calibrated simulation plan, 2) collect data, 3) input data into simulation software and run the model, 4) compare simulation results to measured data, 5) refine model until an acceptable calibration is achieved, 6) produce baseline and post-retrofit models, 7) estimate savings, and 8) report on observations and savings.

Reddy (2006) categorized the sources of error or uncertainties into four categories: 1) improper input parameters due to user related lack of experience and improper specification of material properties and system structures, 2) improper model assumptions and simplifications due to usage of semi-empirical models or even perhaps weaknesses in the physical model, 3) inaccurate numerical algorithms, and 4) errors in simulation code.

ASHRAE Guideline 14 (Gillespie et al., 2002) provides methods for analyzing energy and demand savings from retrofits, as well as instructions on how to use calibrated simulation, but does not give a detailed description on a calibration methodology. It proposes steps for calibration but does not give explanations on how to achieve each step. The most common method of assessing the calibration agreement is to compare the monthly energy values to the corresponding utility bills. The issue with this approach is that the positive and negative differences, regardless of magnitude, could cancel out, giving the impression that there is no difference between the simulated and measured values. Therefore, it is not recommended to express the results only in terms of a mean and a percent difference. The AHSRAE Guideline 14 (ASHRAE (2002)) requires the use of two different statistical indices: the CV-RMSE and NMBE. The root mean squared error (RMSE)

is used to estimate the magnitude of the error of the model, or how much spread exists in the difference between measured and predicted values (Reddy, 2006):

$$RMSE = \sqrt{\frac{\sum (M - P)^2}{n - 1}} \tag{2.2}$$

where:

RSME = root mean squared error;

P = Predicted value;

M = Measured value;

n = number of values.

Another way to represent the measured squared errors between measured and predicted values is by using a dimensionless quantity called the coefficient of variation of the root mean squared error (CV-RMSE). This coefficient quantifies the relative error as well, but is a normalized measure, which is often more appropriate for model evaluation as suggested by Reddy (2011):

$$CV - RMSE = \frac{RMSE}{\mu} \times 100\% \tag{2.3}$$

where:

μ = Mean measured value.

The mean biased error (MBE) represents the difference between the measured values and predicted values (Reddy (2011)):

$$NMBE = \frac{\sum (M - P)}{(n - 1) \times \mu} \times 100\% \tag{2.4}$$

ASHRAE Guideline 14 (Gillespie et al., 2002) suggests that CV-RMSE be a maximum of 15% and NMBE of maximum 5% on a monthly basis, or 30% and 10%, respectively, on an hourly basis should guarantee a calibrated model when the whole building energy use is compared. It is uncertain whether these values are based on experimental work or some statistical analysis. The same values for CV-RMSE and NMBE are found in the Federal Energy Management Program (FEMP) (Webster & Bradford, 2008). The International Performance Measurement & Verification Protocol (IPMVP-Committee, 2002) suggested a CV-RMSE of maximum 5% on a monthly basis or 20% on hourly basis for whole building energy use.

Differences between the predicted and measured values are mostly due to uncertainty in inputs (program defaults or user assumptions), experimental error, mathematical model limitations, and user knowledge of HVAC systems and experience with the software. Users are often forced to assume or predict certain input parameters (such as air infiltration), but a small variation could lead to considerable change in simulated energy consumption.

2.2 Residential Thermostat Use and Heating Control Strategies

The settings of a heating system and the occupant control of the temperature set point have a great effect on energy consumption in buildings. It has been shown that, when compared to a constant temperature set point, that night time set backs reduce overall yearly consumption (Ingersoll & Huang (1985), Manning et al. (2007), Moon & Han (2011a,b), Tariku et al. (2008)). Ingersoll & Huang (1985) found that this night time set back strategy is most effective in loose houses, while the benefits from thermostat setbacks are smaller for tighter houses, and may

actually be counter-productive owing to subsequent effects such as increased peak loads and degradation of system efficiency over time.

In the 2005 RECS, 14% of U.S. households reported having no thermostat, 30% (34.6% of thermostat owners) had a programmable thermostat, and 56% had a manual thermostat (EIA, 2005). In the 2005 heating season, about 60% of U.S. households with programmable thermostats reported using them to reduce temperature at night. Only 45% reduced the temperature during the day; the same survey indicated that approximately 51% of homes have someone home all day, which may explain why fewer household reduce temperature during the day than during the night (Peffer et al., 2011).

A cross cultural study of energy behaviour in Norway and Japan, Wilhite et al. (1996) reveals that less than 50% of Oslo's household's setback temperature at night and 28% did not lower thermostat settings during weekends or vacations. Another northern European survey of 600 homes, Lindén et al. (2006) showed that only 38% of the houses with thermostats lowered their temperature during the night. Of the 35,471 thermostats monitored overall, only 47% were in program mode, in which the thermostat used the schedule previously input by the occupant to control temperature set points.

Meier et al. (2011) performed five investigations related to the usability of residential thermostats. Interviews with occupants revealed widespread misunderstanding of thermostat operation. It was found that most thermostats were selected by previous residents, landlords or other agents. The majority of occupants operated their thermostats manually (rather than using the programmable features available) and almost 90% of respondents reported that they seldom or never adjusted to a weekend or weekday program. It was also found (through photographic evidence) that 45% of low-income families surveyed had their thermostat in hold (constant value), even though 85% claimed to use the programming

features, further showing user misunderstanding with regards to thermostat use.

The accuracy of whole-house building simulations often depends on the accuracy of the input values and how well they reflect "actual values." Whether an input is a defaulted value or measured, discrepancies between the actual value and input value can occur and propagate throughout the simulation, creating errors in the output (Polly et al., 2011). Among the most influential inputs for software-based energy analysis are the thermostat set points and associated indoor air temperatures that drive heat loss calculations. NREL (2013) presents the measured variability in indoor space temperatures in a set of 60 homes located in Florida, New York, Oregon, and Washington. Living room temperatures for the New York area were on average 18.3°C in the heating season, which is lower than many standards (House Simulation Protocols (Hendron & Engebrecht, 2010), (International Code Council, 2009), (RESNET, 2006), Home Energy Rating System (HERS)) heating set point assumptions.

Gunay et al. (2014) studied the user behaviour between those who are personally responsible for their heating bill and those who have their heating bill included in the rent. It was found that those who had personally responsibility for their monthly heating bill were more diligent and active in controlling their indoor temperatures in different zones of the dwelling. On the contrary, those who were not responsible for their energy bills rarely adjusted their thermostat setting or setback their temperature during night or unoccupied times. Also, those not responsible for their energy bill maintained their apartments on average 2°C higher than those responsible for their energy bill.

The World Business Council for Sustainable Development recognized the importance of the occupants' behaviour in reducing energy consumption in its 2007 Report that stated the behaviour of occupants in a building can have as much

impact on energy consumption as the efficiency of equipment (World Business Council for Sustainable Development, 2007).

Huebner et al. (2013) states that 'Smart thermostats' are characterized generally by their communicating capabilities, including web and mobile user interface options, as well as networked control that allows for instantaneous management of multiple thermostats in a facility. Smart thermostats may include occupancy responsive control, adaptive or learning functionality, demand response capability, fault detection and diagnostics, and runtime optimization features. This promises general improvement to programmed set point scheduling, as well as automated schedule and set point optimization.

Kummert et al. (2001) studied the performance of a smart heater control on a passive solar commercial building. It anticipates the building behaviour using a model and a forecasting of the disturbances in order to compute the control sequence that minimizes a given cost function (e.g., thermal comfort, energy consumption, peak load etc.) over the optimization horizon. Simulation-based and experimental results show that it can lead to significant energy savings (9%) while maintaining or improving the comfort level.

Goyal et al. (2013) compared three control algorithms, one that uses feedback from occupancy and temperature sensors, while the other two computes optimal control actions based on predictions of a dynamic model to reduce energy use. Both the optimal-control based schemes use a model predictive control (MPC) methodology; the difference between the two is that one is allowed occupancy measurements while the other is allowed long term occupancy prediction. Simulation results show that each of the proposed controllers lead to significant amount of energy savings over a baseline conventional controller without sacrificing occupant health and comfort.

2.3 Peak Demand and Demand Response

Demand response is regarded as a solution to the issues of uncertain and fluctuating power supply. A key advantage of demand response is the lack of major technological impediments, as much of the required communications and monitoring technology has been developed, with the roll out of advanced metering infrastructure already under-way in a number of regions (Callaway & Hiskens (2011), ICER (2012)).

Demand response is not a new phenomenon and has been employed in various forms across the globe for decades. The most obvious form of demand response is systematic load shedding, a way to avoid system blackout; however more sophisticated approaches have been implemented in a number of power systems.

Time of use (TOU) rates where consumers are subject to expensive tariffs during fixed peak hours, or cheaper rates during night hours, have traditionally been used to incentivise reduced peak consumption, and so-called "night-valley filling" behaviour (Keane & Goett, 1988). Critical peak pricing (CPP) is an event-based tariff scheme employed for larger commercial and industrial consumers with the objective of decreasing peak loads. Under this scheme, higher electricity rates are applied during peak demand events. This approach has been adopted by the Californian independent system operator, and is most commonly employed to reduce loads during hot summer days from noon to 6p.m. when the load from air conditioning units is excessive (Jazayeri et al., 2005).

Many studies involving the residential sector have been done over the years. Studies include California's vast Statewide Pricing Pilot (SPP) (CRA, 2005) and Oregon's Olympic Peninsula (PNNL, 2007). From the detailed analysis of the SPP data (Herter et al., 2007), it was found that automation had a great effect on load reduction, greater than price signal alone.

In the past few years, many studies have been done to evaluate the effect of controlling cooling equipment on the building's total peak load. Most of the work found in literature has been focusing on commercial and institutional buildings. Studies have been done on the reduction of the cooling load using night cooling and on the effect of thermal mass and thermal storage devices (Braun (1990), LBNL (2006), Yin et al. (2010)). Others have focused on optimal control of set points and storage (Henze et al. (2005b), Lee & Braun (2008)). Katipamula & Lu (2006) and Reddy et al. (1991) have studied control strategies for HVAC equipment in residential buildings.

Braun (1990) studied dynamic optimization techniques to computer simulations of buildings and their associated cooling systems for a range of conditions in order to determine the maximum possible savings. Results indicate that both energy costs and peak electrical use can be significantly reduced through optimal control of the intrinsic thermal storage within building structures. However, the cost savings depend strongly on several factors including 1) utility rate structure, 2) part-load characteristics of the cooling plant and air handling system, 3) weather, 4) the occupancy schedule, and 5) building thermal capacitance.

Braun & Lee (2006) developed and evaluated a simple control strategy for limiting demand in two types of small commercial buildings using the building thermal mass. The strategy would be used on days that would be expected to establish the peak demand for the billing-period. The results of the simulations show 30% to 100% reduction in the baseline peak air-conditioning power, depending mostly on climate.

Pietila et al. (2012) studied the viability of achieving a zero peak house (ZPH) in Toronto, Ontario, Canada - a house that draws no electricity from the grid during system-wide peak periods. It was found that 41%- 51% of the goal of eliminating electricity consumption during the summer Ontario on-peak period

(11am to 5pm during weekdays from May 1 through October 31) could be achieved through a combination of architectural, control, efficiency, and occupant behaviour measures.

Research focused on winter peak reduction in cold climates is a continually growing field. Persson et al. (2005) have explored space heating peak load reduction but their solutions involved the use of substitution fuel. Lu & Katipamula (2005) focused on the global effect of controlling thermostatically controlled appliances on the electric grid but not on the effect of this control on occupant thermal comfort. Oregon's Portland General Electric Co. had a pilot project in 2004 on direct load control for electric space heating which showed that residential customers could reduce their peak load by 0.48 to 0.73 kW by reducing their space heating set point by 2-3°C for 2 to 3 hours (PGE, 2004). The Olympic Peninsula pilot project included the control of resistive heating equipment for homes controlled by one or at most two thermostats. The results of this pilot study showed that a significant part of the overall load reduction due to price increase came from a decrease or shift in space heating load (PNNL, 2007).

Leduc et al. (2011) studied space heating strategies for load reduction during critical periods on the grid while also taking into consideration the occupant thermal comfort. They studied three types of strategies: lowering the thermostat set point, storing heat in the building mass during off-peak hours and lowering the set point during critical periods, and limiting the power to the baseboards. Results showed promising reductions of up to 7kW (or 90% of the reference heating load of the average residents).

Reynders et al. (2013) studied the impact of the insulation level and embedded thermal mass of a near net zero house on the ability of its photovoltaic system to cover the power demand of an air-to-water heat pump during grid peak periods. Results show that although the influence on the cover factors is limited, the use of

the structural storage capacity for demand-side management shows strong potential to shift the peak electricity use for heating to off-peak hours. Furthermore, it is shown that not only the availability of the thermal mass, but also the interaction between the heating system and the thermal mass is of significant importance.

Lavigne et al. (2014) studied winter demand response for a commercial building and showed, through using an optimized demand response strategy that the use of DR strategies can lead to significant reductions in the building's total power demand during peak periods while maintaining an acceptable comfort level for the building's occupants.

Ali et al. (2014) optimized the demand response control of partial storage electric space heating, by combining the control of direct electric space heating and partial thermal energy storage in order to minimize the total energy cost of customers without sacrificing user comfort. Ali et al. (2014) concluded that the optimal control model can be easily integrated at the household level.

Fournier & Leduc (2014) used building simulation to study the impact of multiple set point modulation strategies on the demand of a baseboard heater house during winter grid peak periods. This study aimed at evaluating the impact of several set point modulation strategies when applied to selected rooms. Results show that the demand reduction potential, for a specific building and given weather conditions, will depend on both the technology available to materialize the set point modulation strategies and the acceptable disruption from the normal comfort level. While these are common limits associated with DR strategies based only on control modifications, they determined that significant load reduction can be achieved without any added heat storage equipment or building construction modifications.

Most recently, Candanedo et al. (2015) studied the implementation of "near-optimal" trajectory between temperature set points and found a peak reduction

of 8% when compared to a linear ramp profile.

2.4 Conclusion

A great deal of effort has been made to develop suitable energy modelling approaches for buildings and study their thermal response by means of difference mathematical and experimental techniques. Model resolution has an effect on computation time and model accuracy. Model-based thermal control studies have shown that control-oriented modelling is highly beneficial in evaluating different control algorithms and energy efficiency measures. Low-order models using the explicit finite difference method that are well-calibrated are beneficial in control studies and they are appropriate to be implemented into building automation system (BAS) to apply the designed control strategies, though great care must be taken when choosing the approximations used in a mathematical model (Linearization of heat transfer, model complexity reduction and spatial/temporal discretization) depending on the building and system types.

From the above literature, it is evident that advancing controls in buildings offers a way to reduce consumption and peak loads. Settings of a heating system and occupant control of temperature set points have a great effect on energy consumption in buildings, as well as building peak demand. Many residents still do not have programmable thermostats, or if they do, they are not using the programmable features, suggesting lack of care or user knowledge of thermostat operation. Thermostat set point schedules are difficult to predict as an input into building simulations and the results from building simulation studies depend greatly on the input values for temperature set point schedules. If simulation defaults or user inputs do not reflect actual conditions in homes, errors in results can occur. A thermostat user's schedule, personal preferences, their thermostat operation knowledge, and their relationship with their heating bill all affect how

they use their thermostat. All of these variables within the domain of residential heating control suggest simple strategies, and possibly further public education, are necessary for widespread peak load demand response to be implemented.

Chapter 3

Methodology

In this thesis, different levels of thermal modelling detail are studied using data from a real building and benefits of the different models for the application of control strategies in buildings are discussed. This study focuses on the lumped parameter explicit finite difference method as it is appropriate to be implemented into building automation system (BAS) to apply advanced control strategies. Peak power reduction strategies implementing temperature set point adjustments and varying of thermal mass are investigated and evaluated using demand response indicators (describe in Section 3.4). This thesis focuses on simple and physically meaningful models and the investigation of modelling resolution, based off of the guiding principles proposed by Candanedo et al. (2013). Desirable features of appropriate and physically meaningful models for model based control in buildings is considered.

3.1 Experiment Objectives

Full scale experiments are a valuable tool to study system behaviour. The objectives of the experiments at Experimental Houses for Building Energetics (EHBE)

(Fournier & Leduc (2014), Le Bel & Gelinas (2012)) are to obtain a better understanding of the transient thermal behaviour and response of the building due to a set of inputs such as environmental conditions and heating power.

Using the results from full scale building experiments, model resolution and accuracy are evaluated on how well they are able to predict experiment results.

3.1.1 Choice of EHBE

For 74% of those residential customers, electricity is the main energy source for space heating (Le Bel & Gelinas, 2012). Approximately 60% of the commercial & institutional customers (CI market) also use electricity as their main source of energy for space heating. This wide-spread use of electricity for space heating combined with Québec's weather make it a winter-peaking area (its peak demand was approximately 38 800 MW in 2012). Among the residential customers using electricity for space heating, 81% have houses equipped with an electric baseboard and a line-voltage thermostat in each room. On average, their space heating load typically represents 50% of their total annual electricity bill, while during peak periods, the space heating load represents up to 80% of the total load of a residence.

The test bench consists of two 2-storey detached homes with excavated basements, each with a 60m^2 footprint, excluding the single detached garage. The reason to build two identical houses side by side is to have one of them as the test house while the other is the reference; it allows to determine precisely the impact of a technology or a strategy in reference to a base case subjected to the exact same environmental conditions. Further details of EHBE are given in Chapter 4.

3.2 Data Acquisition

There are approximately 500 sensors in each house with recordings every 15 minutes. The thermocouples instrumented in the homes are special T type and the data acquisition equipment and computers are located in the garage of each house. The sensors measure the following:

- Weather (temperature, solar etc.)
- Room by room electric baseboard heating (in Wh)
- Plug and lighting loads
- Air temperature, relative humidity, air velocity, globe temperature (Figure 4.5)
- Surface temperatures of structure (walls, floors, ceiling layers etc.)
- Temperatures and water content of surrounding soils in several locations

For this study, weather conditions, room temperatures and heating data were required for the evaluation of the thermal models. Surface temperature are also used for thermal comfort analysis.

3.3 Building Thermal Modelling

Simulation and analysis of the thermal and energy fluxes in a building facilitates the choice of the materials, subsystems and control strategies for the local climatic characteristics and building function (Athienitis & O'Brien, 2015). Many thermal processes are relevant in the assessment of building thermal behaviour, such as:

- Heat conduction through exterior walls, roofs, ceilings, floors and interior partitions;
- Solar radiation through transparent surfaces;

- Latent and sensible heat generated in the space by occupants, lights, and appliances;
- Heat transfer through ventilation and infiltration of outdoor air and other miscellaneous heat gains

One of the most important items in the above process is the thermal conduction through a multi-layered wall that is calculated in several ways such as:

- Finite difference methods
- Finite element methods
- Transform methods (frequency domain and time domain), including time series methods

There are two main steps in creating a suitable mathematical model that describes the energy transfer processes in a building. First, the thermal exchanges must be modeled as accurately as is necessary. While an acceptable level of precision is desired, too much complexity or detail can limit the model usefulness in analysis and design. Second, an appropriate method must be chosen to determine the room temperature and auxiliary energy loads.

Modelling the long-wave radiant heat exchanges of the zone interior is more important with direct gain than with indirect gain systems and generally requires more modelling detail, particularly if a floor heating system is integrated (Athienitis & O'Brien, 2015). As for this study, direct gains and floor heating systems are not main factors in the zones, therefore a simplified modelling approach for long-wave radiant heat exchanges is employed and explained in a later section.

The following three types of approximations are commonly introduced in mathematical models to facilitate representation of the building thermal behaviour (Athienitis & O'Brien, 2015):

1. *Linearization of heat transfer*: Convective and radiative heat transfer are nonlinear processes and the respective heat transfer coefficients are usually linearized so that the system energy balance equations can be solved by direct linear algebra techniques and, if desired, represented by a linear thermal network. Linearization generally introduces less error for long-wave radiant exchanges between surfaces than convection between surfaces and room air. In some cases heat flow reversal can occur such as between a cold floor and warm air when the convective heat transfer coefficient can be of the order of 1 W/m^2K versus 3 W/m^2K for a heated floor and cold air. A linear lumped parameter system can be represented by a set of ordinary differential equations and thermal networks. An important subset of linear systems are those with time varying coefficients – an important case in building energy analysis, where we can often represent thermal conductances such as a known variable level of natural ventilation or time-varying infiltration. It should be noted that when thermal storage undergoes phase change (e.g. phase change materials – PCM) a linear approximation may not be possible in some cases and specialized modelling will be required.

2. *Spatial and/or temporal discretization*: Transient heat conduction is described by a parabolic, diffusion type partial differential equation. Thus, when using finite difference methods, a conducting medium with significant thermal capacity such as concrete or brick must be discretized into a number of regions, commonly known as control volumes, which may be modelled by lumped network elements (thermal resistances and capacitances). Also, time domain discretization is required in which an appropriate time step is employed.

3. *Approximations for reduction in model complexity - (establishing appropriate model resolution)*: These approximations are employed in order to reduce the number of simultaneous equations to be solved and the required data input

or to enable the derivation of closed form analytical solutions. They are the most important approximations (Athienitis & O'Brien, 2015). Examples include combining radiative and convective heat transfer coefficients, assuming that surfaces are at the same temperature, or considering certain heat exchanges as negligible. These approximations must be carefully selected and applied by considering the expected temperature variations (spatial and temporal) in a zone. As an example, a zone with large windows or floor heating may exhibit large spatial temperature variations, in which case the use of combined film coefficients would results in high errors in room operative temperature or floor heating rate calculations.

3.3.1 Lumped Parameter Finite Difference Method

This approach is based on a space discretization of the material into control volumes, each one of which describes a layer. A node is located at the centroid of the control volume. The heat flux between adjacent nodes is described by using resistance analogies: the flux is calculated as proportional to the difference between the temperatures of the two nodes. Between control volumes, the conductance is calculated as kA/L, where k is the thermal conductivity of the material, A the area of the surface of contact, and L the distance between adjacent nodes. If the node has considerable thermal mass, a node may be assigned a capacitance, which represents the heat storage capacity of the control volume. By performing a heat balance on the control volume, the differential equation of a node can then be written as (Athienitis et al., 1990, Athienitis & Santamouris, 2002):

$$C_i \frac{dT_i}{dt} = q_i + \sum_j U(i,j)\,(T(j,n) - T(i,n)) \tag{3.1}$$

Where q_i represents the heat generated at a node or received directly by it from a source, $U_{i,j}$ represents the thermal conductance (inverse of resistance), T is the temperature, and C is the thermal capacitance of each node. A strategy commonly implemented to determine the transient solution is the application of time discretization (Athienitis & Santamouris, 2002). The fully explicit approach assumes that the current temperature of a given node depends only on its temperature and the temperature of the surrounding nodes at a previous time step (Athienitis, 1994). The term having the time derivative can then be discretized as follows (Athienitis, 1994):

$$C_i \frac{dT_i}{dt} \approx C_i \frac{\Delta T_i}{\Delta t} = C_i \left(\frac{T(i, n+1) - T(i, n)}{\Delta t} \right) \tag{3.2}$$

By solving for the temperature at the next time step (Athienitis, 1994):

$$T(i, n+1) = \left(\frac{\Delta t}{C_i} \right) \cdot \left(q_i + \sum_j \frac{T(j, n) - T(i, n)}{R(i, j)} \right) + T(i, n) \tag{3.3}$$

Heat conduction calculations based on this method are applied in building simulation tools such as ESP-r and EnergyPlus. The calculation of conduction through massive building envelope components become a part of a larger thermal network representing the zone being analyzed (often linked to other zones).

Figure 3.1 shows a schematic of a simple one-zone thermal network with combined radiative and convective heat transfer coefficients. The air node (node 1) is linked to the internal surfaces by combined interior convective film coefficients and radiative heat transfer coefficients. It is also linked to the outdoor temperature directly by a resistance representing infiltration and conduction through elements of negligible thermal mass (windows and doors). The air node also receives a heat contribution q_{aux} from the heating system . By representing radiation and

convection with linear approximations, methods from circuit analysis can be used to study the building.

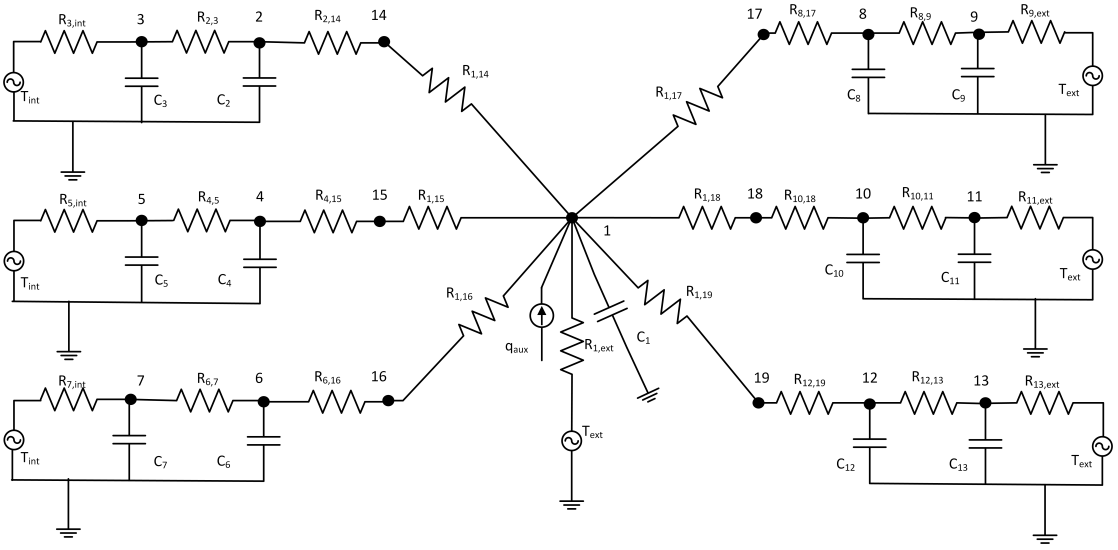

Figure 3.1: Finite Difference Thermal Network of a zone

Kummert et al. (2006) states that parameter identification on a detailed building model is a complex problem due to the large number of parameters and to the possibility of achieving the same result through different actions (e.g., increasing the infiltration rate or increasing the thermal conductivity of a low-mass wall or window).

The large number of parameters in the building model makes parameter identification a complex problem, and the desired level of accuracy is very high - performance differences of less than 10% must be reproduced. For those reasons, among others, a simpler model may be an attractive alternative to complex building simulation tools.

Using the explicit finite difference method, several thermal network models of varying resolution (based off of the network in Figure 3.1) were created and compared to experimental data. The purpose is to study the level of modelling detail adequate to represent a zone heated convectively and with minimal solar gains.

3.4 Demand Response Strategies

Demand reduction indicators can be computed to quantitatively compare the resulting demand profiles over peak periods with the reference scenario. Depending on the demand strategy implemented, the possible rebound of demand after the typical peak hours could also create new peaks, . The demand impact of the hours following the peak period is therefore also of interest.

Table 3.1 lists the most important power demand indicators used to evaluate the efficiency of the DR strategies (Fournier & Leduc, 2014). Every indicator can be expressed in terms of the daily power demand profile vector components:

$$\overrightarrow{Q_x} = [q_{x,0.25}, q_{x,0.5}, q_{x,0.75}, \ldots, q_{x,24}] \tag{3.4}$$

Table 3.1: Power demand reduction indicators

	Indicator	**Definition**
AM	q_{am}^{max}	maximum power demand from 6:00-9:00
	$\overline{q}_{am}$	mean power demand from 6:00-9:00
	$rebound_{am}$	maximum power demand from 9:00-11:00
PM	q_{pm}^{max}	maximum power demand from 16:00-20:00
	$\overline{q}_{pm}$	mean power demand from 16:00-20:00
	$rebound_{pm}$	maximum power demand from 20:00-22:00

3.5 Summary

Full scale experiments are a valuable tool to study system behaviour. The objectives of the experiments at Experimental Houses for Building Energetics (EHBE)

are to obtain a better understanding of the transient thermal behaviour and response of the building due to a set of inputs such as environmental conditions and heating power. Using the results from full scale building experiments, model resolution and accuracy are evaluated on how well they are able to predict experiment results. Using the explicit finite difference method, several thermal network models of varying resolution (based off of the network in Figure 3.1) were created and compared to experimental data. The purpose is to study the level of modelling detail adequate to represent a zone heated convectively and with minimal solar gains.

Adding simulation results to the experimental comparison allows the researcher to estimate yearly savings and to study the behaviour of different DR strategies, therefore adding useful information to the study.

Kummert et al. (2006) showed that it can be easier to reach a high level of accuracy with simple models that allow a greater flexibility in parameter identification. Detailed building models that are commonly used to optimize building designs require thousands of parameters. While a purely experimental comparison based on two identical buildings is probably still preferable it the resources are available, the hybrid comparison combining experiments and simulation allows one to infer useful information.

Chapter 4

Experimental Description and Results

Experiments were conducted at Hydro-Québec's LTE (Laboratoire des technologies de l'énergie), in Shawinigan, Québec, where two identical homes are located and are commonly called the "twin homes", shown in Figure 4.1. The objective of the first experiments was to study the dynamic response of a room in the homes to a temperature step change with different floor coverings. The objective of the second set of experiments was to implement peak power (due to space heating loads) reduction control strategies using advanced communicating thermostats, and observe the building thermal behaviour.

4.1 Experimental Houses for Building Energetics

The homes used for the experiments are the Experimental Houses for Building Energetics (EHBE) (Fournier & Leduc (2014), Le Bel & Gelinas (2012)). The test bench consists of two 2-storey detached homes with excavated basements,

each with a 60m^2 footprint, excluding the single detached garage. Floor plans are shown in Figures 4.2, 4.3 and 4.4. The houses are 25 ft x 26 ft, three bedrooms, one and a half bathroom cottages with a full basement and a 15 ft x 24 ft attached garage. The wall assemblies of the building were chosen to represent a typical light-weight wood framed house in Québec. The total fenestration area is 19m^2, consisting of vinyl framed windows with double glass and air gap. They were completed in February 2011.

The homes are located in Shawinigan, Québec (46°34'N 72°45'W) and are oriented 35° west of south. The homes are heated with baseboard space heating in each room with individual electronic room thermostats. There is also electric radiant floor heating in the kitchen and bathroom.

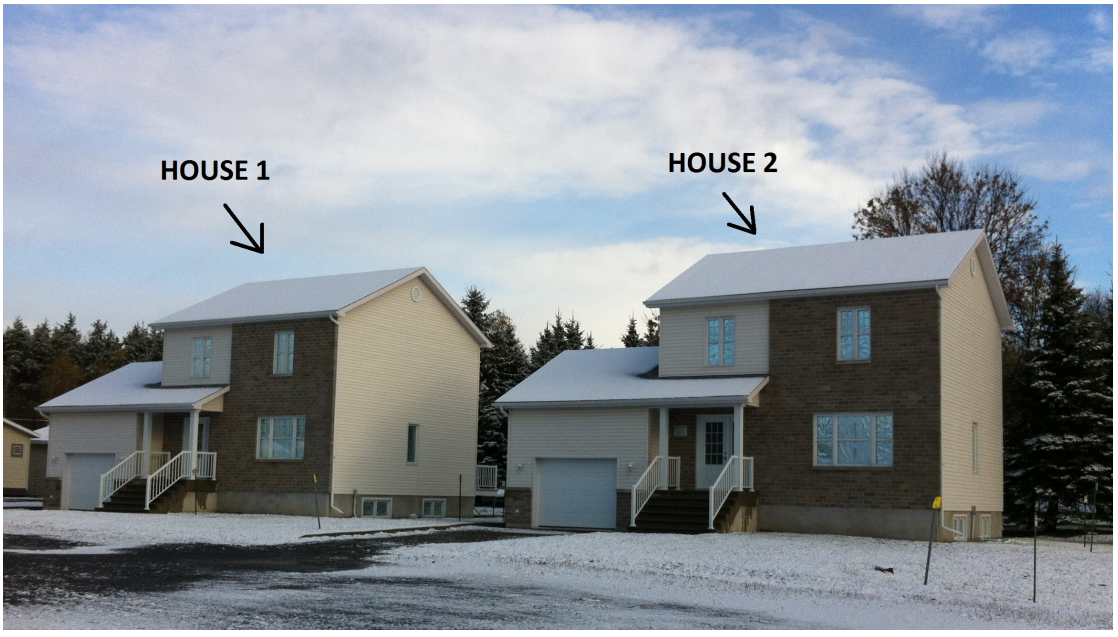

Figure 4.1: Twin houses

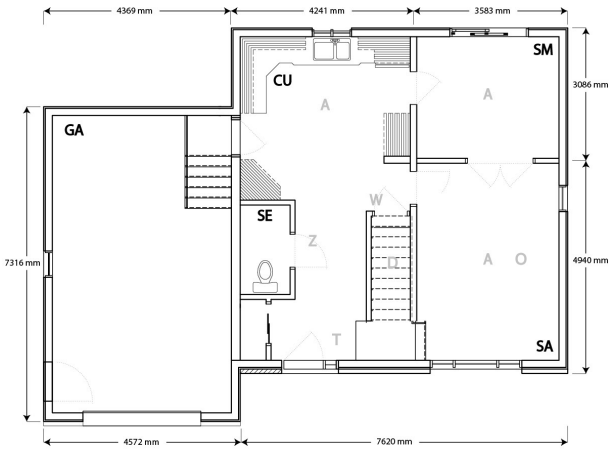

Figure 4.2: Main level of twin houses

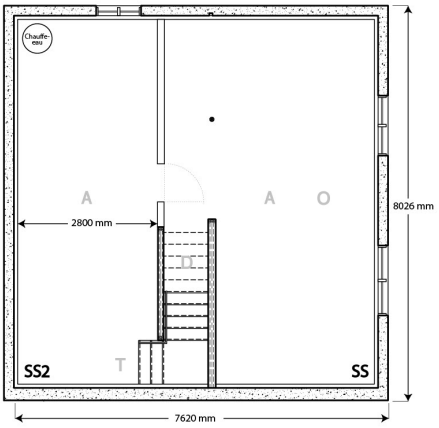

Figure 4.3: Basement of twin houses

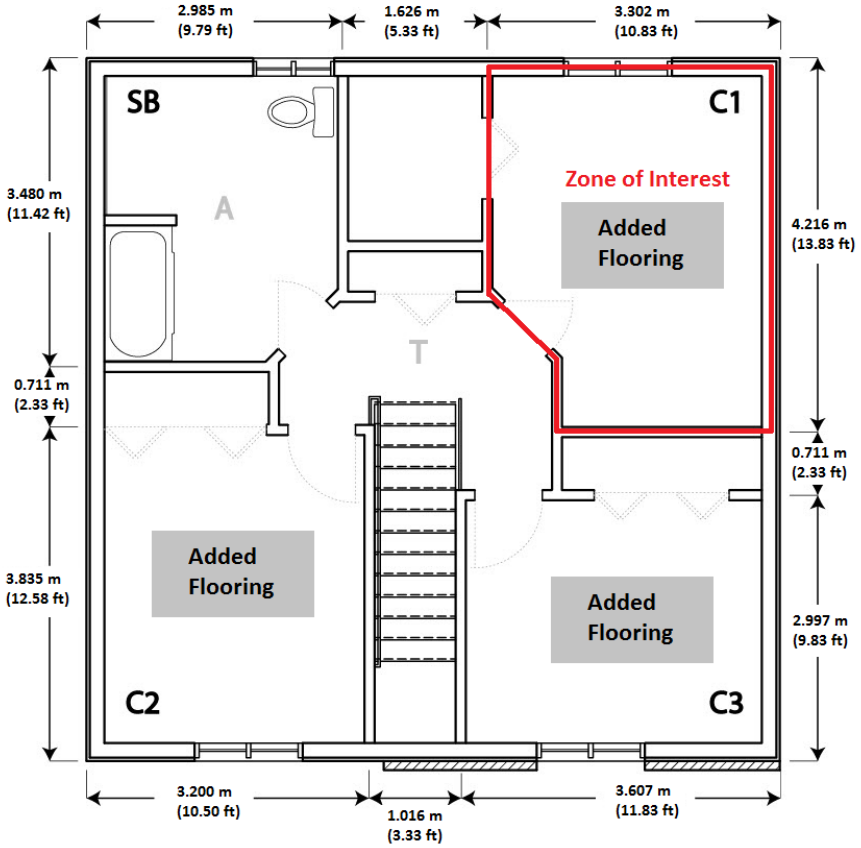

Figure 4.4: 2nd storey of twin houses

The homes are of normal construction for Québec with a building envelope consisting of (from exterior to interior) vinyl cladding or brick, air-space, air barrier, fibreboard, R-20 glass-fiber, Enermax, air-space, drywall and R-30 insulation

in the roof instead of R-20. The windows are of double clear glass with an air gap and no coatings, with a total window area of 208 square feet for each house. The interior of the houses is finished with drywall and wood floors except for the kitchen and bathrooms which have ceramic tile floor.

The baseboard heater in each room is controlled by a line-voltage (204 V) electronic thermostat with pulse width modulation at 15 second cycles. The heating capacity in the basement is 4000 W, 4750 W each for the main and second floor, and 2000 W in the garage. The bedrooms each have a rated capacity of 1250 watts. The houses have been fitted with all the air ducts necessary for a central heating/cooling system, though the system is not yet installed. In addition, the kitchen and second storey bathroom are equipped with electric radiant floor heating.

There are approximately 500 sensors in each house with recordings every 15 minutes. The thermocouples instrumented in the homes are special T type and the data acquisition equipment and computers are located in the garage of each house. The sensors measure the following:

- Weather (temperature, solar etc.)
- Room by room electric baseboard heating (in Wh)
- Plug and lighting loads
- Air temperature, relative humidity, air velocity, globe temperature (Figure 4.5)
- Surface temperatures of structure (walls, floors, ceiling layers etc.)
- Temperatures and water content of surrounding soils in several locations

Figure 4.5: Globe thermometer

4.2 Experiment 1 Description - Room Dynamics

Experiments were conducted at Hydro Québec's LTE (Energy technology laboratory). The objective of the experiment 1 was to study the dynamic response of a room in the homes to a temperature step change with different floor coverings. Experiment 1 occurred between October 23rd and November 4th, 2013 following the experiment schedule shown in Table 4.1.

The following are the conditions of the homes during the experiments:

- Night time set back at 7pm = 21°C
- Day time step up at 7am = 26°C
- Three floor coverings tested: plywood, carpet, tile

- Experiments with interior doors open and closed
- South windows covered by interior foil
- All windows covered by interior blinds
- Garage and basement kept at constant 21°C & doors closed

Figure 4.6 shows the temperature set point profile used for the duration of the experiment and material properties of the floor coverings are shown in Table 4.2.

Table 4.1: Experiment 1 schedule

	House 1		**House 2 - Reference**	
	Interior Doors	**Flooring**	**Interior Doors**	**Flooring**
Test 1	Open	Carpet	Open	Plywood
Test 2	Closed	Carpet	Closed	Pywood
Test 3	Open	Tile	Open	Plywood
Test 4	Closed	Tile	Closed	Plywood

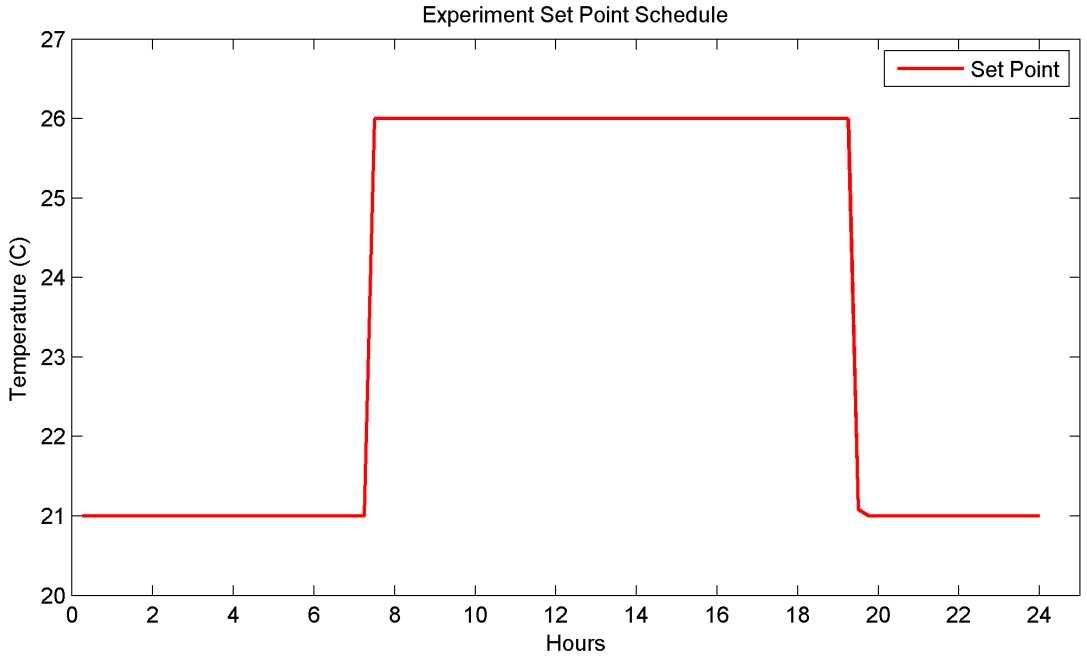

Figure 4.6: Experiment 1 set point profile

Table 4.2: Material properties of floor coverings

	Density ρ (kg/m^3)	**Specific Heat** C_p (J/kgK)	**Conductivity** k (W/mK)	**Thickness** L (mm)	**Thermal Capacitance** $C = C_p \times \rho \times L \times A_{floor}$ (J/K)
Wood	650	2,200	0.12	34.5	6.88×10^5
Tile	1,600	1,000	0.195	9.5	1.03×10^6
Carpet	200	1,300	–	9.5	–

The indoor set point temperatures were higher than normal during the experiments as a way to increase the temperature difference between indoor and outdoor environments. Because the experiments were conducted in the fall, the outdoor temperature was mild and performing energy consumption (due to heating) analysis at these mild conditions could be difficult.

4.2.1 Experiment 1 Results

Figures 4.7 and Figure 4.8 show air temperature results for all tests of experiment 1 for bedroom 1. The first part of the graph are tests with interior doors open while the second part is the tests with doors closed. A repeated air temperature profile can be seen through the days.

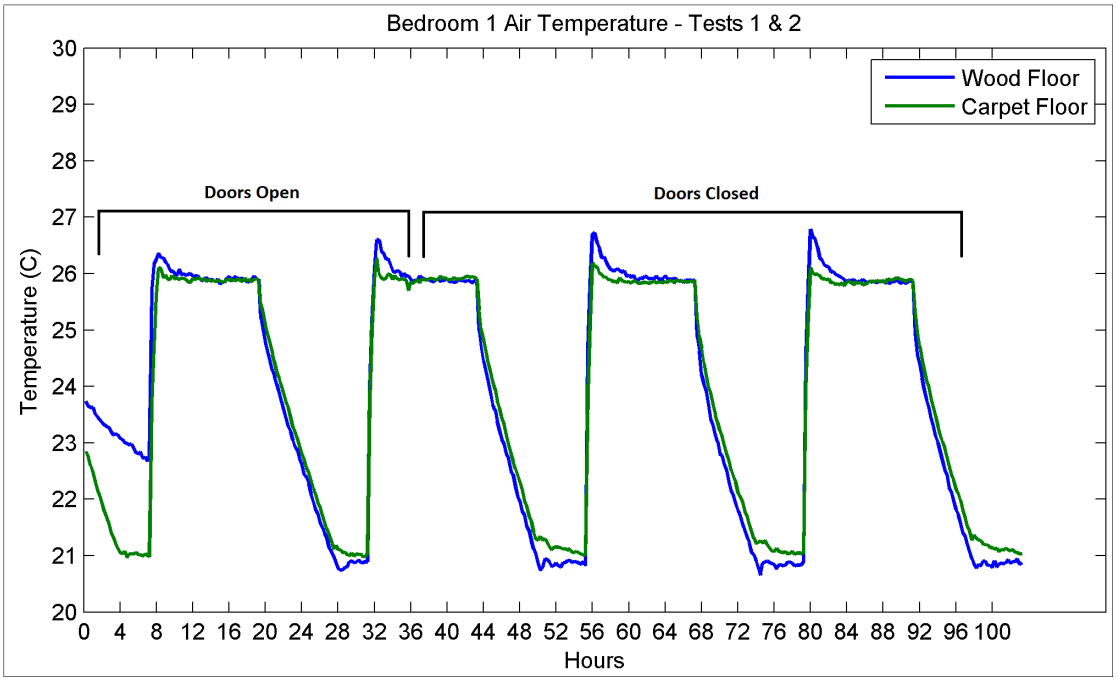

Figure 4.7: Interior temperature - tests 1 & 2

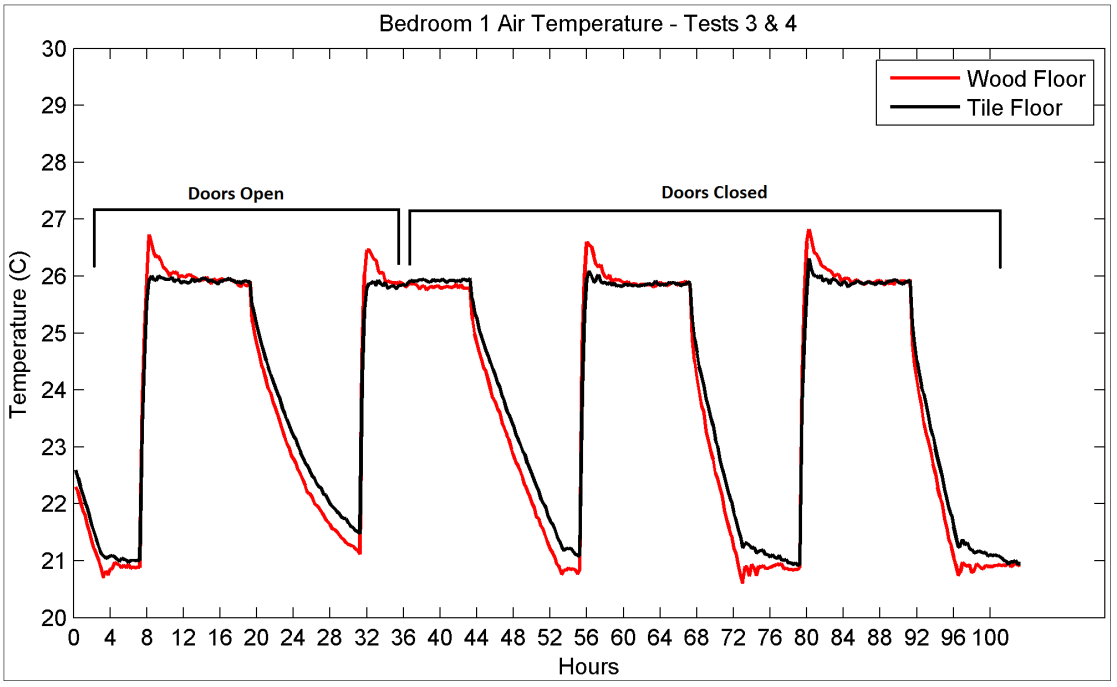

Figure 4.8: Interior temperature - tests 3 & 4

Figures 4.7 and Figure 4.8 shows room air temperature for the tests, while Figures 4.9 & 4.10 display the weather conditions during the experiments. outdoor air temperature.

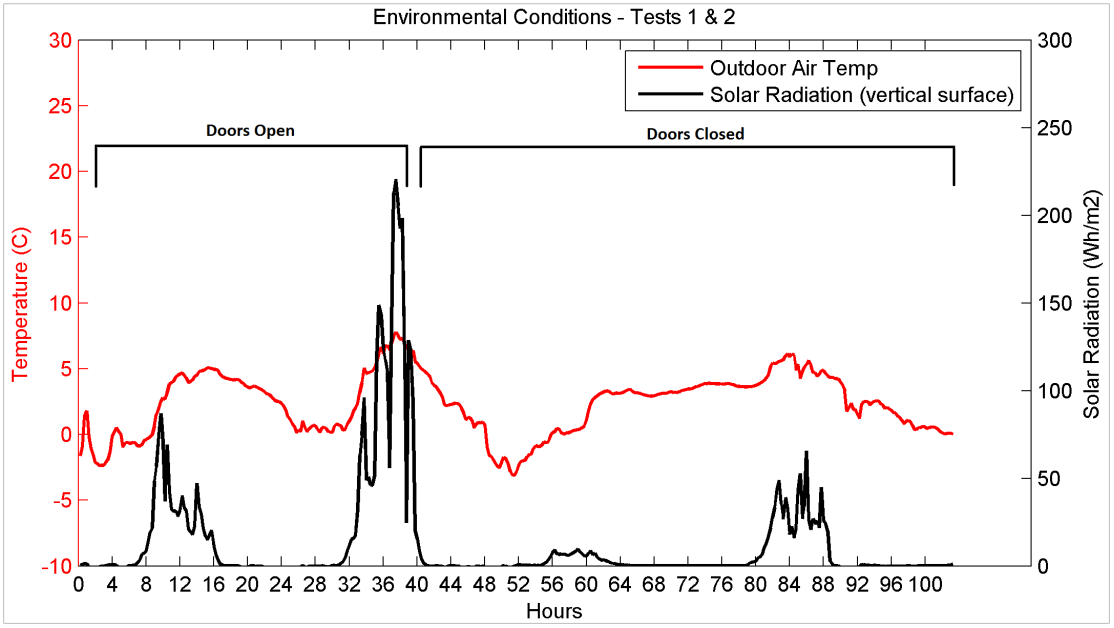

Figure 4.9: Weather - tests 1 & 2

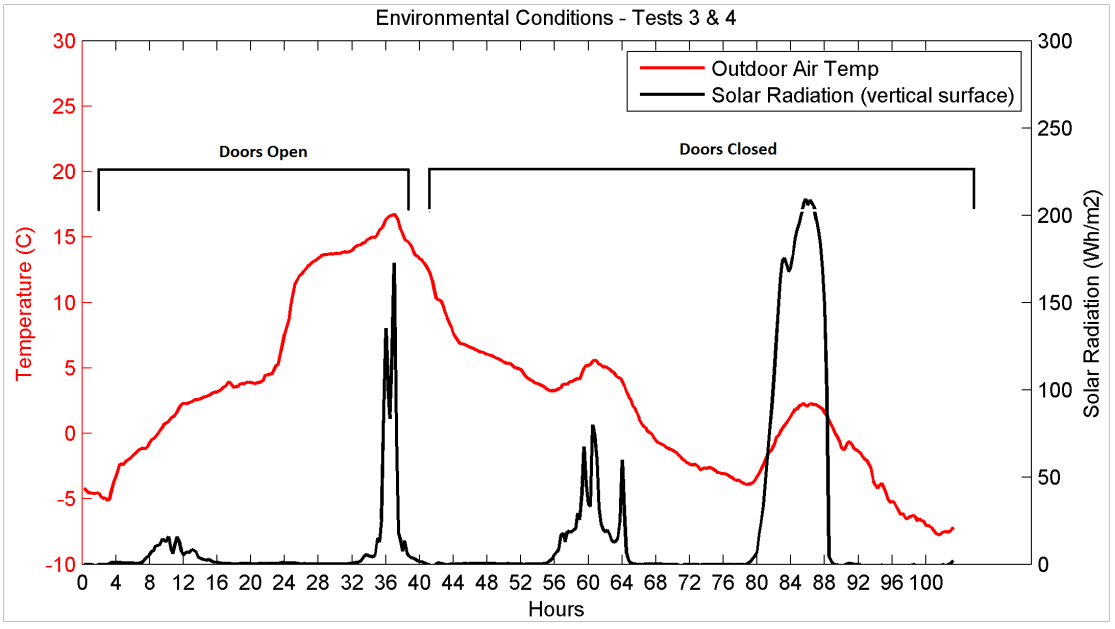

Figure 4.10: Weather - tests 3 & 4

Figures 4.11 and 4.12 shows room air temperature and heating power for the tests. The higher energy consumption comes at a time with lower air temperature, even though at that time, solar radiation is high. This can also be seen in Figure 4.13, where low whole building energy consumption correlates well with a higher outdoor temperature.

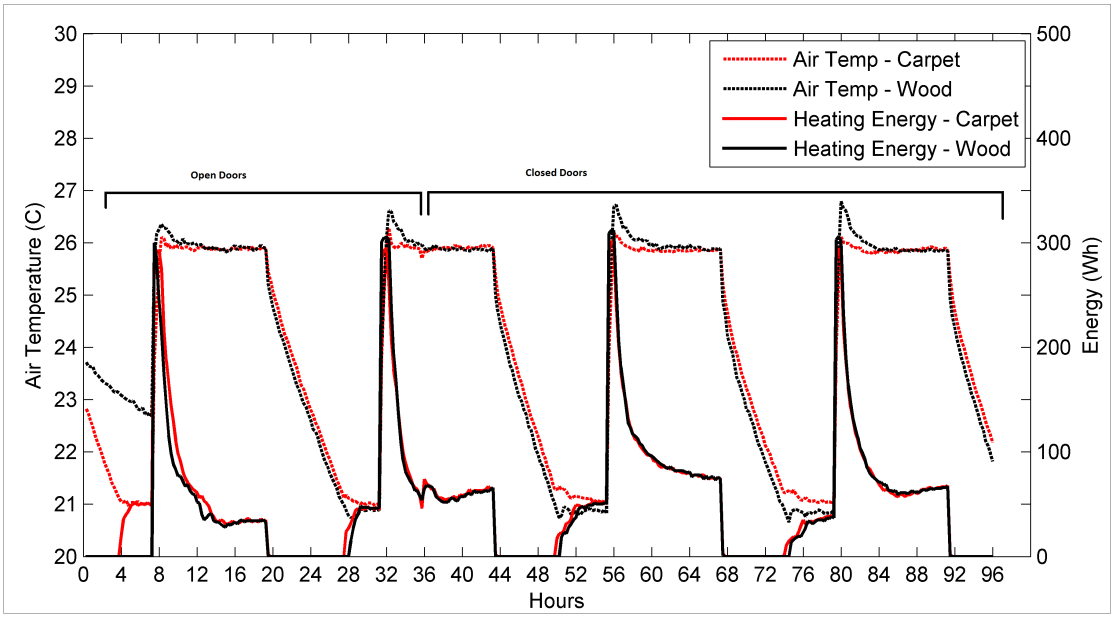

Figure 4.11: Air temperature and heating power - tests 1 & 2

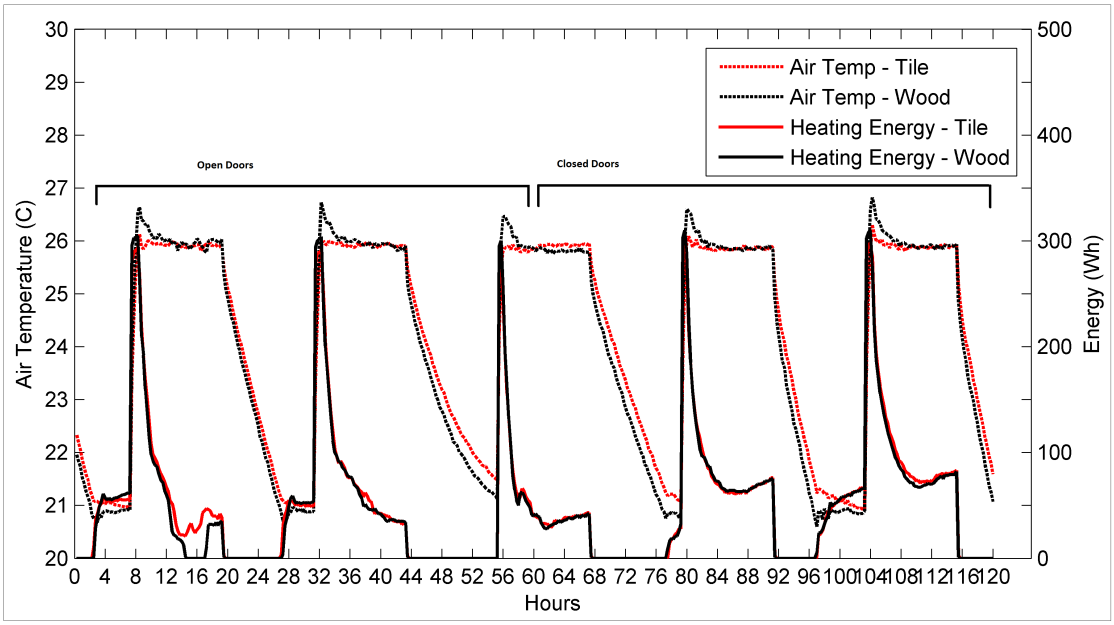

Figure 4.12: Air temperature and heating power - tests 3 & 4

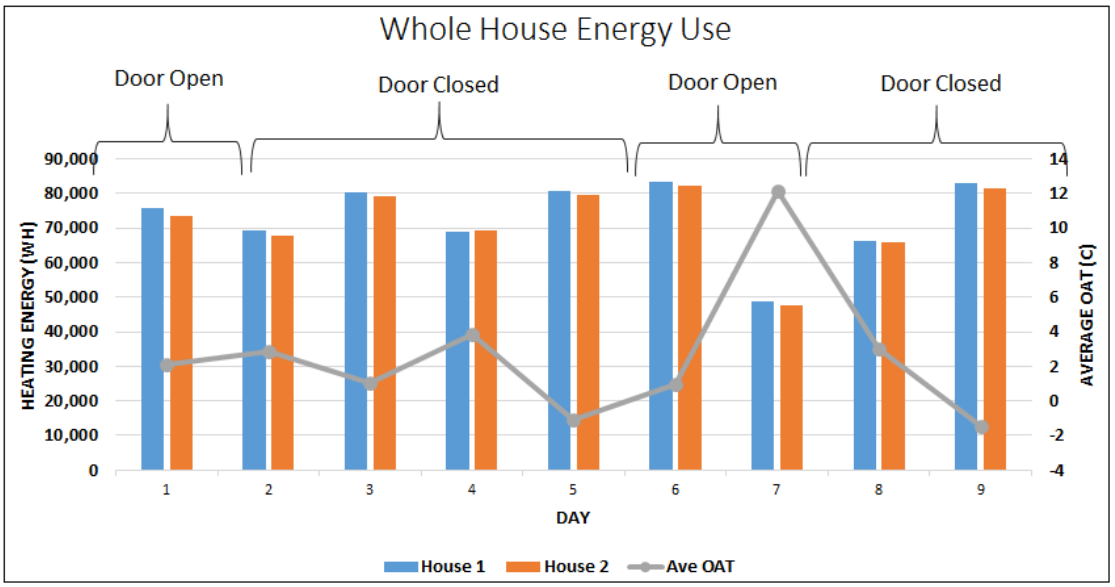

Figure 4.13: Whole house energy use

4.2.2 Thermal Comfort Considerations

Thermal comfort refers to "that condition of mind that express satisfaction with the thermal environment" [ASHRAE standard 55; as cited in (ASHRAE, 2005)]. ASHRAE Standard 55-2004, "Thermal Environmental Conditions for Human Occupancy," specifies conditions in which a specified fraction of the occupants will find the environment thermally acceptable. Thermal comfort occurs in narrow temperature ranges, at low skin moisture levels and with minimal physiological effort of regulation. It is strongly dependent on the levels of activity, physiological and psychological state, nature of clothing as well as the surrounding environment.

Mean Radiant Temperature

Mean Radiant Temperature (MRT) was calculated with the simplified area weighted equation as follows:

$$T_{mr} = T_1A_1 + T_2A_2 + \cdots + T_NA_N/(A_1 + A_2 + \cdots + A_N) \tag{4.1}$$

where:

T_{mr} = mean radiant temperature

T_N = surface temperature of surface N (calculated or measured)

A_N = area of surface N

This is the simplest and least accurate way to calculate MRT, it is a homogeneous steady state area weighted average of the uncontrolled or unconditioned surface temperatures. This method does not reflect the geometric position, posture and facing orientation of the occupant, nor the ceiling height, nor the thermal comfort influence of extraordinary items such as cooled and heated surfaces. Figure 4.14 shows MRT results using Equation 4.1.

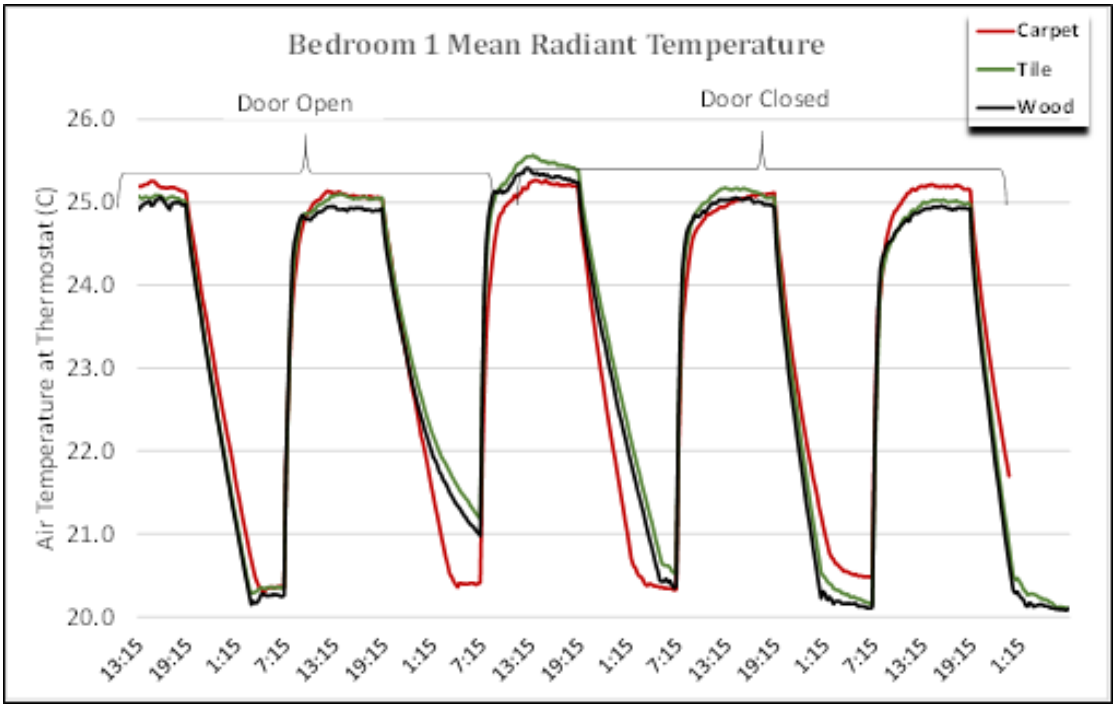

Figure 4.14: Mean radiant temperature experiment 1

Mean radiant temperature can also be measured using a black-globe thermometer, which can be seen in Figure 4.5. The black-globe thermometer consists of a black globe in the centre of which is placed a temperature sensor. The globe can in theory have any diameter, though a diameter of 0.15m is generally recommended to use for calculating mean radiant temperature.

Using the globe to measure the globe temperature (GT), mean radiant temperature (MRT) can be determined using the following equations:

$$MRT = \left[(GT + 273)^4 + \frac{1.1 \times 10^8 \cdot v_a^{0.6}}{\epsilon \cdot D^{0.4}}(GT - T_a)\right]^{1/4} - 273 \tag{4.2}$$

And for standard globe (D = 0.15m, $\epsilon = 0.95$):

$$MRT = \left[(GT + 273)^4 + 2.5 \times 10^8 \cdot v_a^{0.6} \cdot (GT - T_a)\right]^{1/4} - 273 \tag{4.3}$$

where:

MRT = mean radiant temperature, °C

GT = globe temperature, °C

v_a = air velocity at the level of the globe, m/s

ϵ = emissivity of the globe

D = diameter of the globe, m

T_a = air temperature, °C

The globes in the bedrooms are home-made and are of an ellipsoid shape, thus further analysis should be done on how to properly calculate MRT with this shape of globe. At this time, the calculations of MRT in this analysis assumed diameter of 0.15m for the globes. Results of MRT using the black-globe thermometer are seen in Figure 4.15.

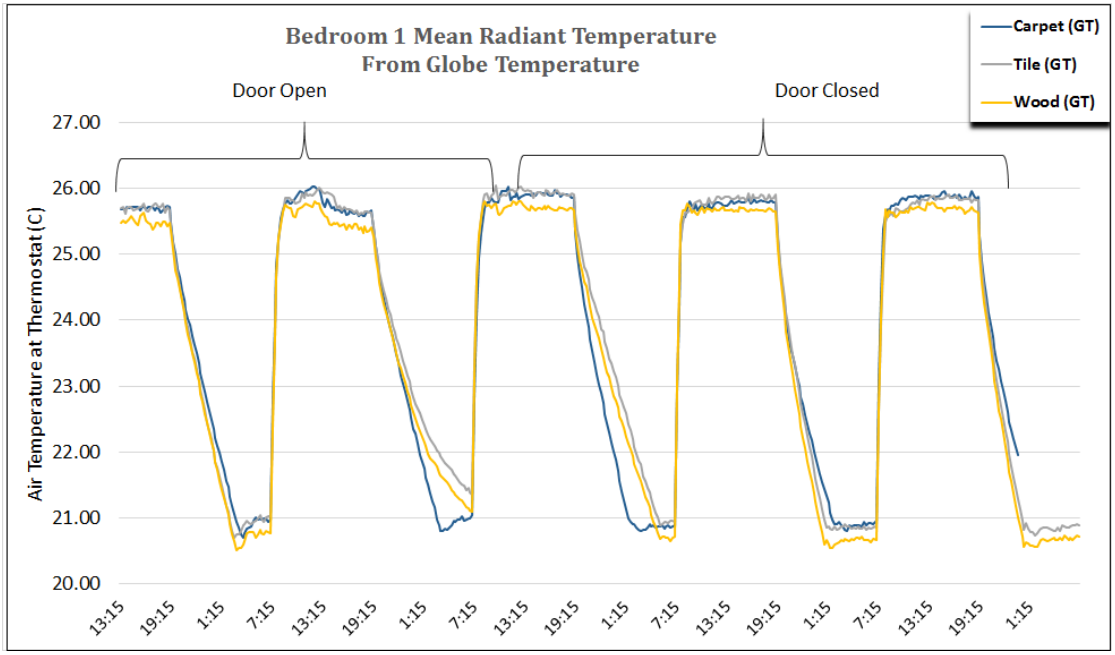

Figure 4.15: Mean radiant temperature experiment 1 (from globe temperature)

Operative Temperature

The operative temperate (T_o) is what humans experience thermally in a space. It is the combined effects of the mean radiant temperature and air temperature. T_o can be mathematically expressed as:

$$T_o = (h_r T_{mr} + h_c T_{db})/(h_r + h_c) \tag{4.4}$$

where:

h_c = convective heat transfer coefficient, $W/(m^2K)$

h_r = linear radiative heat transfer coefficient, $W/(m^2K)$

T_{db} = air (dry bulb) temperature, °C

T_{mr} = mean radiant temperature, °C

The linear radiative heat transfer coefficient can be calculated as:

$$h_r = 4\sigma f_{eff} \left[273 + \frac{(t_r + t_a)}{2}\right]^3 \tag{4.5}$$

where:

h_r = linear radiative heat transfer coefficient, $W/(m^2K)$

f_{eff} = ratio of radiating surface of the human body to its total DuBois surface area AD = 0.71

σ = Stefan-Boltzmann constant = $5.67 \times 10^{-8} W/(m^2K^4)$

The convective heat transfer coefficient for an occupant depends on the relative velocity between the occupant and the surrounding air, as well as the occupant's activity. For this study it was assumed a sedentary occupant with moving air less than 0.23 m/s (typical value measured in the homes), therefore, h_c = 3.1 W/(m2K). Operative temperature results are shown in Figure 4.16.

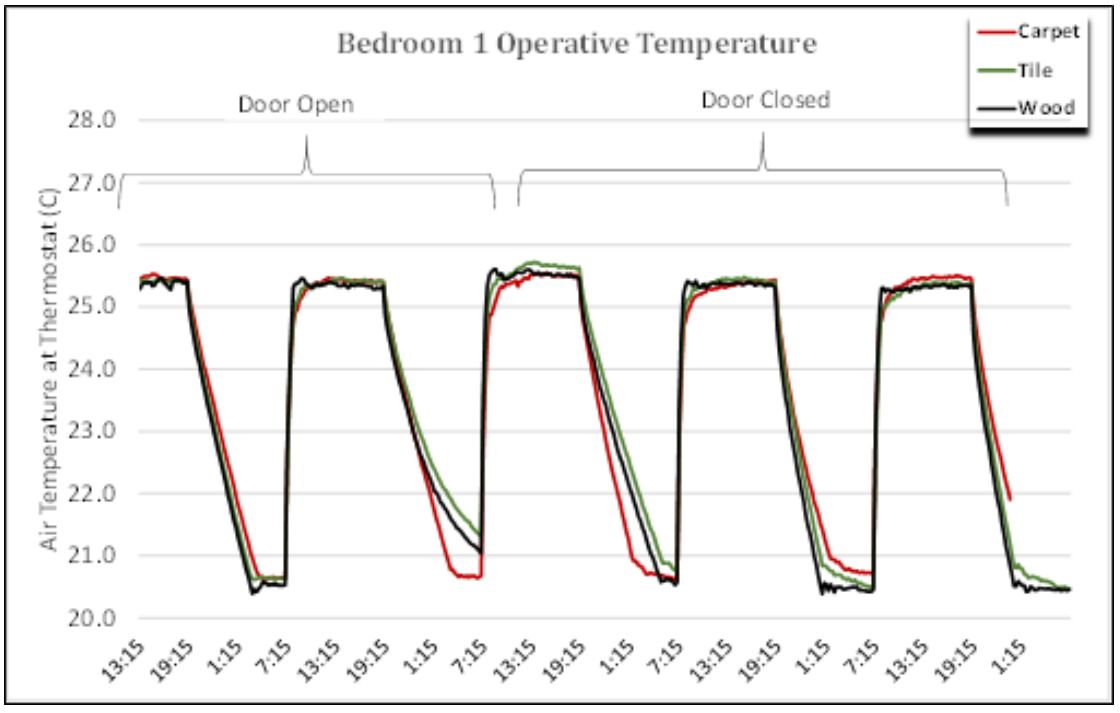

Figure 4.16: Operative temperature experiment 1

Radiant Temperature Asymmetry

The thermal radiation field about the body may be non-uniform due to hot and cold surfaces and direct sunlight. This asymmetry may cause local discomfort and reduce the thermal acceptability of the space. In general, people are more sensitive to asymmetric radiation caused by a warm ceiling than that caused by hot and cold vertical surfaces. Radiant asymmetry is the difference between the plane radiant temperatures in opposite directions. The plane radiant temperature is defined similarly to mean radiant temperature except that it is with respect to a small planar surface element exposed to the thermal radiation from surfaces from one side of that plane. The vertical radiant asymmetry is with plane radiant temperatures in the upward and downward direction. The horizontal radiant asymmetry is the maximum difference between opposite plane radiant temperatures for all horizontal directions. The radiant asymmetry is determined at waist level (0.6m or 24 in.) for a seated person and 1.1m (43in) for a standing occupant. The maximum vertical asymmetry of 3.8°C occurred for a seated person in a carpeted bedroom. This value is nearing the maximum allowable value of 5°C for a scenario of a warm ceiling. Figure 4.17 shows values of plane radiant asymmetry calculated for the duration of all experiments, and Table 4.3 shows maximum values for all scenarios tested.

Table 4.3: Radiant asymmetry measured extremes experiment 1

	Carpet Floor		**Tile Floor**		**Wood Floor**	
	Seated	Standing	Seated	Standing	Seated	Standing
Max Vertical Asymmetry (°C)	3.8	2.5	2.3	1.3	2.2	2.0
Max Horizontal Asymmetry (°C)	1.3	1.4	1.5	1.7	1.7	1.9

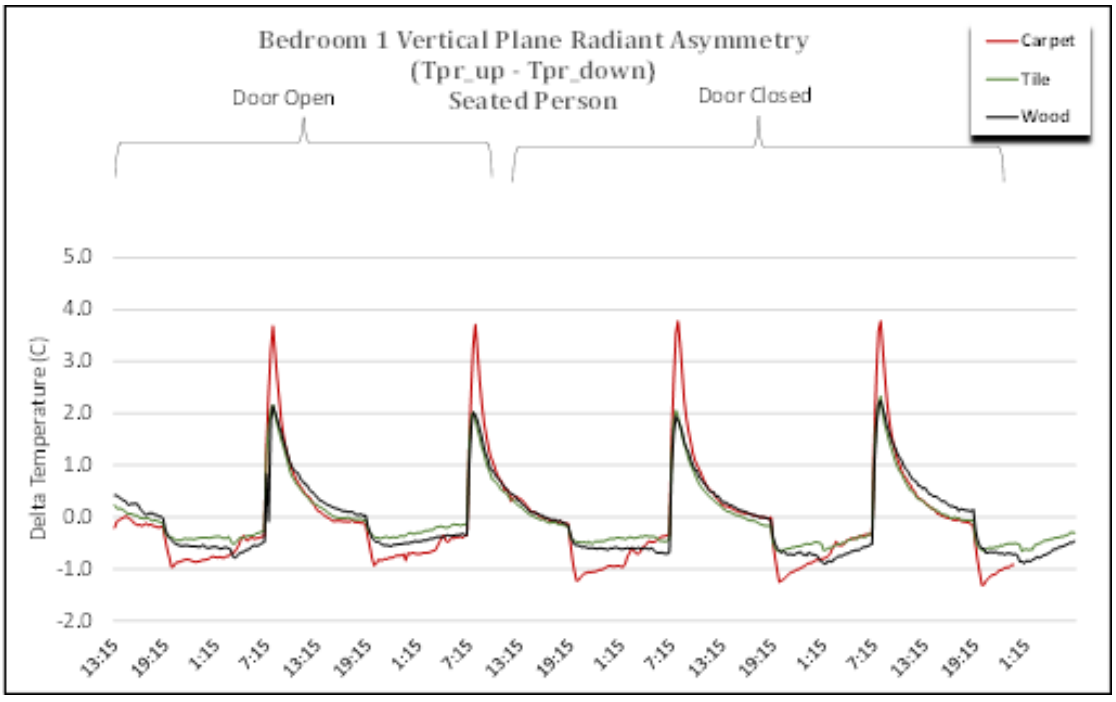

Figure 4.17: Bedroom 1 vertical radiant temperature asymmetry (seated person)

Air Temperature Vertical Stratification

Thermal stratification that results in the air temperature at the head level being warmer than at the angle level may cause thermal discomfort. The allowable vertical air temperature difference between head and ankles is less than 3°C.

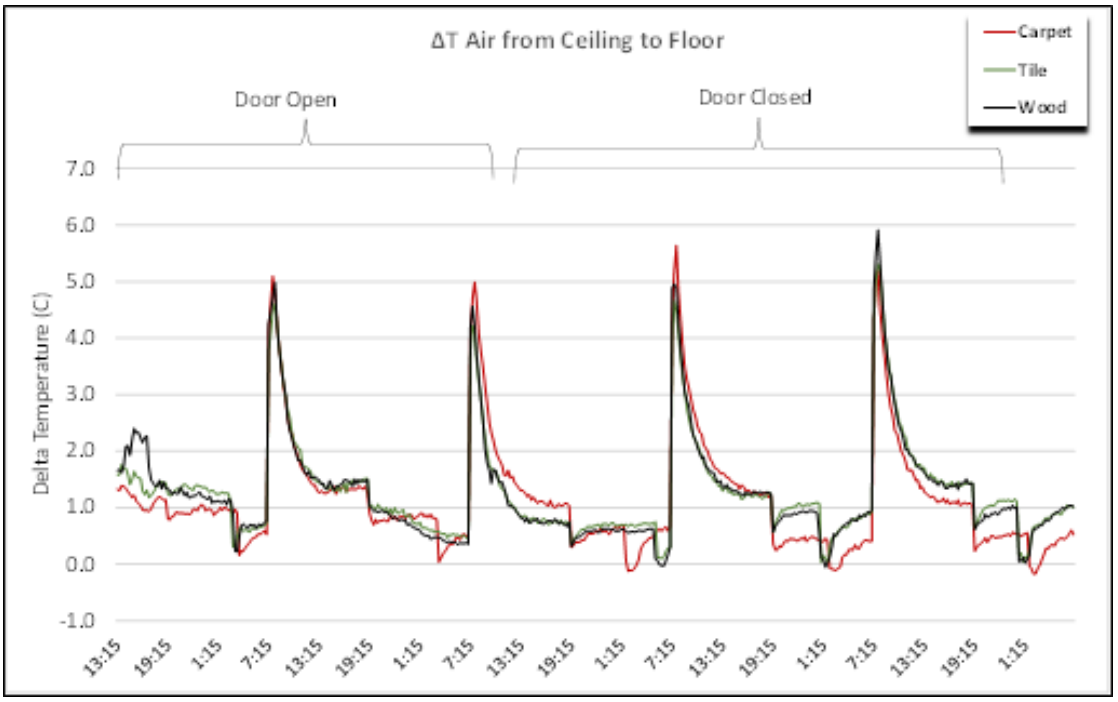

Figure 4.18: Delta air temperature between ceiling and floor

In experiment 1 an air temperature difference in the vertical direction of 5°C was observed, therefore there could be issues with occupant satisfaction, especially in the morning when daytime temperature step up begins. Figure 4.18 shows vertical air gradient during the experiments and Table 4.4 displays the maximum gradients for the three floor covering cases. At Δ T = 5°C, 30% of occupants are dissatisfied with indoor environment conditions.

Table 4.4: Room air temperature properties experiment 1

	Carpet	**Tile**	**Wood**
Delta T Max - Vertical (°C)	4.5	4.3	4.9
Peak Air Temp at ankle (°C)	25.3	25.1	25.3
Peak Air Temp at head (°C)	27.1	27.1	27.7

Floor Surface Temperature

Occupants may feel uncomfortable due to contact with floor surfaces that are too warm or too cool. The temperature of the floor, rather than the material of the floor covering, is the most important factor for foot thermal comfort for people wearing shoes. The acceptable range of floor temperature is 19-29°C. From the Figure 4.19 it can be seen that for all three types of floor covering the surface temperature is always in the acceptable range for the days during the experiment.

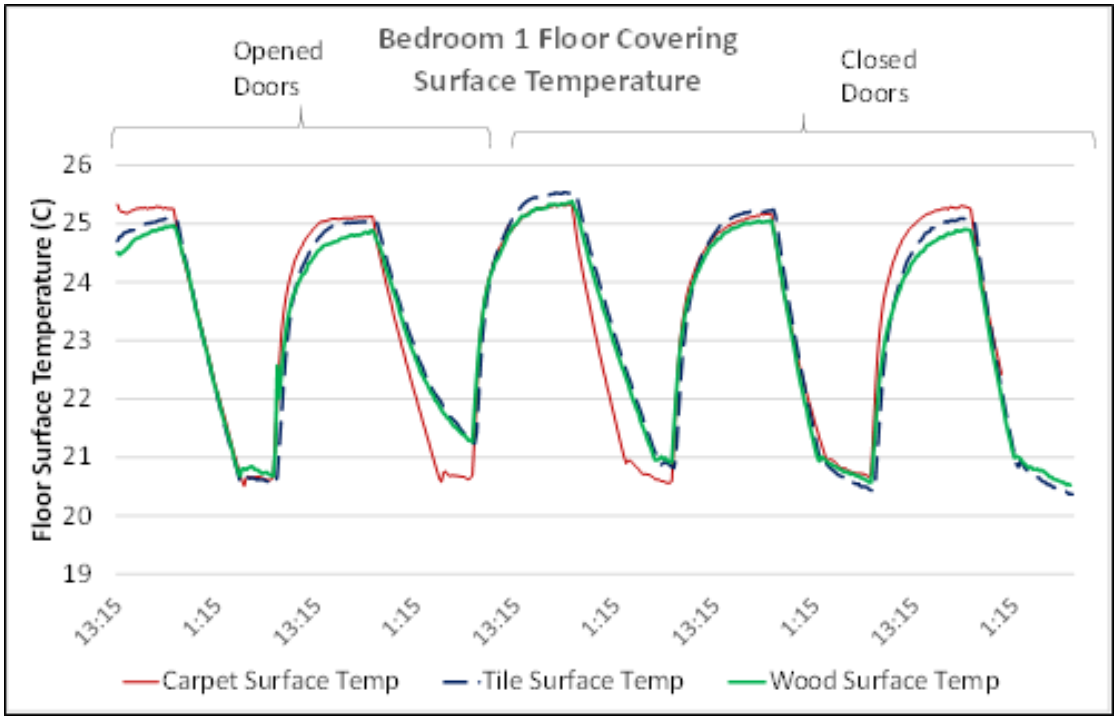

Figure 4.19: Bedroom 1 floor covering surface temperature

4.3 Experiment 2 Description - Ramping Profiles

Between experiments 1 and 2, the thermostats in the twin homes were switched from Ouellet standard programmable thermostats (www.ouellet.com) to Sinopé communicating thermostats (www.sinopetech.com). The Sinopé thermostats were

altered to have minimum increments at 1 minute intervals and resolution of 0.1°C. Standard Sinopé communicating thermostats have resolution of 0.5°C and allow six temperature set point changes per day. Experiment 2 lasted a total of seven days from Nov. 12 to 18, 2014. The objectives of experiment 2 were to implement ramping profiles in a real building to validate developed models. One house had wood flooring and the other house had carpet flooring, tile was not used in experiment 2. Figure 4.20 shows the temperature profile for the seven days of experiments. The first two days were kept at a constant temperature of 21°C. Starting on the third day, two temperature changes using different ramping lengths between 21°C and 26°C were implemented. Ramping profiles provide a simple yet effective way to reduce the peak load when compared to a temperature step change. Ramping lengths of 1, 2 and 3 hours were implemented in the experiments to determine their impact on peak demand reduction due to space heating.

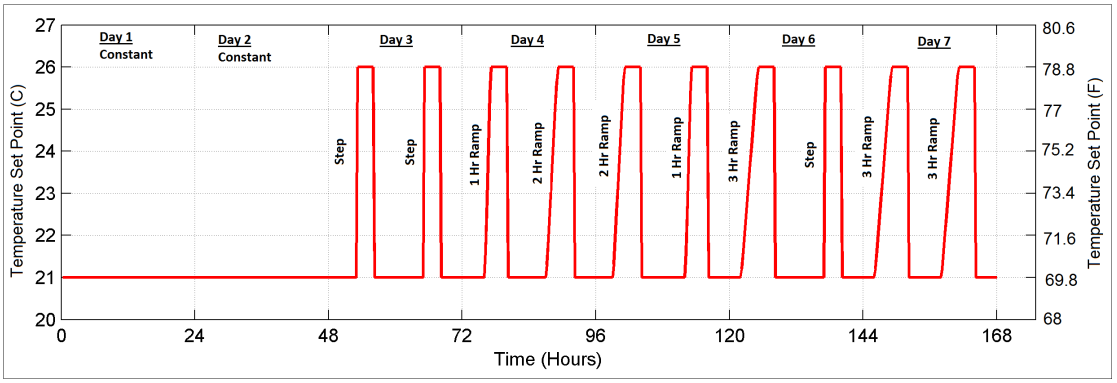

Figure 4.20: Experiment 2 temperature profile

4.3.1 Experiment 2 Results

Figure 4.21 displays the heating power and air temperature of bedroom 1 with wood floors. We see clearly the peak power is reduced with ramping profiles when compare to the step changes. Table 4.5 shows the corresponding peak values for each step or ramp temperature change during the experiment.

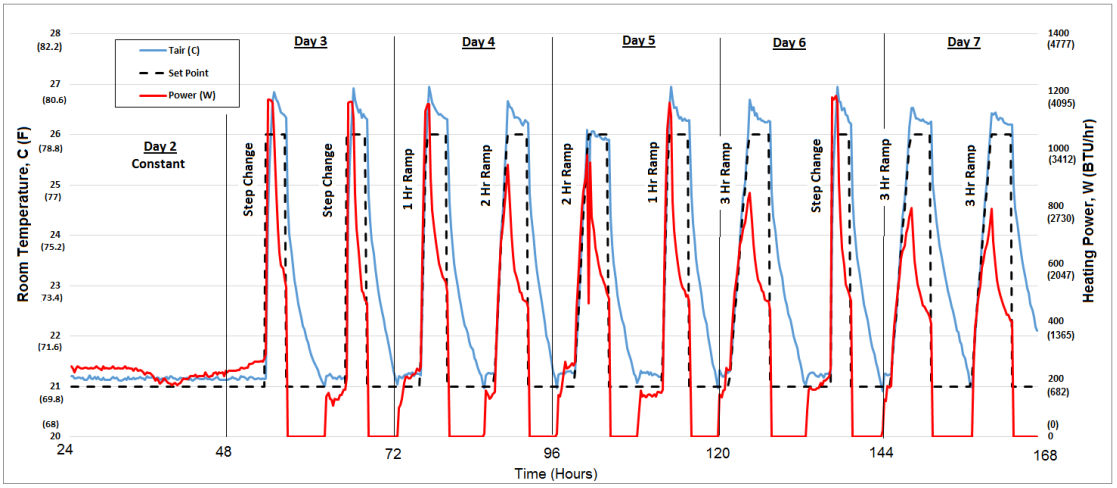

Figure 4.21: Experiment 2 results - bedroom 1 wood floors

Table 4.5: Experiment 2 peak power values - bedroom 1 wood floors

	Day 2	Day 3	Day 4	Day 5	Day 6	Day 7
Peak 1 [W] (Reduction)	—	1172 (1%)	1156 (2%)	980 (17%)	848 (28%)	796 (33%)
Peak 2 [W] (Reduction)	—	1164 (1%)	944 (20%)	1160 (2%)	1184 (0%)	792 (33%)

Weather conditions for the duration of the experiment 2 are shown in Figure 4.22. As seen, outdoor air temperature was relatively mild, therefore exaggerated set point values were used to obtain a larger temperature difference between indoor and outdoor environments.

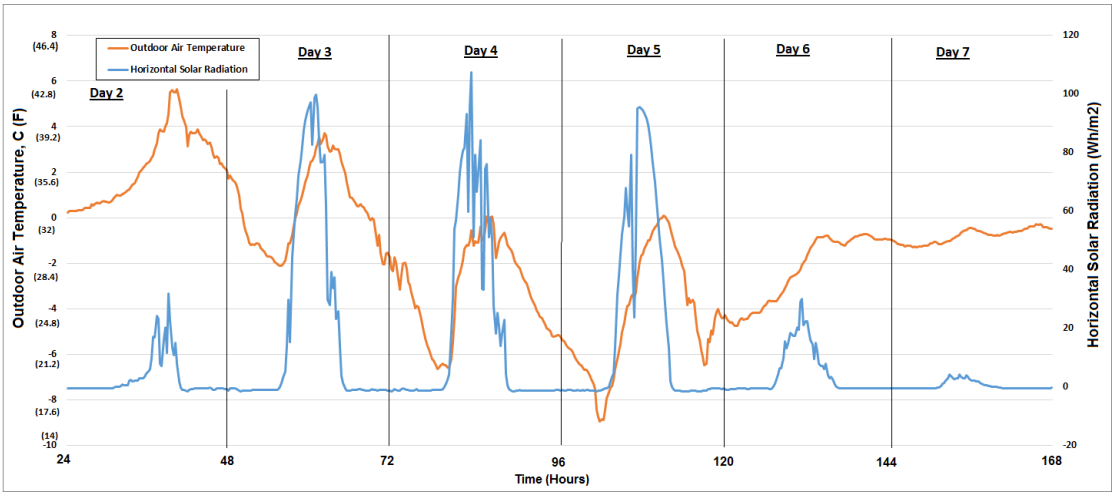

Figure 4.22: Experiment 2 weather

Figure 4.23 shows the air temperatures of bedroom one for each house (carpet floor vs. wood floor). We see that the air temperature in the carpeted room is slighting higher (possibly due to uncalibrated thermocouples) but tends to decay faster when there is set point temperature step down.

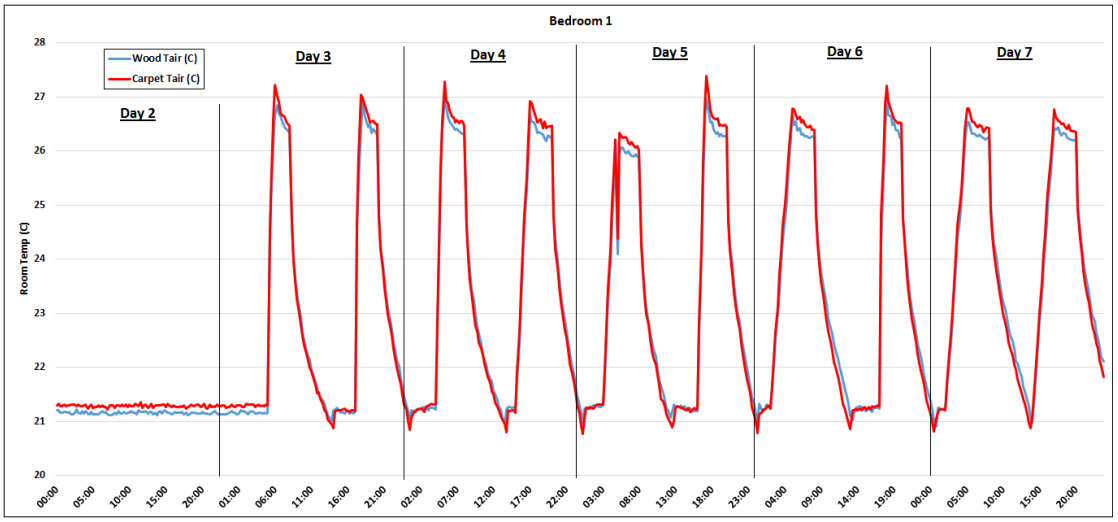

Figure 4.23: Experiment 2 air temperature

Focusing on day 6 of experiment 2, shown in Figure 29, the measured air temperature in bedroom 1 with wood floors compared the Temperature set point profile. The air temperature always heats up higher to the set point when there is an increase in the set point values (from 21°C to 26°C). This phenomena is difficult to capture in a model since the reason for this could simply be how the thermostat is designed. The sensor used to measure air temperature is located next to the thermostat, typically located at the entrance of each room.

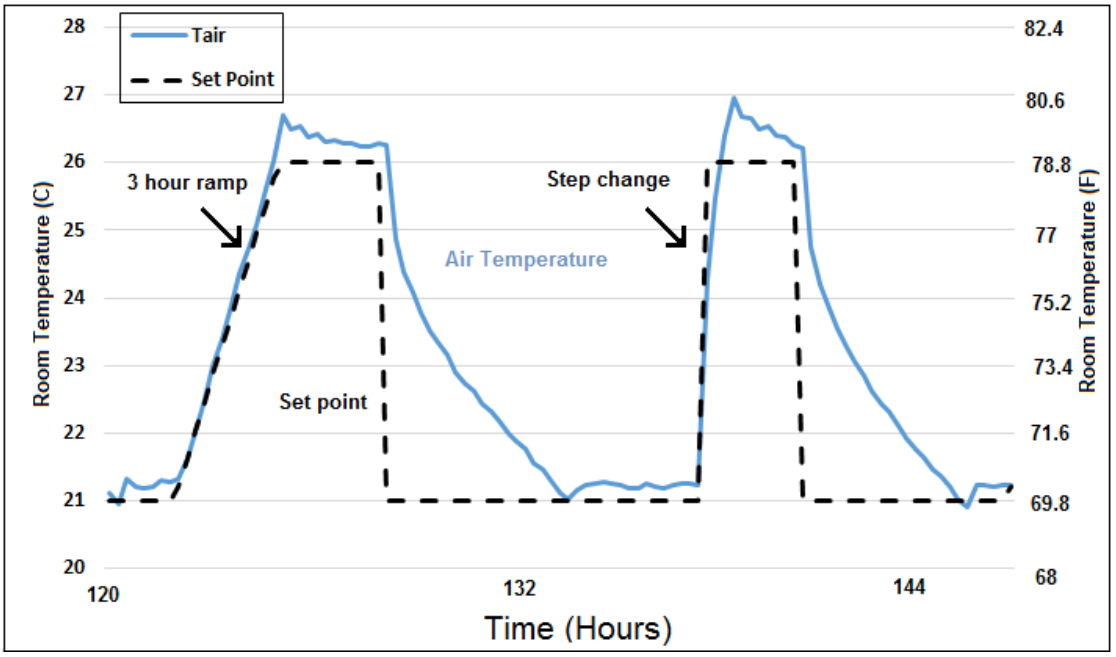

Figure 4.24: Experiment 2 air temperature - wood floors

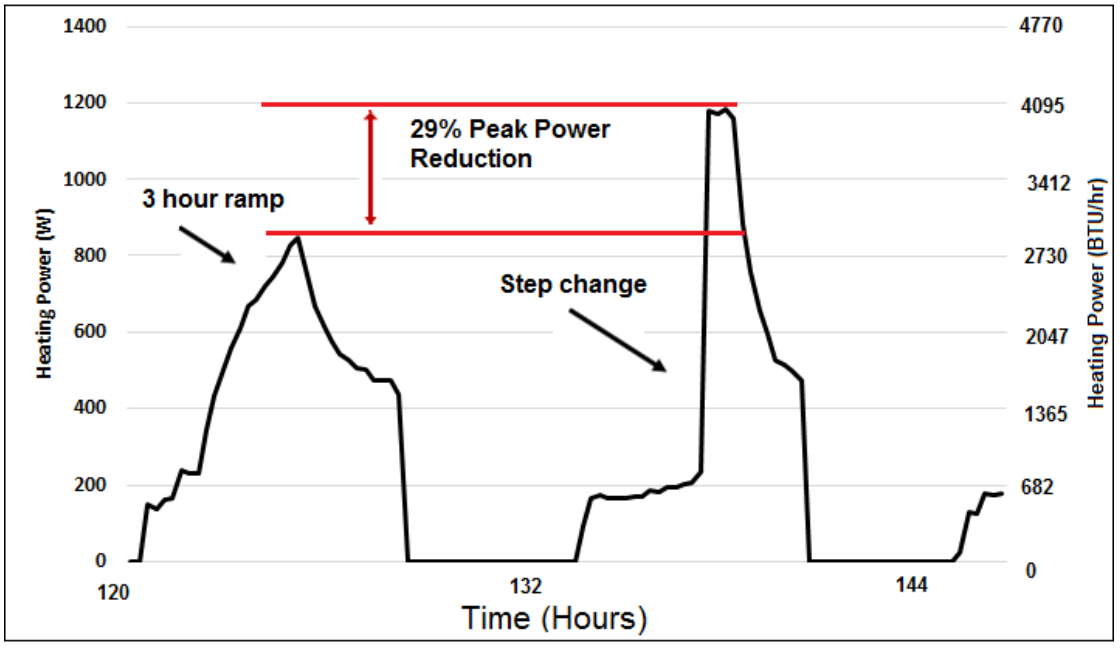

Figure 4.25: Experiment 2 peak power reduction

Figure 4.25 shows that on day 6 the peak heating for the three hour ramp is 29% less than the peak for a temperature step change of 21°C to 26°C. This is a significant reduction of peak heating power from easily implemented and only slightly more advanced temperature set point profile. Climate conditions were

fairly constant during day 6 of the experiments and was slightly colder during the 3 hour ramping period despite the fact that in the afternoon solar radiation is higher too.

Chapter 5

Thermal Modelling Description and Results

The one dimensional heat transfer process for a wall is governed by the following parabolic, diffusion-type partial differential equation:

$$\frac{\partial T}{\partial t} = \alpha \frac{\partial^2 T}{\partial x^2} \tag{5.1}$$

where thermal diffusivity $\alpha = k/(\rho c)$, k is thermal conductivity, ρ is the density and c is the thermal capacitance.

In explicit finite difference schemes, the temperature at time n+1 depends explicitly on the temperature at time n. The explicit finite difference discretization of equation 5.1 is:

$$\frac{T_i^{n+1} - T_i^n}{\Delta t} = \alpha \frac{T_{i+1}^n - 2T_i^n + T_{i-1}^n}{\Delta x^2} \tag{5.2}$$

This assumes α and Δx^2 are the same on all sides of node i.

This can be rearranged in the following manner (with all quantities at time n+1 on the left-hand-side and quantities at time n on the right-hand-side):

$$T_i^{n+1} = T_i^n + \alpha \Delta t \frac{T_{i+1}^n - 2T_i^n + T_{i-1}^n}{\Delta x^2} \tag{5.3}$$

Since we know T_{i+1}^n , T_i^n and T_{i-1}^n , we can compute T_i^{n+1}. This is schematically shown on Figure 5.1. The main advantage of explicit finite difference methods is that they are relatively simple and computationally fast. However, the main drawback is that stable solutions are obtained only when:

$$0 < \frac{\alpha \Delta t}{\Delta x^2} < 0.5 \tag{5.4}$$

If this condition is not satisfied, the solution becomes unstable and starts to wildly oscillate.

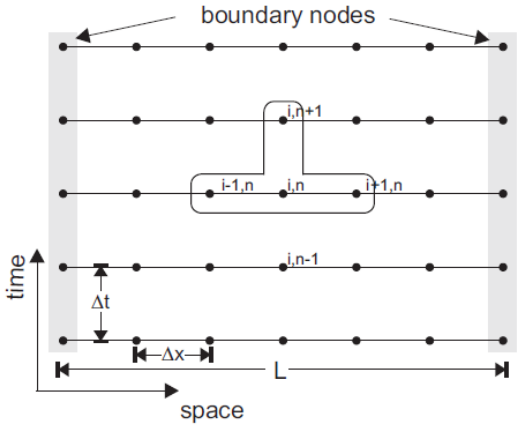

Figure 5.1: Explicit finite difference discretization

The boundary conditions of a wall shown in Figure 5.2 will include convective heat transfer, absorbed solar radiation (heat source) and long-wave radiations exchange with other surfaces. Boundary conditions (x = 0 corresponds to exterior surface) are:

(i) At x = 0

$$q = -k\frac{\partial T}{\partial x} = G + h_o\,(T_o - T_1) = h_o\,(T_{eo} - T_1) \tag{5.5}$$

where sol-air temperature is:

$$T_{eo} = T_o + \alpha_s G/h_o \tag{5.6}$$

(ii) At x = L (thickness of wall)

$$q = h_i\,(T_2 - T_r) \tag{5.7}$$

where thermal diffusivity $\alpha = k/(\rho c)$, k is thermal conductivity, α_s is solar absorptance of the wall, q is the heat flux, h is the heat transfer coefficient and G is solar radiation.

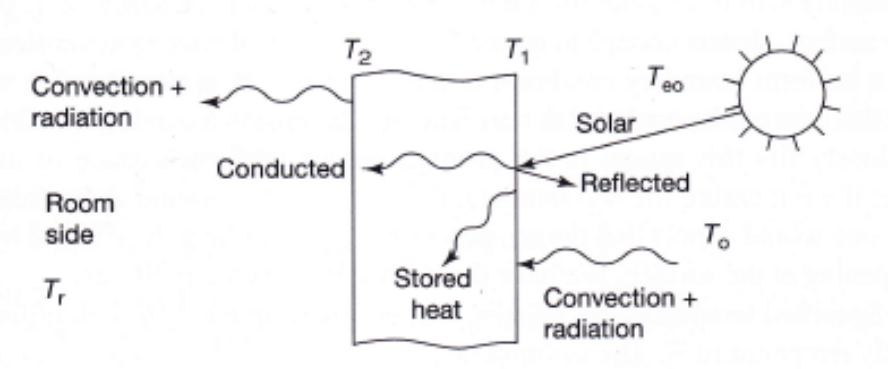

Figure 5.2: Heat exchange mechanisms for a layer of thermal mass (Athienitis & Santamouris, 2002)

One dimensional conduction through the walls is generally assumed, as well as uniform irradiation of their surfaces by solar radiation (Athienitis and Santmouris 2002). However, when thermal bridges are present, such as at corners in rooms

and for heat loss through the floor, two-dimensional or three-dimensional analysis is required.

Transient thermal analysis of walls or rooms may be performed with the following objectives:

1. Peak heating or cooling load calculations

2. Calculation of dynamic temperature variation within walls, including solar effects, room temperatures swings, and condensation on wall interior surfaces.

For a multi-layered wall, an energy balance is applied at each node at regular time intervals to obtain the temperature of the nodes as a function of time. These equations may be solved with the implicit method as a set of simultaneous equations or with the explicit method in which we march forward in time from a set of initial conditions.

Wall transient thermal response analysis with finite difference techniques may generally provide a more accurate estimation of temperatures and heat flows owing to the capability to model non-linear effects such as convection and radiation. One disadvantage is that the initial conditions are usually unknown, thus, the simulation must be repeated until a steady periodic response is obtained.

The explicit finite difference method is particularly suitable for modelling of non-linear heat diffusion problems such as heat transfer through a wall. It can easily accommodate non-linear heat transfer coefficients and control actions.

In the transient one-dimensional finite difference thermal network method, each wall layer is represented by one or more sub-layers. Each sub-layer is represented by a node with a thermal capacitance C connected to two thermal resistances, R, each equal to half the R-Value of the layer, forming a T-section. For a multi-layered wall, an energy balance is applied at each node at regular time intervals to obtain the temperature of the nodes as a function of time. These

equations may be solved with implicit method as a set of simultaneous equations or with the explicit method which we march forward in time from a set of initial conditions.

The general form of the explicit finite difference formulation corresponding to node i and time interval n is:

$$T(i,n+1) = \left(\frac{\Delta t}{C_i}\right) \cdot \left(q_i + \sum_j \frac{T(j,n) - T(i,n)}{R(i,j)}\right) + T(i,n) \tag{5.8}$$

Where $n+1$ indicates the next time step, j is all nodes connected to i and q is a heat sources at node i. When the thermal capacitance C can be negligible the equation is as follows:

$$T(i,n+1) = \frac{q_i + \sum_j \frac{T(j,n)-T(i,n)}{R(i,j)}}{\sum_j \frac{1}{R(i,j)}} \tag{5.9}$$

In this investigation, heating control was approximated with proportional-integral control. In proportional-integral (PI) control, which is most common in building control, the auxiliary heating is equal to the error between the set point temperature and the actual room temperature multiplied by a proportional constant plus the magnitude of the error and the duration of the error multiplied by an integral constant. The relationship can be expressed as:

$$q_{aux_n} = K_p e_n + K_i \sum_{n=1}^{p} (e_n \cdot \Delta t) \tag{5.10}$$

where:

K_p = proportional control constant

K_i = integral control constant

Δt = time step

and

$$e_n = (T_{sp})_n - (T_{air})_n \tag{5.11}$$

where:

T_{sp} = air temperature set point

T_{air} = actual measured air temperature

5.1 Thermal Modelling of EHBE North Zone

5.1.1 Model Resolution

Using the explicit finite difference method, several thermal models of varying resolution were created for a north zone in the house to study a simple modelling approach. Resistance-capacitance (RC) circuit thermal models of varying levels of resolution were developed for a zone and compared to the physical measurements in order to study how model resolution has an effect on model accuracy. The model detail is different in modelling of heat conduction, but for radiation and convection the models are the same. Radiative and convective heat transfer coefficients have been combined for this study. Simple models are not just an oversimplification of a system: they are an acutely understood selection of relevant system information. The development and application of simple models require a good understanding of all phenomena involved, a coherent choice of significant parameters and variables, and much care and thinking when analyzing and interpreting the data (B. Lachal, 1992).

For a vertical surface, the correlation for the convective heat transfer coefficient is as follows (McAdams, 1959):

$$h_c = 1.13 \cdot |T_{surface} - T_{air}|^{1/3} \tag{5.12}$$

For a hot ceiling, the correlation for convective heat transfer is:

$$h_c = 0.59 \cdot \left(\frac{|T_{ceiling} - T_{air}|}{x} \right)^{0.25} \tag{5.13}$$

where x is the characteristic dimension.

For a cold floor, the correlation for convective heat transfer is:

$$h_c = 1.52 \cdot |T_{floor} - T_{air}|^{1/3} \tag{5.14}$$

While the correlation for radiative heat transfer is:

$$h_r = \varepsilon \cdot \sigma \cdot 4 \left(\frac{T_{surface} + 273 + T_{air} + 273}{2} \right)^3 \tag{5.15}$$

where:

ε = emissivity of walls

σ = Stefan-Boltzman constant ($5.6703 \times 10^{-8} W m^{-2} K^{-4}$)

and

$$Tm = \left(\frac{T_{surface} + 273 + T_{air} + 273}{2} \right) \tag{5.16}$$

where $4Tm^3$ is a linearization factor for radiation heat transfer.

Comparisons were done between models with calculated heat transfer coefficients at each time step from the above equations and models with averaged constant values and results are shown and discussed later in this chapter.

Three Capacitance Model

The simplest model created for a zone is shown in Figure 5.3 and consists of three capacitances. There is one capacitance for the effective interior capacitance, one for the interior partitions and floor, while the third capacitance is for the walls and roof exposed to the exterior environment. Table 5.2 displays the capacitance and resistance values for the third order RC circuit.

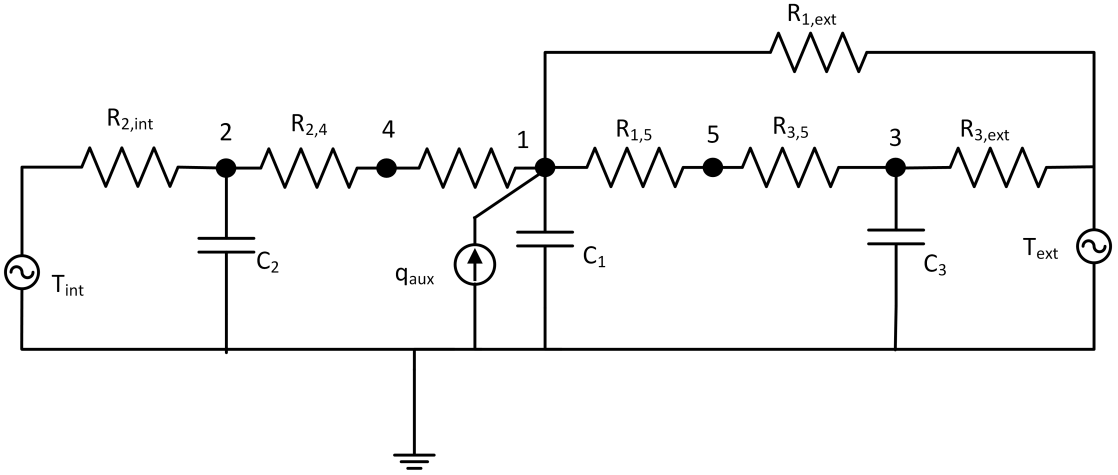

Figure 5.3: Third order equivalent RC network - combined surfaces

Table 5.1: Node descriptions: third order model - combined surfaces

Node	Description
1	air node
2	interior walls node
3	exterior walls node
4	interior surfaces node
5	exterior surfaces node

Table 5.2: Parameter values: third order model - combined surfaces

Capacitances (J/K)		Resistances (K/W)	
C_1=	159,667	$R_{1,4}$ =	0.0045
C_2=	862,235	$R_{1,5}$ =	0.0050
C_3=	287,847	$R_{1,ext}$ =	0.2200
		$R_{2,4}$ =	0.0018
		$R_{2,int}$ =	0.0280
		$R_{3,5}$ =	0.0013
		$R_{3,ext}$ =	0.1453

Five Capacitance Model

The next thermal model is a five capacitance RC circuit and is shown in Figure 5.4. The walls, ceiling, and floor capacitances have been discretized into two capacitances with circuit parameter values shown in Table 5.4.

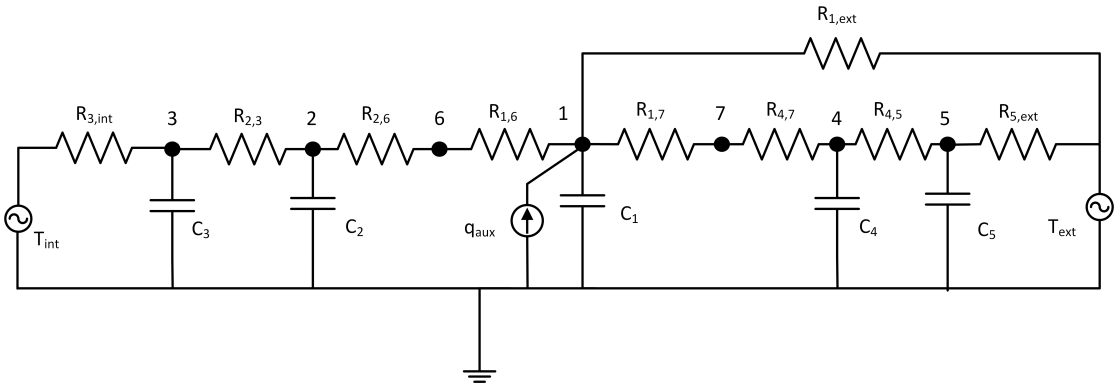

Figure 5.4: Fifth order equivalent RC network - combined surfaces

Table 5.3: Node descriptions: fifth order model - combined surfaces

Node	Description
1	air node
2,4	interior walls nodes
3,5	exterior walls nodes
6	interior surfaces node
7	exterior surfaces node

Table 5.4: Parameter values: fifth order model - combined surfaces

Capacitances (J/K)		Resistances (K/W)	
C_1=	159,667	$R_{1,6}$=	0.0052
C_2=	433,178	$R_{1,7}$=	0.0053
C_3=	433,178	$R_{1,ext}$=	0.2202
C_4=	147,323	$R_{2,3}$=	0.0012
C_5=	147,323	$R_{2,6}$=	0.0012
		$R_{3,int}$=	0.0257
		$R_{4,5}$=	8.7947 x 10^{-4}
		$R_{4,7}$=	8.7947 x 10^{-4}
		$R_{5,ext}$=	0.1444

Nine Capacitance Model

The nine capacitance RC circuit model is shown in Figure 5.5. The surface capacitances of the three capacitance model have been discretized into four capacitances each and the circuit parameter values are shown in Table 5.6. As capacitance values of a wall layer are increasingly discretized, the model theoretically becomes closer to physical reality, with the assumption of good model calibration

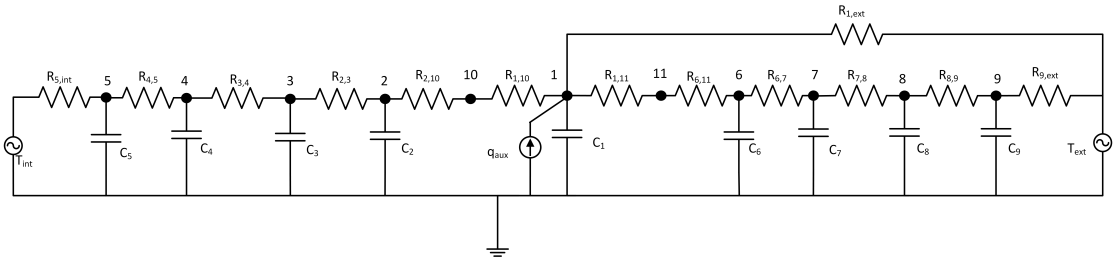

Figure 5.5: Ninth order equivalent RC network - combined surfaces

Table 5.5: Node descriptions: ninth order model - combined surfaces

Node	Description
1	air node
2,3,4,5	interior walls nodes
6,7,8,9	exterior walls nodes
10	interior surfaces node
11	exterior surfaces node

Table 5.6: Parameter values: ninth order model - combined surfaces

Capacitances (J/K)		**Resistances (K/W)**	
$C_1 =$	119,750	$R_{1,10} =$	0.0051
$C_2 =$	216,589	$R_{1,11} =$	0.0050
$C_3 =$	216,589	$R_{1,ext} =$	0.2202
$C_4 =$	216,589	$R_{2,3} =$	7.2024×10^{-4}
$C_5 =$	216,589	$R_{2,10} =$	7.2024×10^{-4}
$C_6 =$	73,661	$R_{3,4} =$	7.2024×10^{-4}
$C_7 =$	73,661	$R_{4,5} =$	7.2024×10^{-4}
$C_8 =$	73,661	$R_{5,int} =$	0.0249
$C_9 =$	73,661	$R_{6,7} =$	5.277×10^{-4}
		$R_{6,11} =$	5.277×10^{-4}
		$R_{7,8} =$	5.277×10^{-4}
		$R_{8,9} =$	5.277×10^{-4}
		$R_{9,ext} =$	0.1437

Seven Capacitance Models

There are two models consisting of seven capacitances. The first seven capacitance model shown in Figure 5.6 is similar to the five capacitance model except now the floor has been separated on to its own. Interior partitions are represented as two capacitances, the outer walls and ceiling are represented as two capacitances and the floor connected to the lower level is represented as two capacitances. Table 5.8 displays the parameter values of the RC circuit.

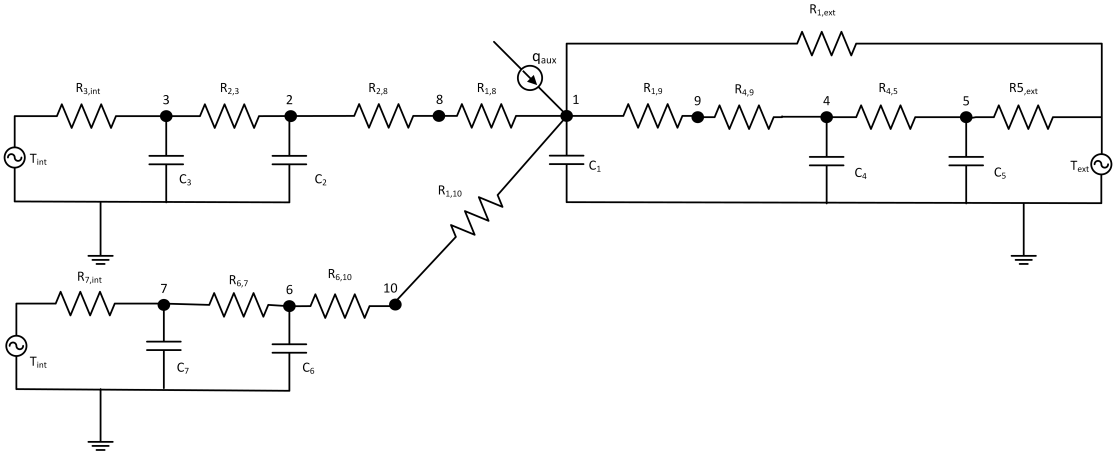

Figure 5.6: Seventh order equivalent RC network - separated floor

Table 5.7: Node descriptions: seventh order model - separated floor

Node	Description
1	air node
2,3	interior walls nodes
4,5	exterior walls nodes
6,7	floor nodes
8	interior surfaces node
9	exterior surfaces node
10	floor surface node

Table 5.8: Parameter values: seventh order model - separated floor

Capacitances (J/K)		**Resistances (K/W)**	
C_1=	279,417	$R_{1,8}$=	0.0091
C_2=	89,305	$R_{1,9}$=	0.0053
C_3=	89,305	$R_{1,10}$=	0.0129
C_4=	147,323	$R_{1,ext}$=	0.2202
C_5=	147,323	$R_{2,3}$=	0.0022
C_6=	343,873	$R_{2,8}$=	0.0011
C_7=	343,873	$R_{3,int}$=	0.0382
		$R_{4,5}$=	0.0013
		$R_{4,9}$=	6.5960 x 10^{-4}
		$R_{5,ext}$=	0.1442
		$R_{6,7}$=	0.0104
		$R_{6,10}$=	0.0052
		$R_{7,int}$=	0.0778

The second of the seven capacitance models is one where all four walls, floor,

and ceiling are each represented by their own capacitance and the seventh capacitance is the effective interior air capacitance. The RC network is shown in Figure 5.7 and parameter values are shown in Table 5.10.

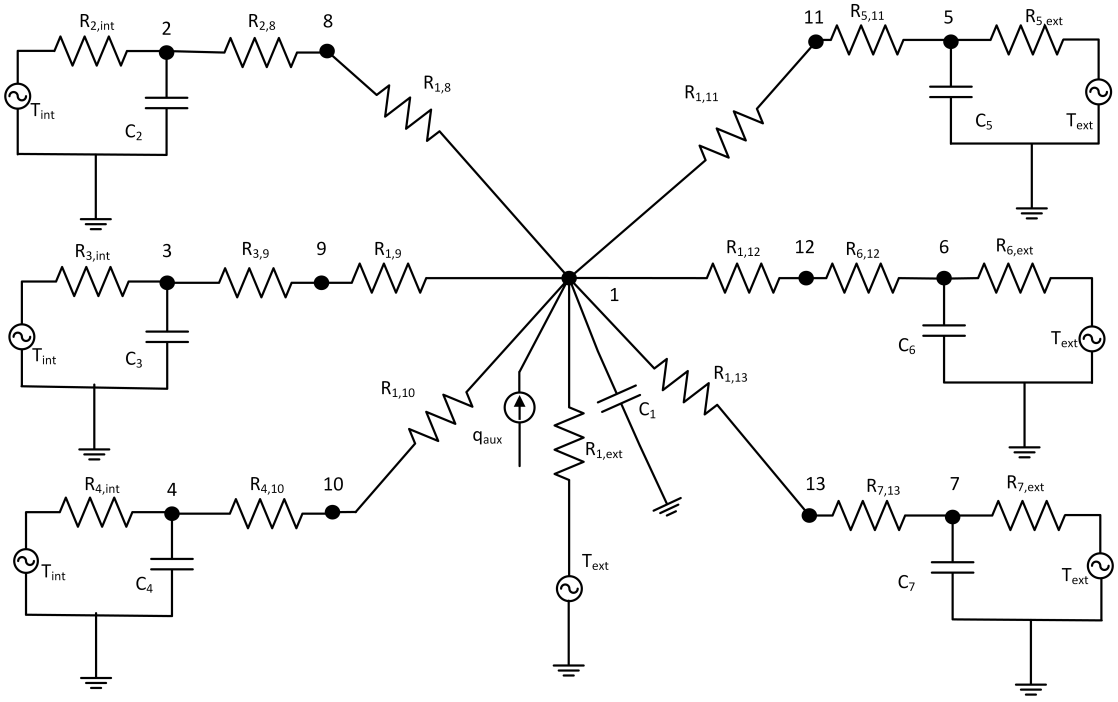

Figure 5.7: Seventh order equivalent RC network - separated surfaces

Table 5.9: Node descriptions: seventh order model - separated surfaces

Node	Description
1	air node
2,3,4	interior walls nodes
5,6,7	exterior walls nodes
8,9,10	interior surfaces node
11,12,13	exterior surfaces node

Table 5.10: Parameter values: seventh order model - separated surfaces

Capacitances (J/K)		**Resistances (K/W)**	
C_1=	279,417	$R_{1,8}$=	0.0210
C_2=	76,775	$R_{1,9}$=	0.0154
C_3=	97,713	$R_{1,10}$=	0.0116
C_4=	687,747	$R_{1,11}$=	0.0241
C_5=	60,582	$R_{1,12}$=	0.0149
C_6=	97,713	$R_{1,13}$=	0.0109
C_7=	129,552	$R_{1,ext}$=	0.2463
		$R_{2,8}$=	0.0048
		$R_{2,int}$=	y0.1010
		$R_{3,9}$=	0.0038
		$R_{3,int}$=	0.0793
		$R_{4,10}$=	0.0104
		$R_{4,int}$=	0.0798
		$R_{5,11}$=	0.0061
		$R_{5,ext}$=	0.6651
		$R_{6,12}$=	0.0038
		$R_{6,ext}$=	0.4123
		$R_{7,13}$=	0.0029
		$R_{7,ext}$=	0.3623

Thirteen Capacitance Model

Lastly, the most detailed thermal network is shown in Figure 5.8 and consists of 13 capacitances. Each surface is represented with two capacitances and the 13th

capacitance is the effective interior air capacitance. Table 5.8 shows parameter values for the 13 capacitance RC thermal network. The thirteen capacitance model was chosen as the most detailed for a few reasons. First, geometrically the walls, ceiling, floor and windows are individually representated in the model. Second, due relatively to low thermal inertia of the zone, two capacitances were chosen for each surface. Lastly, since the zone is heated by convection and the windows are covered, radiative exchanges are assumed not significant factors and therefore the heat transfer coefficients were combined to effective values.

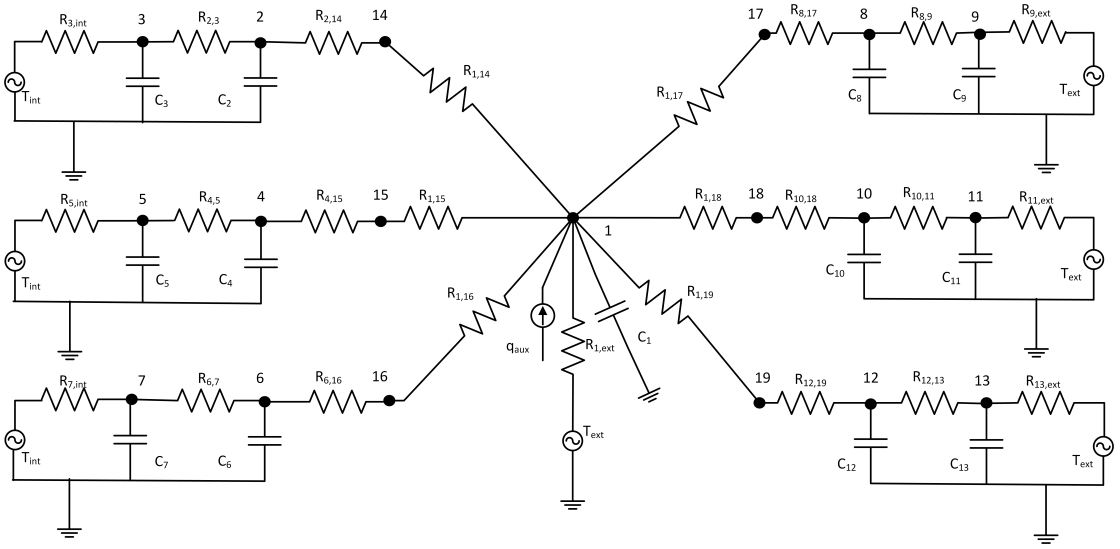

Figure 5.8: Thirteenth order equivalent RC network - separated surfaces

Table 5.11: Node descriptions: Thirteenth order equivalent RC network - separated surfaces

Node	Description
1	air node
2,3,4,5,6,7	interior walls nodes
8,9,10,11,12,13	exterior walls nodes
14,15,16	interior surfaces node
17,18,19	exterior surfaces node

Table 5.12: Parameter values: thirteenth order equivalent RC network - separated surfaces

Capacitances (J/K)		**Resistances (K/W)**		**Resistances (K/W)**	
C_1=	279,417	$R_{1,14}$=	0.0206	$R_{6,7}$=	0.0070
C_2=	38,387	$R_{1,15}$=	0.0154	$R_{6,16}$=	0.0070
C_3=	38,387	$R_{1,16}$=	0.0116	$R_{7,int}$=	0.0763
C_4=	48,856	$R_{1,17}$=	0.0241	$R_{8,9}$=	0.0041
C_5=	48,856	$R_{1,18}$=	0.0149	$R_{8,17}$=	0.0041
C_6=	343,873	$R_{1,19}$=	0.0109	$R_{9,ext}$=	0.6630
C_7=	343,873	$R_{1,ext}$=	0.2463	$R_{10,11}$=	0.0025
C_8=	30,291	$R_{2,3}$=	0.0032	$R_{10,18}$=	0.0025
C_9=	30,291	$R_{2,14}$=	0.0032	$R_{11,ext}$=	0.4111
C_{10}=	48,856	$R_{3,int}$=	0.0993	$R_{12,13}$=	0.0019
C_{11}=	48,856	$R_{4,5}$=	0.0025	$R_{12,19}$=	0.0019
C_{12}=	64,776	$R_{4,15}$=	0.0025	$R_{13,ext}$=	0.3614
C_{13}=	64,776	$R_{5,int}$=	0.0781		

5.1.2 Thermal Model Verification

The statistical indices of coefficient of variation of the root-mean-square error (CV-RSME) and normalized mean bias error (NMBE) were used for the model verification process. ASHRAE Guideline 14 (Gillespie et al., 2002) suggests that a maximum CV-RMSE of 15% and NMBE of 5% on a monthly basis, or 30% and 10%, respectively on an hourly basis ensures a calibrated model when the whole building energy use is compared. There are no known guidelines for sub-hourly or sub-whole building energy use, thus for this study, hourly guidelines were followed.

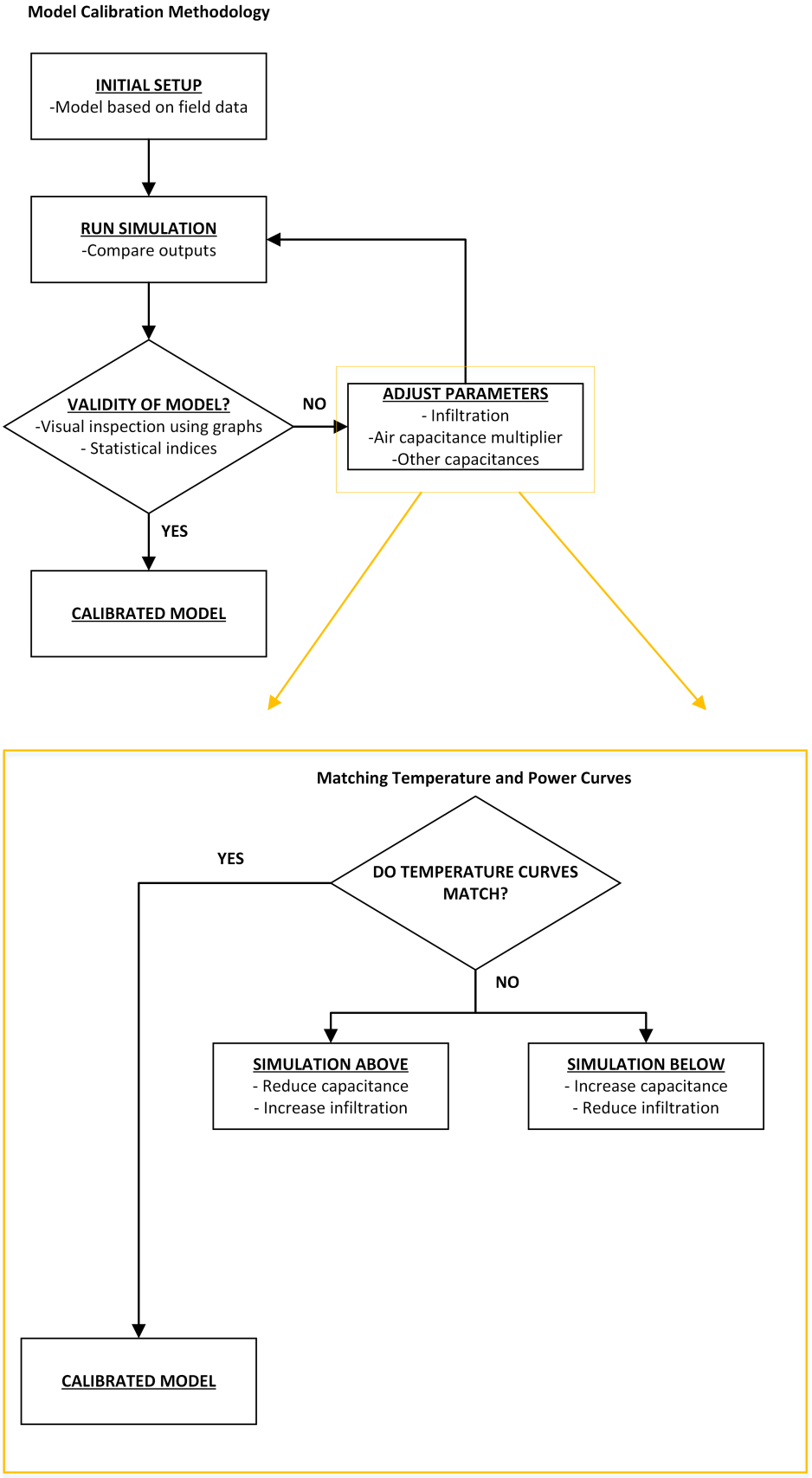

Figure 5.9: Calibration methodology

Tables 5.13 and 5.14 displays the statistical indices generated from comparing measurement data from experiment 1 to model results of the six models created. Table 5.13 compares against models with average constant heat transfer coefficients, while Table 5.14 compares against those models with temperature dependent heat transfer coefficients calculated at each time step. From these values of statistical indices, we can say that the model is validated to simulate the conditions with which the house was under (closed interior doors, no solar radiation, temperature step change etc.), and that a more detailed model does not necessarily result in higher model accuracy. A manually iterative calibration process was used, shown in Figure 5.9. As a model becomes more detailed, the number of parameters that can be adjusted increases, which can result in a complex calibration problem (Kummert et al., 2006).

Table 5.13: Power model calibration - constant heat transfer coefficients (experiment 1)

Model Order	**Wood**		**Tile**		**Carpet**	
	CVRSME	NMBE	CVRSME	NMBE	CVRSME	NMBE
3	13.07%	-1.15%	10.87%	-6.72%	14.00%	-1.49%
5	12.94%	-1.16%	6.55%	1.2%	15.49%	-1.38%
7(a)	13.25%	-1.12%	11.10%	3.51%	14.27%	-5.38%
7(c)	15.43%	-5.34%	11.13%	-3.68%	14.15%	-2.02%
9	14.23%	-1.55%	6.05%	1.19%	14.78%	-1.38%
13	12.19%	-1.77%	11.20%	-3.83%	16.51%	1.60%
Guideline 14-2002	30%	10%	30%	10%	30%	10%

Table 5.14: Power model calibration - temperature dependent heat transfer coefficients (experiment 1)

Model Order	Wood		Tile		Carpet	
	CVRSME	NMBE	CVRSME	NMBE	CVRSME	NMBE
3	13.05%	0.37%	6.88%	0.94%	14.23%	0.03%
5	13.57%	-1.52%	6.01%	1.01%	15.74%	-1.50%
7(a)	13.33%	-1.16%	11.85%	4.37%	15.63%	-7.62%
7(c)	15.67%	-5.48%	11.00%	-3.70%	13.85%	-1.95%
9	17.70%	-7.04%	6.55%	0.91%	15.48%	-1.37%
13	13.90%	-5.25%	11.14%	-3.88%	16.00%	-1.82%
Guideline 14-2002	30%	10%	30%	10%	30%	10%

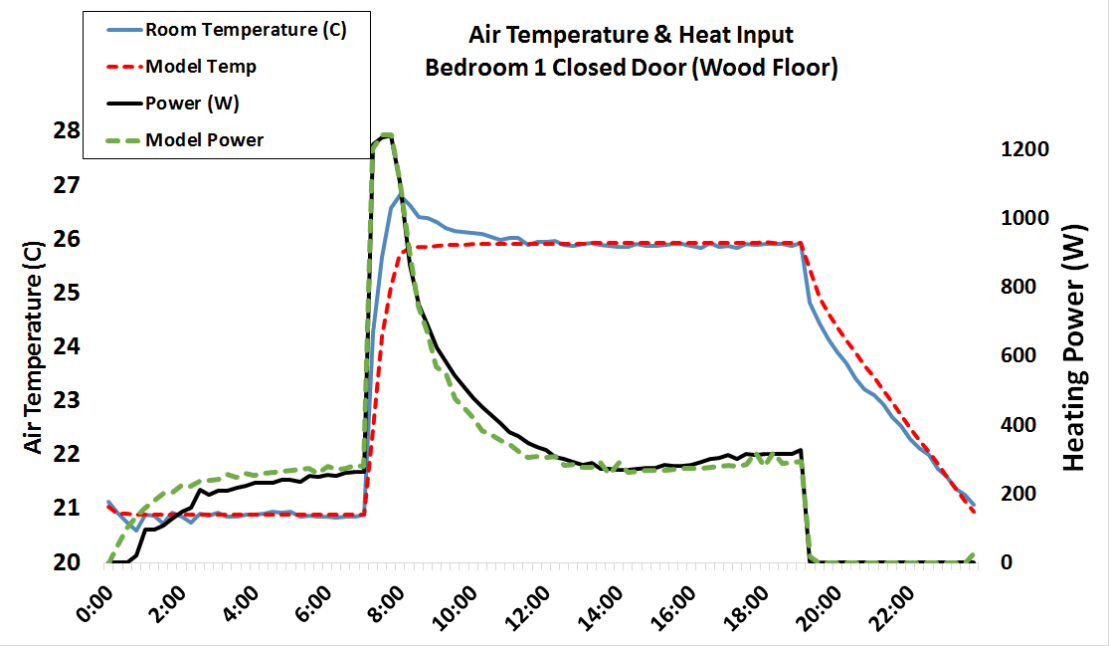

Figure 5.10: Results from 3 capacitance model with constant heat transfer coefficients (Exp 1)

Figure 5.10 shows results for one day of the 3 capacitance model with constant heat transfer coefficients (the simplest model of the 12 models investigated). Good correlation of heating power and air temperature can be seen. Figure 5.11 shows the results of the 13 capacitance model with constant heat transfer coefficients. When comparing, visually, the results from the 3 capacitance model and the 13

capacitance model, we can see that both models accurately predict heating power and air temperature for the experimental conditions.

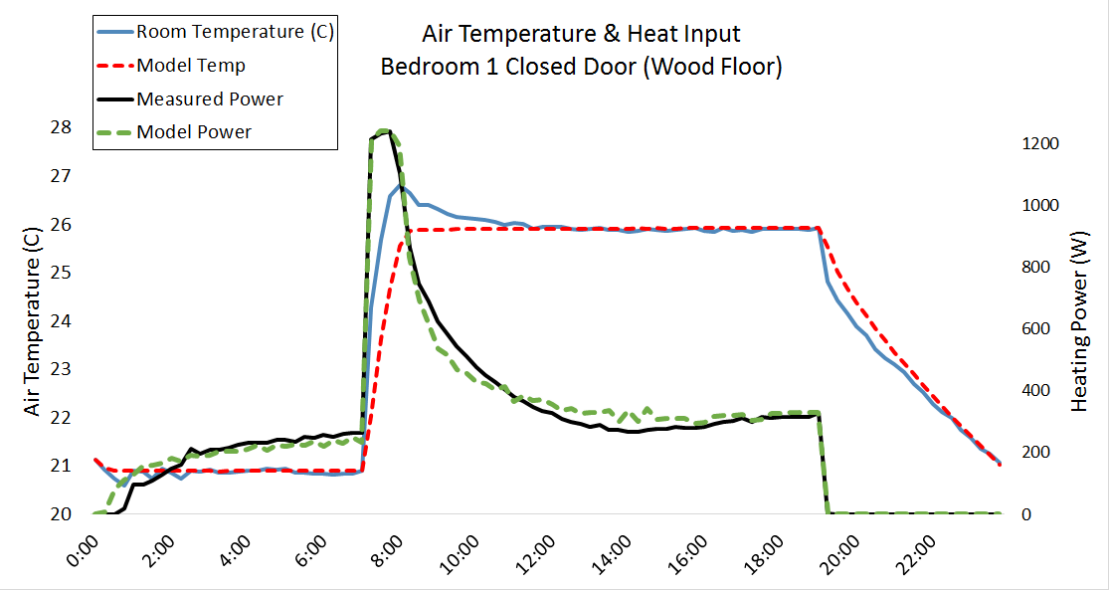

Figure 5.11: Results from 13 capacitance model with constant heat transfer coefficients (Exp 1)

Next, the models were compared to 7 days from experiment 2 data. Table 5.15 shows statistical indices for models with constant heat transfer coefficients, while Table 5.16 shows results for models with temperature dependent heat transfer coefficients. Again, all models meet ASHRAE limits for statistical indices values. The simple and detailed models for the zone with wood flooring in Figure 5.13 show good accuracy and adequate statistical indices, with small differences between the simple and more detailed models. The discrepancy in power calculation at the beginning of the simulation (Figures 5.13 and 5.14) is due to the assumed initial states. When using the explicit finite difference method, one must assume all initial states as inputs to the model. It was assumed that the room temperature was initially equal to the set point temperature. The heating calculation depends on the error between air temperature and set point temperature, so if they are equal to each other, the power will be calculated as zero since the error is zero.

Table 5.15: Power model calibration - constant heat transfer coefficients (experiment 2)

Model Order	Wood		Carpet	
	CVRSME	NMBE	CVRSME	NMBE
3	17.57%	0.98%	19.76%	4.43%
5	17.72%	-0.26%	19.33%	-0.65%
7(a)	19.35%	-0.20%	17.83%	3.30%
7(c)	17.37%	2.05%	18.01%	1.73%
9	19.11%	1.00%	19.89%	-0.50%
13	17.47%	-3.39%	22.22%	2.87%
Guideline 14-2002	30%	10%	30%	10%

Table 5.16: Power model calibration - temperature dependent heat transfer coefficients (experiment 2)

Model Order	Wood		Carpet	
	CVRSME	NMBE	CVRSME	NMBE
3	17.90%	2.27%	20.17%	5.69%
5	18.28%	2.30%	19.51%	-0.84%
7(a)	19.11%	0.80%	19.10%	-3.40%
7(c)	17.56%	3.23%	18.12%	2.20%
9	18.74%	1.13%	19.80%	-0.64%
13	17.18%	3.38%	20.56%	2.43%
Guideline 14-2002	30%	10%	30%	10%

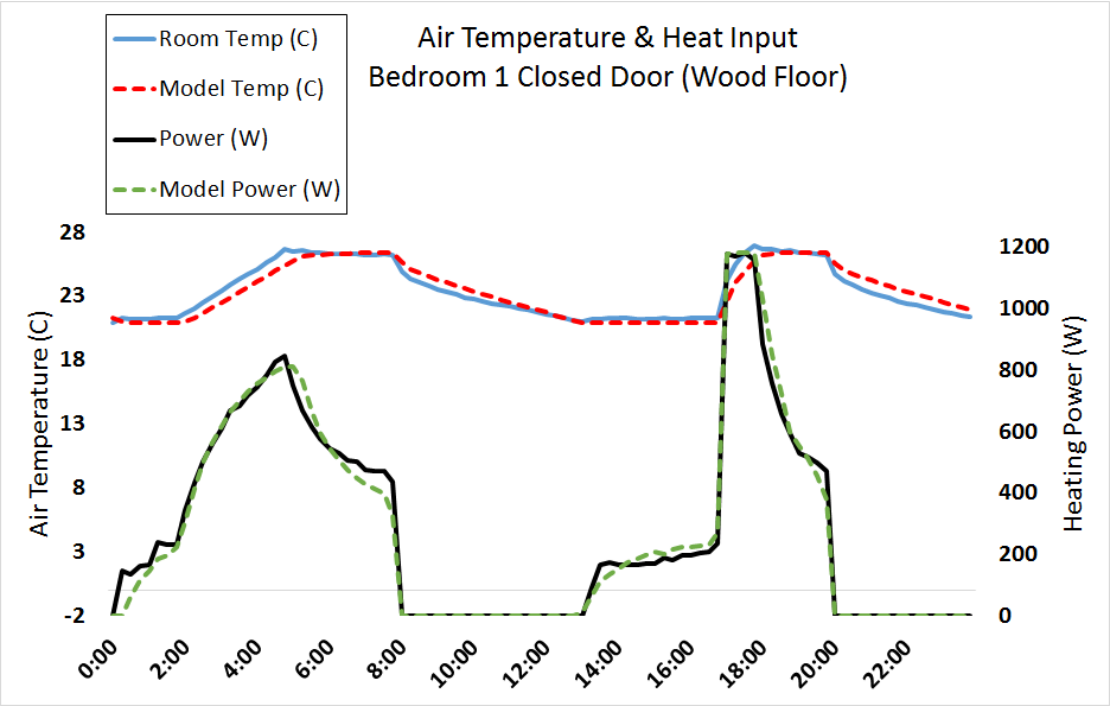

Figure 5.12: Results from 3 capacitance model with temperature dependent heat transfer coefficients

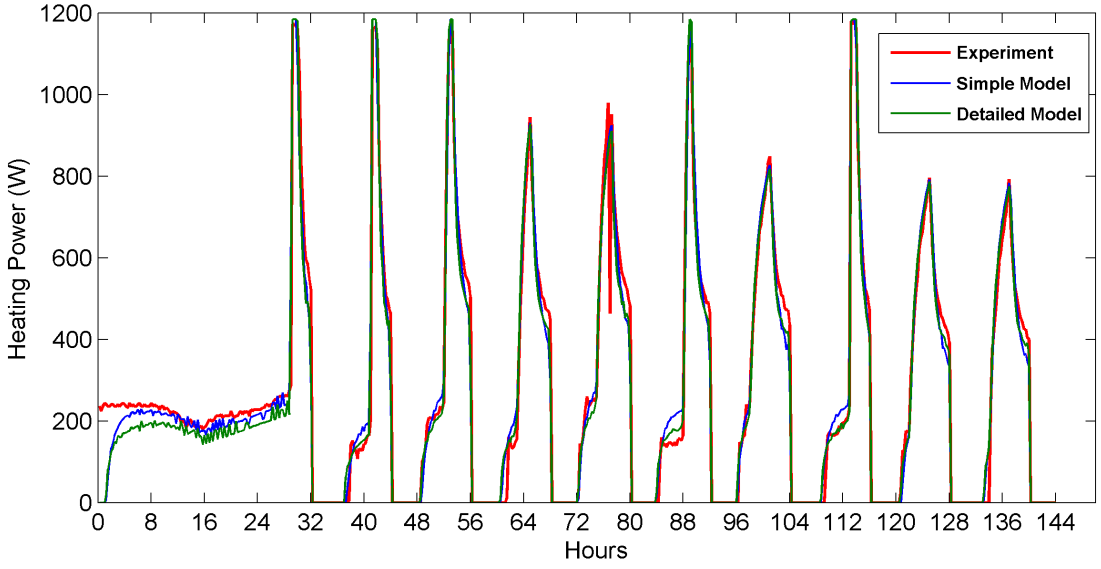

Figure 5.13: Heating power, experimental, simple model, and detailed model results – Bedroom 1 wood floors

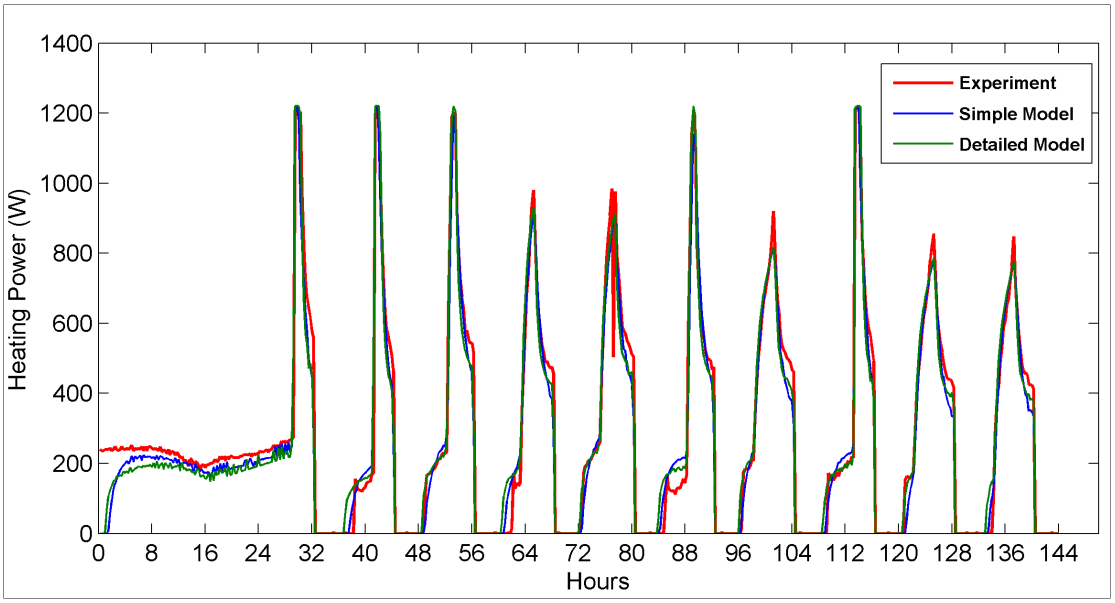

Figure 5.14: Heating power, experimental, simple model, and detailed model results – Bedroom 1 carpet floors

The models of the carpet floored room are not as accurate, especially at the peaks during ramping profiles, as seem in Figure 5.14, yet the statistical indices are within the reasonable limits (CV-RMSE below 30% and NMBE below 10%). Therefore, it is important to use visual comparison techniques as well as statistical comparison techniques when the load profile at sub hourly intervals if of importance.

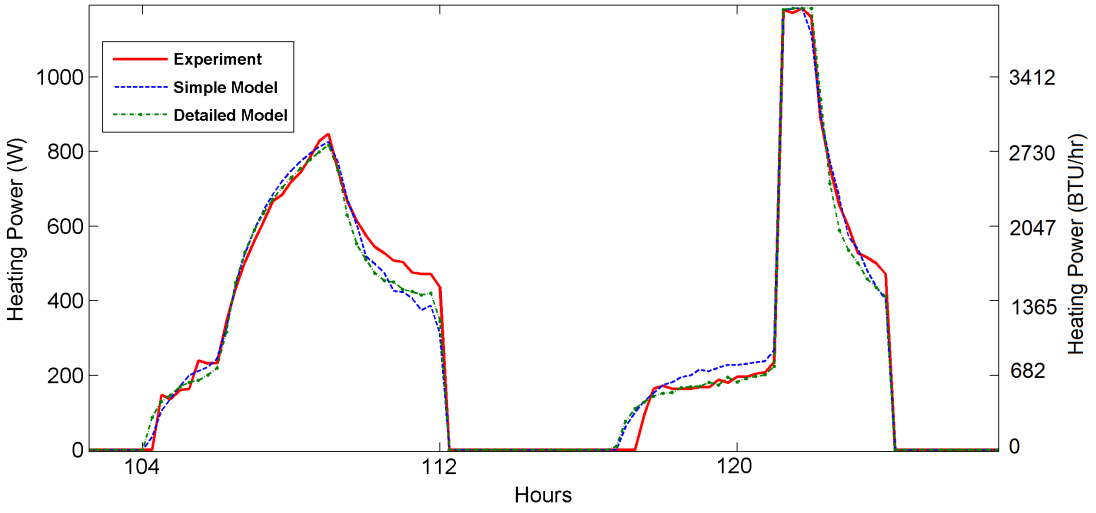

Figure 5.15: Day 6 power demand model predictions - wood floors

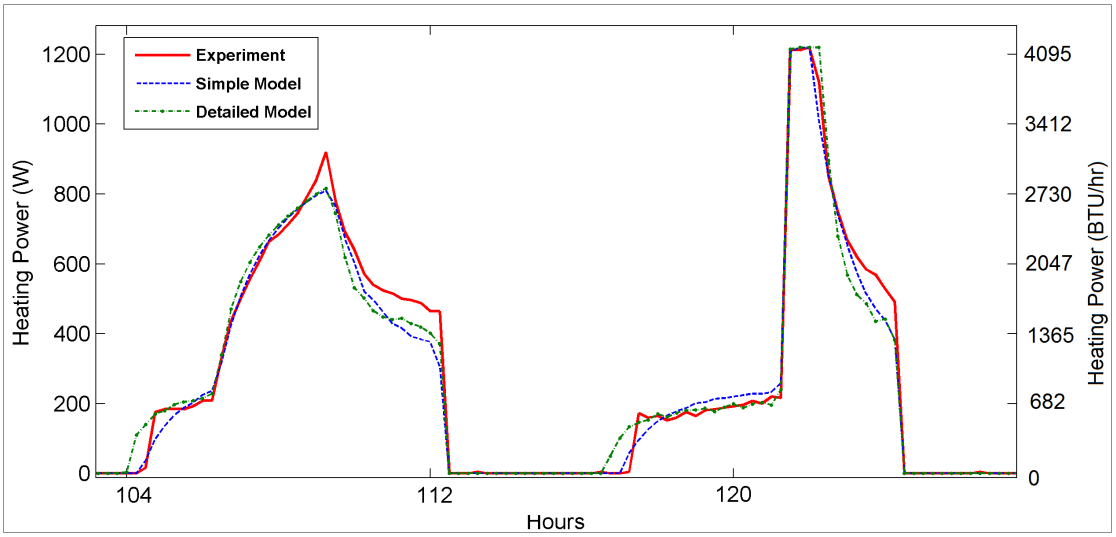

Figure 5.16: Day 6 power demand model predictions - carpet floors

5.2 Thermostat Set Point Strategies for Peak Power Reduction

Realistic behaviour concerning temperature set point adjustments is notoriously less regular than a fixed schedule (Urban & Gomez, 2013). It is however difficult to obtain realistic user behaviour profiles, especially during extreme weather conditions which cause DR events. While fixed schedules allowed comparing strategies, the resulting reduction potential values should only be considered as an approximation.

In winter, the electricity grid peak demand in Québec occurs on weekdays between 6am and 9am and between 4pm and 8pm. There are many strategies that could be effective for peak heating reduction, but here have been narrowed to the effect of different ramp lengths and "near optimal" trajectories introduced in (Candanedo et al., 2015). The reference profile is the step change from 18°C to 21°C, as a night time temperature setback is common practice for reducing energy consumption (Manning et al., 2007). The temperatures set points are

within acceptable comfort conditions. Using the procedure in (Candanedo et al., 2015), "near optimal" transition curves were determined for transition times of 1, 2, and 3 hours. Their effectiveness will be compared to the simpler ramp profiles. The different strategies were simulated using the simplest model and most detailed model with an outdoor air temperature profile of the winter peak day shown in Figure 5.17.

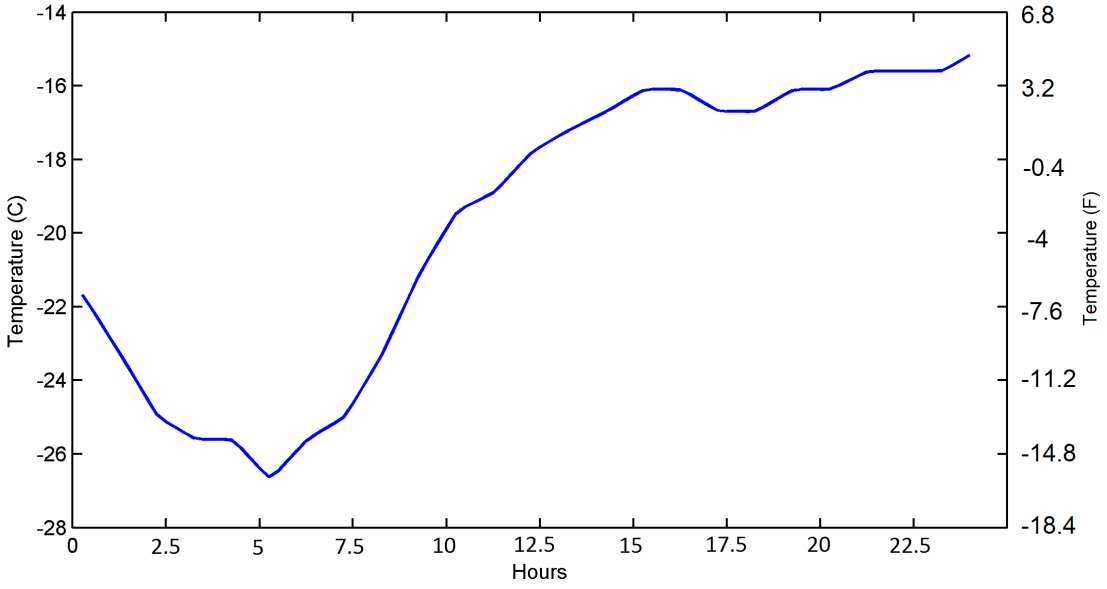

Figure 5.17: Peak winter day outdoor air temperature

Acceptable Daytime Comfort Temperature Set Point Profiles

Figure 5.18 shows the reference step temperature profile (A0) and the three ramp profiles with acceptable daytime comfort (A1-A3). Figure 15 shows the three optimal transition curves (A4-A6) for transition times of 1, 2 and 3 hours.

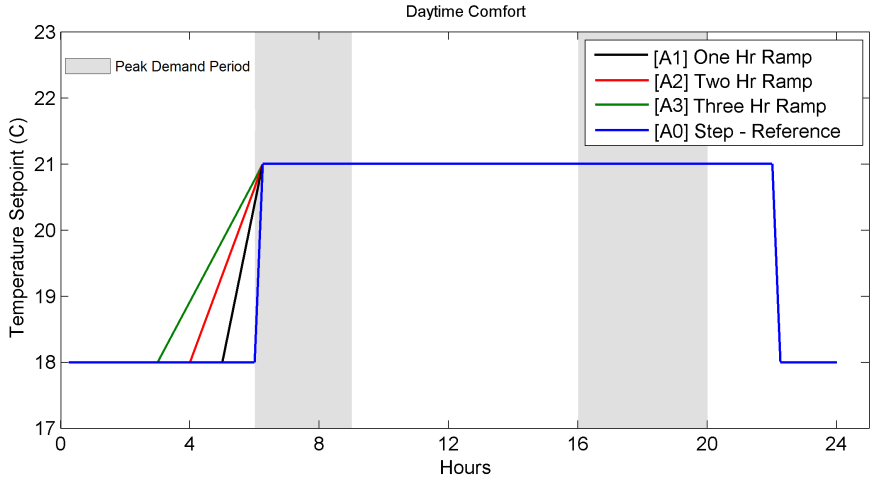

Figure 5.18: Ramping strategies - acceptable daytime comfort

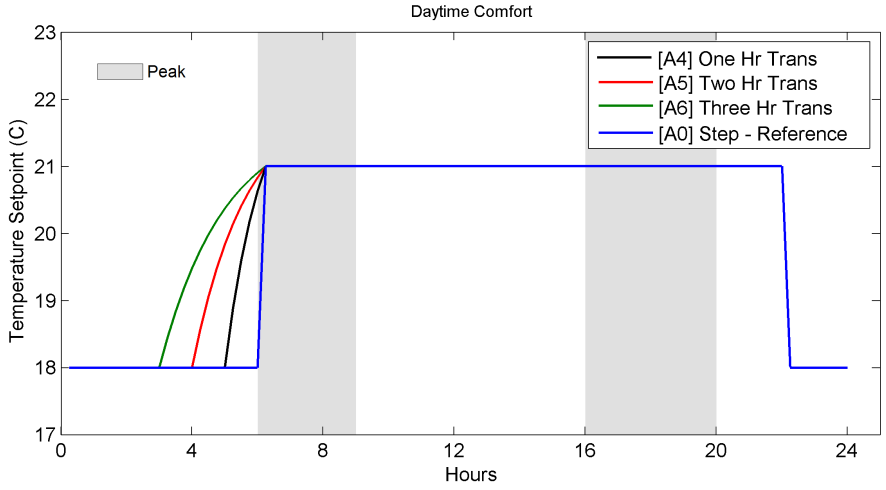

Figure 5.19: Optimal transition curves - acceptable daytime comfort

Below are results for aforementioned temperature set point profiles for the objective of peak heating demand reduction. Figure 5.20 shows the results using the 3 capacitance model for acceptable daytime comfort ramping profiles. Figure 14 shows the results using the detailed 13 capacitance model with temperature dependent heat transfer coefficients. Significant peak reductions can be observed when a step change is replaced by simple 1, 2, or 3 hour ramps.

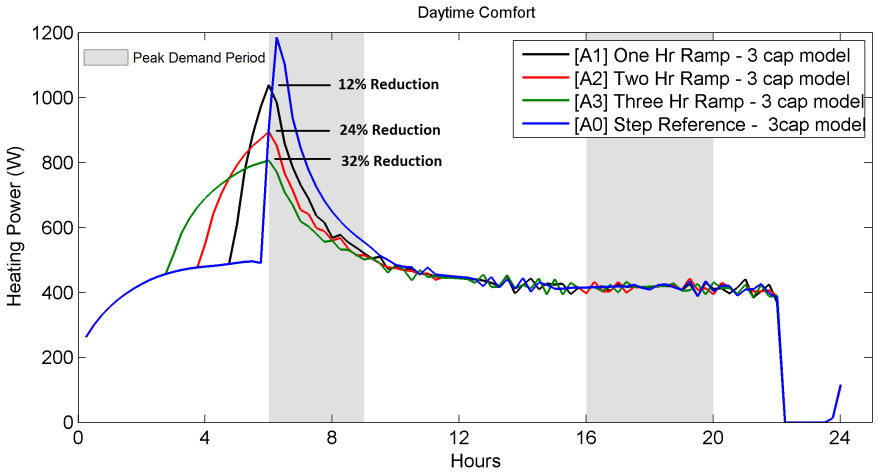

Figure 5.20: Ramping strategies power results - acceptable daytime comfort - 3 capacitance model

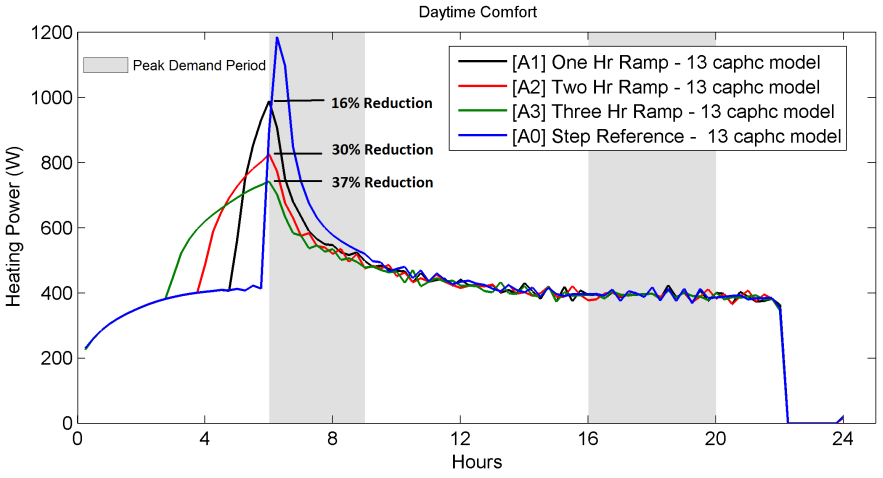

Figure 5.21: Ramping strategies power results - acceptable daytime comfort - 13 capacitance model with temperature dependent HT coefficients

On the peak day with very cold outdoor temperature, the low order model, when compared to the detailed model, underestimates the impact of the ramping profiles on peak reduction. For a two hour ramp, the less detailed model predicts a reduction of 24%, while the more detailed model predicts 30%, and for the three hour ramp, 32% versus 37%, respectively. On the experiment days, the simple model and detailed model both calculate the same reductions of 21% for a 2 hour ramp and 31% for a three hour ramp. This difference could be due to the fact that cold outdoor air on the peak day has greater effect, and the temperature step up

was 5°C in the experiments rather than 3°C on the peak day simulations. Table 1 shows the demand response indicators for strategies with acceptable daytime comfort for a transition time of 3 hours. Peak power results for the optimal transition curve profiles can be seen in Figure 16.

Table 5.17: Demand response indicators for strategies with acceptable daytime comfort (3 capacitance model)

		[A0] Reference	[A3] 3 Hr Ramp		[A6] 3 Hr Transition	
		[W]	Demand [W]	Impact [%]	Demand [W]	Impact [%]
Zone peak		1184	806	-32%	790	-33%
AM	q_{am}^{max}	1184	770	-35%	690	-42%
	$\overline{q}_{am}$	770	595	-23%	566	-26%
	$rebound_{am}$	490	470	-4%	469	-4%
PM	q_{pm}^{max}	436	433	-1%	441	1%
	$\overline{q}_{pm}$	413	412	0%	413	0%
	$rebound_{pm}$	16	16	0%	16	-3%
Zone daily consumption [kWh]		10.67	10.73	1%	10.75	1%

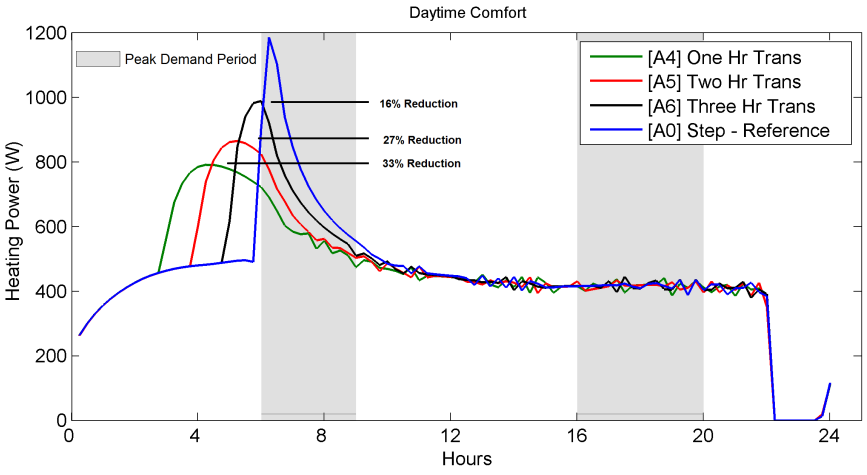

Figure 5.22: Optimal transition curves - acceptable daytime comfort - 3 capacitance model

Temperature Set Point Profiles without Acceptable Daytime Comfort

Figure 17 shows the reference step temperature profile (B0) and the three ramp profiles without acceptable daytime comfort (B1-B3). Figure 19 shows the three

optimal transition curves (B4-B6) for transition times of 1, 2 and 3 hours.

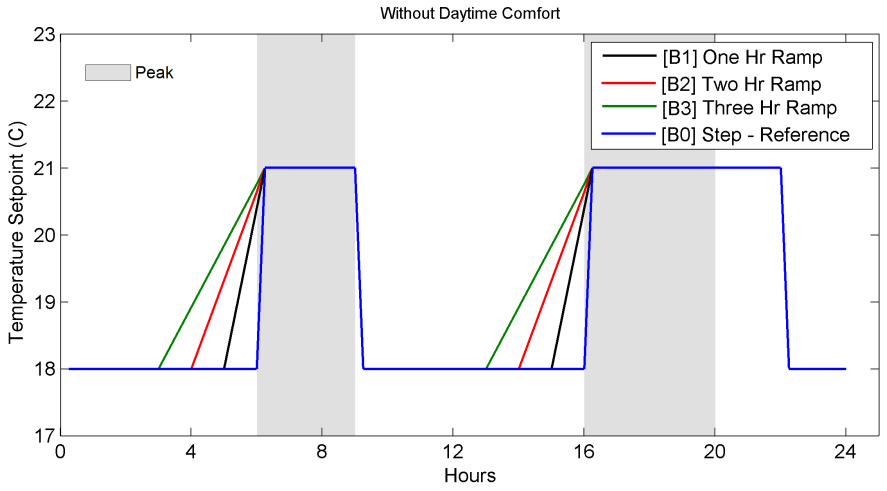

Figure 5.23: Ramping strategies - without acceptable daytime comfort

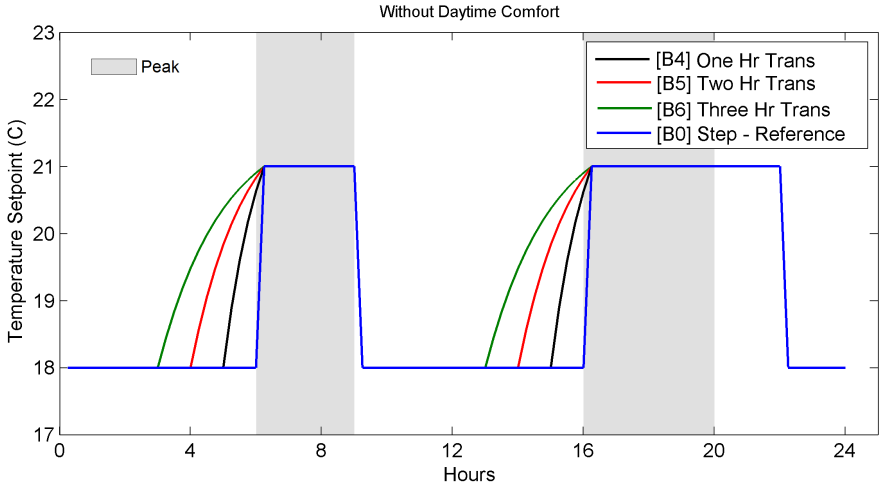

Figure 5.24: Optimal transition curves - without acceptable daytime comfort

Seen in Figure 18 are results for ramping strategies with a night time set back as well as a day time set back (profile without acceptable daytime comfort). This is a suitable profile for dwellings with no one at home during the weekday, as this reduces the overall energy consumption from 9.81 kWh to 9.38 kWh for the reference step profile (B0 compared to A0) on the winter peak day. This profile also shows good results in peak reduction as well as having no peak during the rebound period.

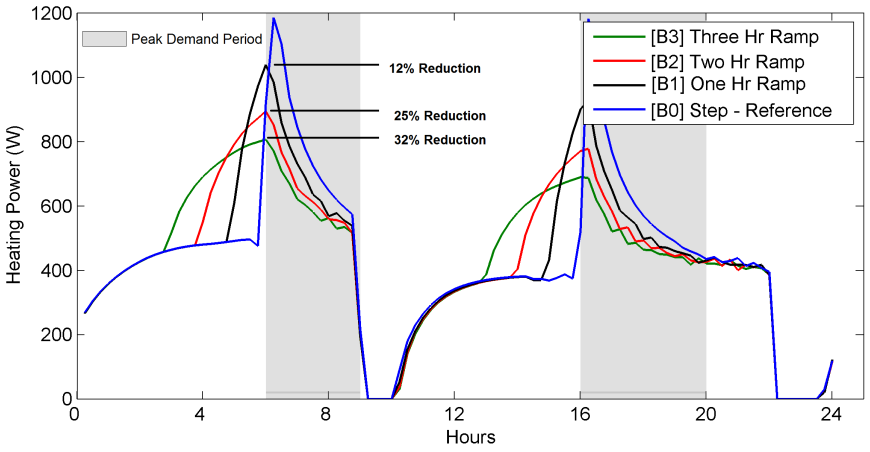

Figure 5.25: Ramping strategies power results - without acceptable daytime comfort - 3 capacitance model

Table 5.18: Demand response indicators for strategies without acceptable daytime comfort (3 capacitance model)

		[B0] Reference	[B3] 3 Hr Ramp		[B6] 3 Hr Transition	
		[W]	Demand [W]	Impact [%]	Demand [W]	Impact [%]
Zone peak		1184	806	-32%	791	-33%
AM	q_{am}^{max}	1184	770	-35%	690	-42%
	$\overline{q}_{am}$	742	570	-23%	542	-27%
	$rebound_{am}$	96	77	-19%	75	-22%
PM	q_{pm}^{max}	1181	687	-42%	596	-50%
	$\overline{q}_{pm}$	567	465	-18%	449	-21%
	$rebound_{pm}$	19	18	-6%	17	-10%
Zone daily consumption [kWh]		10.44	10.55	1%	10.58	1%

Figure 20 shows the power profiles for the corresponding optimal transition curves without acceptable daytime comfort. Detailed demand response indicators for profiles without acceptable daytime comfort are found in Table 3 for 3 hour ramps and optimal curves. Optimal transition curve profiles again give slightly better results than the ramp profiles.

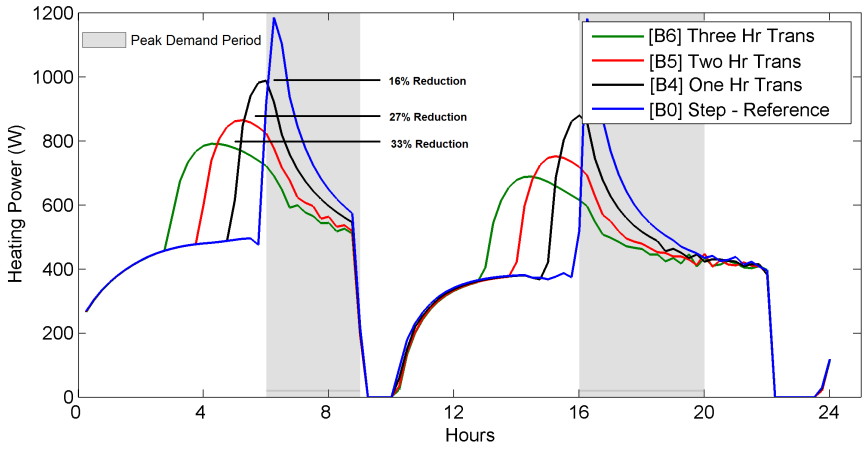

Figure 5.26: Optimal transition curves power results - without acceptable daytime comfort - 3 capacitance model

Temperature Set Point Profiles with Pre Heating and Acceptable Daytime Comfort

Figure 21 shows ramp profiles with preheating for one hour prior to peak times and acceptable daytime comfort (C1-C3). Figure 23 shows the three optimal transition curves (C4-C6) for transition times of 1, 2 and 3 hours.

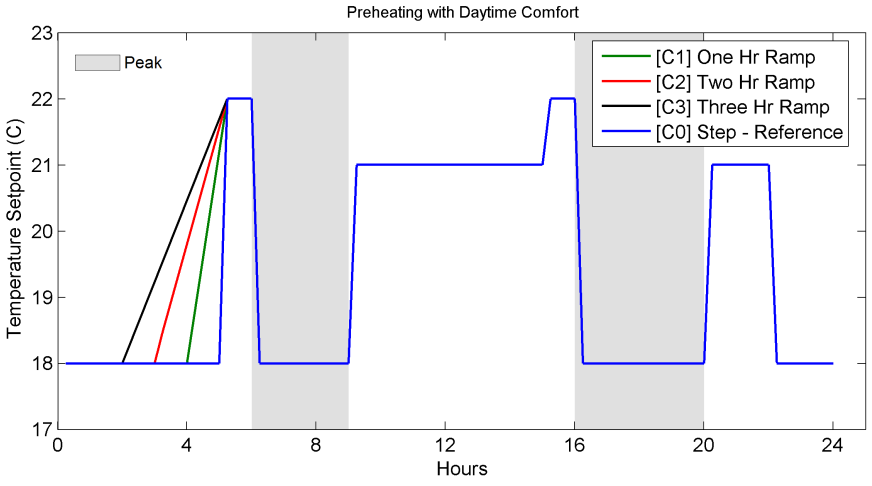

Figure 5.27: Ramping strategies - preheating with acceptable daytime comfort

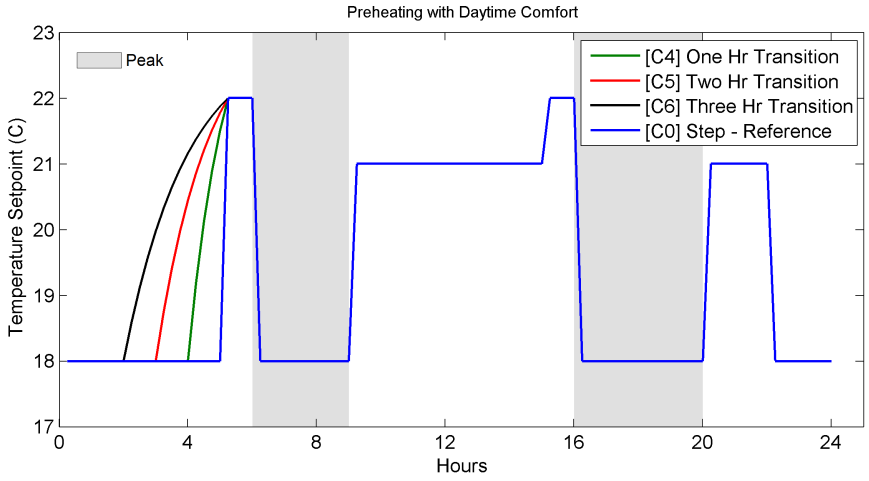

Figure 5.28: Optimal transition curves - preheating with acceptable daytime comfort

Next, preheating before peak hours were tested with ramp profiles. The zone was preheated for one hour at one degree higher than the normal comfort temperature at 22°C. During the peak hours the set point was readjusted to the setback temperature of 18°C and then at the end of the peak hours the temperature is returned to 21°C.

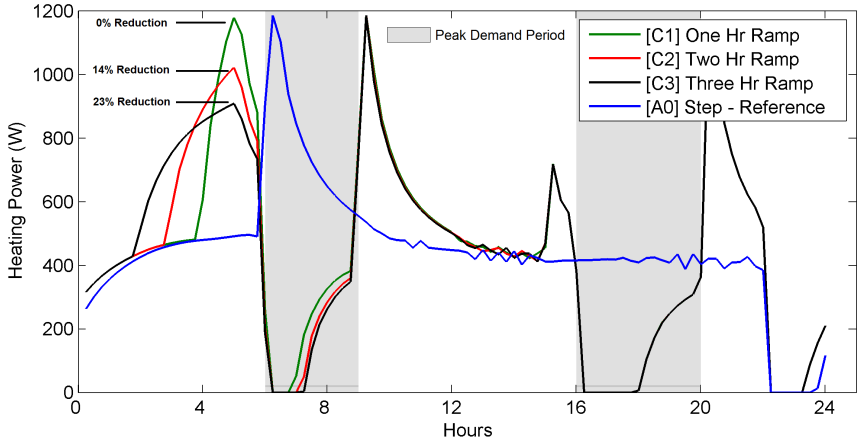

Figure 5.29: Ramping strategies power results - preheating with acceptable daytime comfort

Table 5.19: Demand response indicators for strategies with preheating and acceptable daytime comfort (3 capacitance model)

		[A0] Reference	[C3] 3 Hr Ramp		[C6] 3 Hr Transition	
		[W]	Demand [W]	Impact [%]	Demand [W]	Impact [%]
Zone peak		1184	1184	0%	1184	0%
AM	q_{am}^{max}	1184	752	-36%	745	-37%
	$\overline{q}_{am}$	770	195	-75%	181	-76%
	$rebound_{am}$	490	783	60%	779	59%
PM	q_{pm}^{max}	436	1147	163%	1147	163%
	$\overline{q}_{pm}$	413	341	-18%	341	-18%
	$rebound_{pm}$	16	57	248%	57	248%
Zone daily consumption [kWh]		10.67	10.57	-1%	10.57	-1%

As seen in Figure 22, results for ramping profiles with preheating and acceptable daytime comfort are not so favourable. Although the morning peak load during peak hours is significantly reduced, there is an undesirable by-product of a very large rebound load after the peak hours, shown in Table 5. Since this is an investigation of implementing relatively simple profiles, it is probable that any more modifications to this style of profile to reduce unfavourable results will just result in a too complicated temperature set point profile.

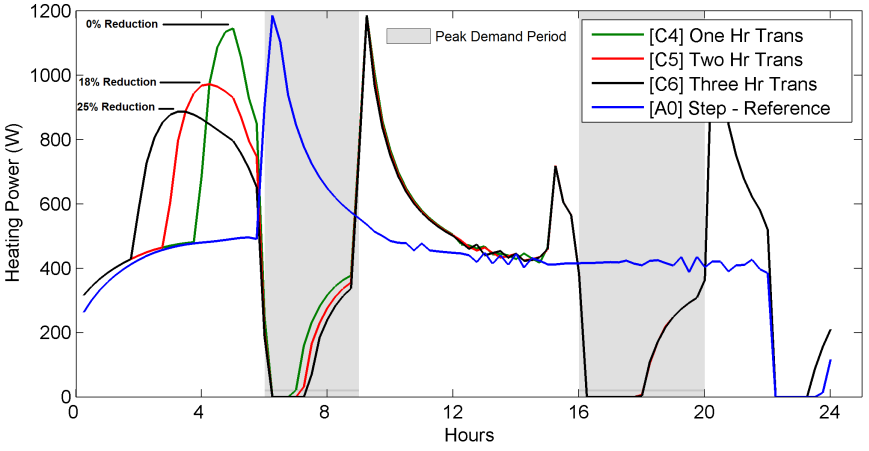

Figure 5.30: Optimal transition curves power results - preheating with acceptable daytime comfort

Temperature Set Point Profiles with Pre Heating and without Acceptable Daytime Comfort

Figure 25 shows ramp profiles with preheating for one hour prior to peak times and without acceptable daytime comfort (D1-D3). Figure 27 shows the three optimal transition curves (D4-D6) for transition times of 1, 2 and 3 hours.

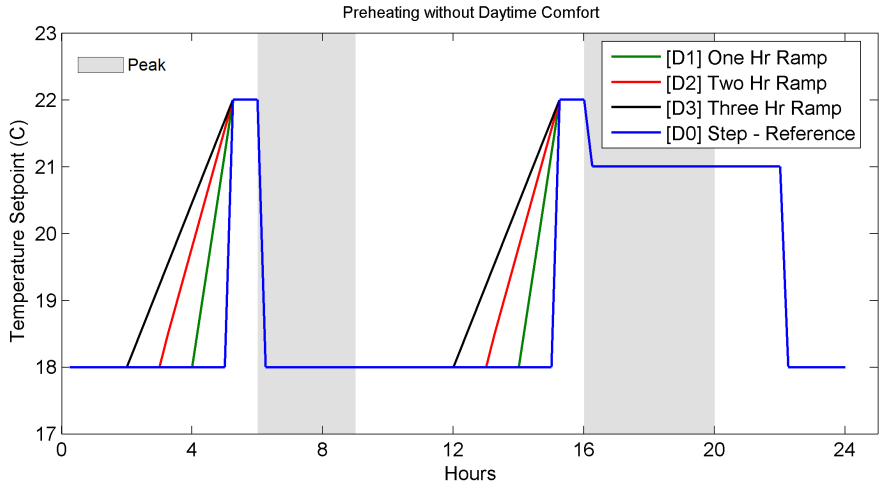

Figure 5.31: Ramping strategies - preheating without acceptable daytime comfort

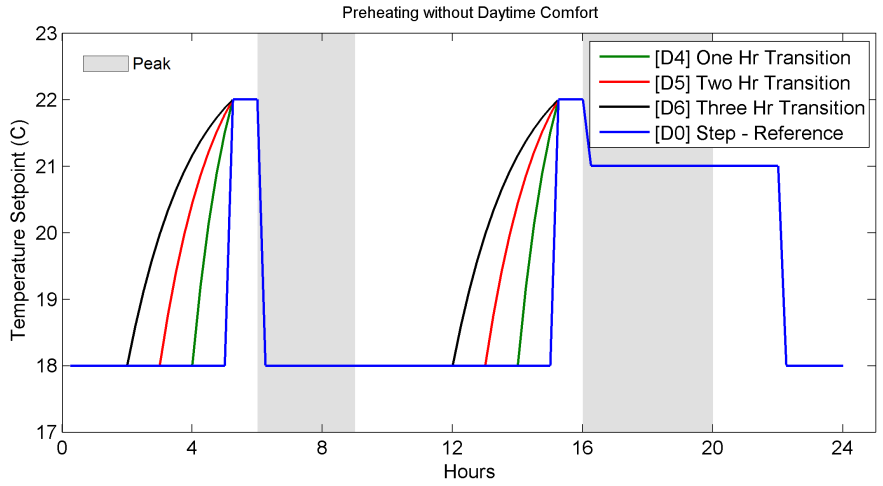

Figure 5.32: Optimal transition curves - preheating without acceptable daytime comfort

The last style of temperature set point profiles studied for the zone on a winter peak consist of one hour of preheating and without acceptable daytime

comfort, shown in Figures 25 and Figure 27. For the demand response indicators shown in Table 7, these ramps and transition curve profiles were compared against the simple step change without acceptable daytime comfort profile B0, shown in Figure 17, to give a better understanding of the impact of ramping or transition curves with preheating on the a typical step profile. The main observation is the morning rebound load is increased, though it is still a low value, otherwise the preheating without acceptable daytime comfort profiles seem to have good peak load reduction capabilities.

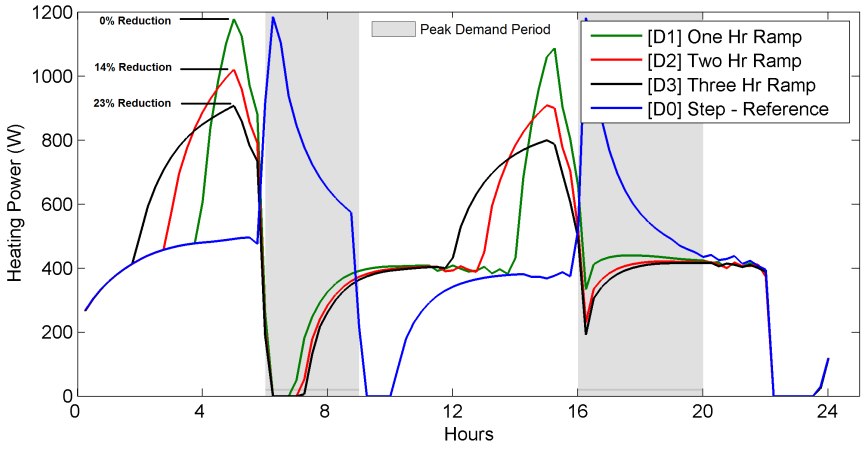

Figure 5.33: Ramping power results - preheating without acceptable daytime comfort

Table 5.20: Demand response indicators for strategies without preheating and acceptable daytime comfort (3 capacitance model)

		[B0] Reference	[D3] 3 Hr Ramp		[D6] 3 Hr Tranisiton	
		[W]	Demand [W]	Impact [%]	Demand [W]	Impact [%]
Zone peak		1184	907	-23%	881	-26%
AM	q_{am}^{max}	1184	363	-69%	335	-70%
	$\overline{q}_{am}$	742	163	-78%	150	-80%
	$rebound_{am}$	96	391	310%	387	305%
PM	q_{pm}^{max}	1181	417	-65%	420	-64%
	$\overline{q}_{pm}$	567	390	-31%	381	-33%
	$rebound_{pm}$	19	18	-6%	18	-4%
Zone daily consumption [kWh]		10.44	10.57	1%	10.61	2%

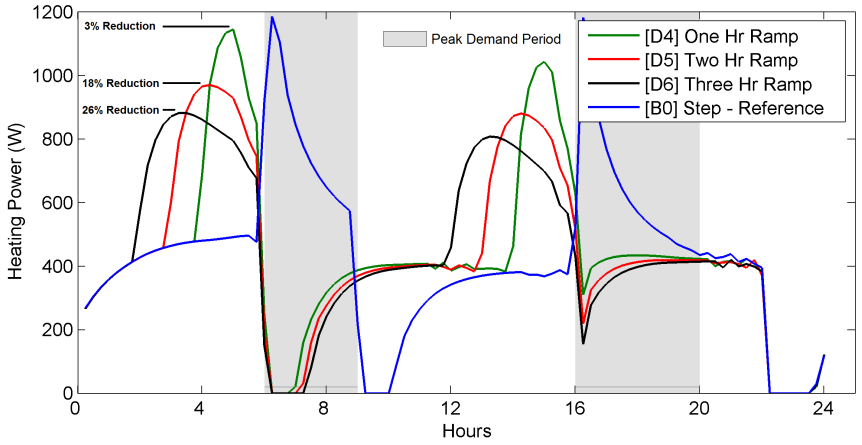

Figure 5.34: Optimal transition curves power results - preheating without acceptable daytime comfort

5.2.1 Final Remarks

Several temperature set point strategies have been suggested and investigated for their effectiveness in peak load reduction due to heating for a residential building. The aim was to suggest simple profiles which could be easily implemented by homeowners in advanced communicating thermostats. Ramping profiles with or without acceptable daytime comfort temperature set points seem to result in a good compromise between peak load reduction and simplicity, as there is more steps required in order to obtain optimal transitions curves for a given zone depending on the zone time constant. Optimal transition curves are better suited for peak reduction in building with higher thermal mass levels. Preheating of one hour at one degree Celsius higher did not produce effective results, therefore a longer preheating time should be used. However, a longer preheating period could lead to occupant thermal discomfort as well as increased energy consumption. This is not an exhaustive investigation of temperature set point modulation strategies, as there are an infinite amount of strategies that could potentially be effective in

peak load reduction while maintaining occupant thermal comfort. The next potential step to further study this topic is to implement an optimization procedure to identify suitable set point strategies.

Based on simulation results using the experiment weather conditions, the 3 capacitance low order model will give sufficient prediction for the zone. The number of nodes in an RC model and their arrangement may vary depending on the requirements of the control strategy or other factors (e.g. time scale, energy storage device). If the purpose of the simulation is to select a ramp duration or predict future thermal behaviour of a low mass zone such as the one studied here, both models could be used, however, the low order model is better suited to be implemented in the context of model-based control due to faster computation time, simplicity of the model and the fact that, if anything, it will underestimate rather than overestimate the peak reduction from a given strategy.

5.3 Zone Thermal Mass Alterations

Using the model, alterations to the walls and ceilings were done in order to different thermal capacity and conductivity levels in the zone. The effects of ramping on the different zones were then analyzed. The materials are shown in Table 5.21. Hypothetical materials that are based on increasing the thickness of the gypsum board (by a factor of two) and increasing its conductivity between 1-4 times are considered. This type of analysis can inform development of new materials.

Table 5.21: Material property alterations of walls and ceiling

Gypsum Board	**Density** ρ (kg/m^3)	**Specific Heat** C_p (J/kgK)	**Conductivity** k (W/mK)	**Thickness** L (mm)	**Thermal Capacitance** $C = C_p \times \rho \times L \times A_{floor}$ (J/K)	**Thermal Resistance** (m^2K/W)
$1 \times L, 1 \times k$	640	1,150	0.16	13	4.62×10^5	0.08
$2 \times L, 1 \times k$	640	1,150	0.16	26	9.25×10^5	0.16
$1 \times L, 2 \times k$	640	1,150	0.32	13	4.62×10^5	0.04
$2 \times L, 2 \times k$	640	1,150	0.32	26	9.25×10^5	0.08
$1 \times L, 3 \times k$	640	1,150	0.48	13	4.62×10^5	0.03
$2 \times L, 3 \times k$	640	1,150	0.48	26	9.25×10^5	0.05
$1 \times L, 4 \times k$	640	1,150	0.64	13	4.62×10^5	0.02
$2 \times L, 4 \times k$	640	1,150	0.64	26	9.25×10^5	0.04

Figures 5.35 displays, for a wood floored room, the reduction in peak load due to ramping profiles of 1, 2 or 3 hours, for zones with mass properties found in Table 5.21. It can be seen that thickness and the conductivity play an important role in the room thermal dynamics and behaviour.

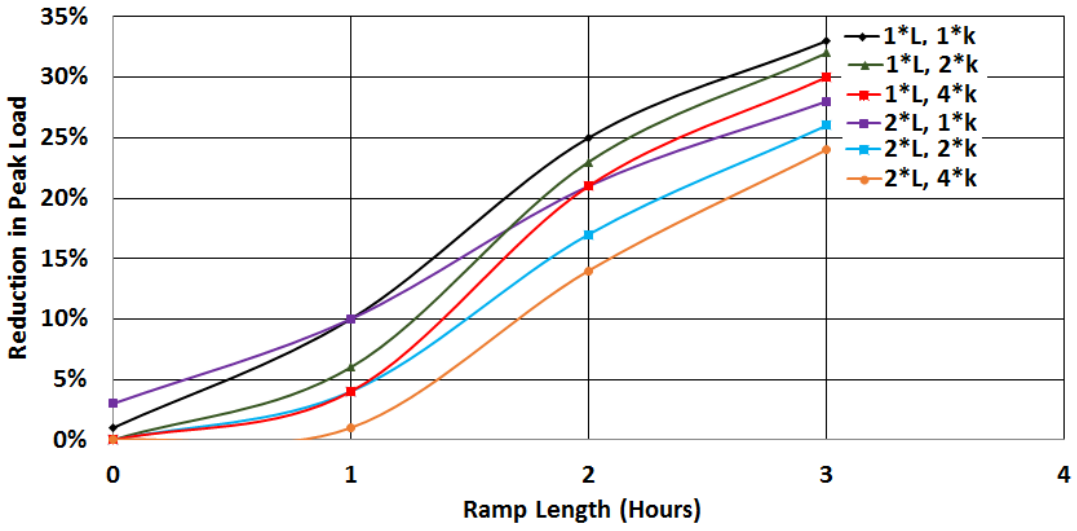

Figure 5.35: Thermal Mass Alterations - Ceiling & Walls - Wood Floors

Figures 5.36 and 5.37 show peak power profiles for a 3 hour ramping profile with acceptable daytime comfort and 3 hour optimal transition curve, respectively. The results are for various zones with the mass properties found in Table 5.21.

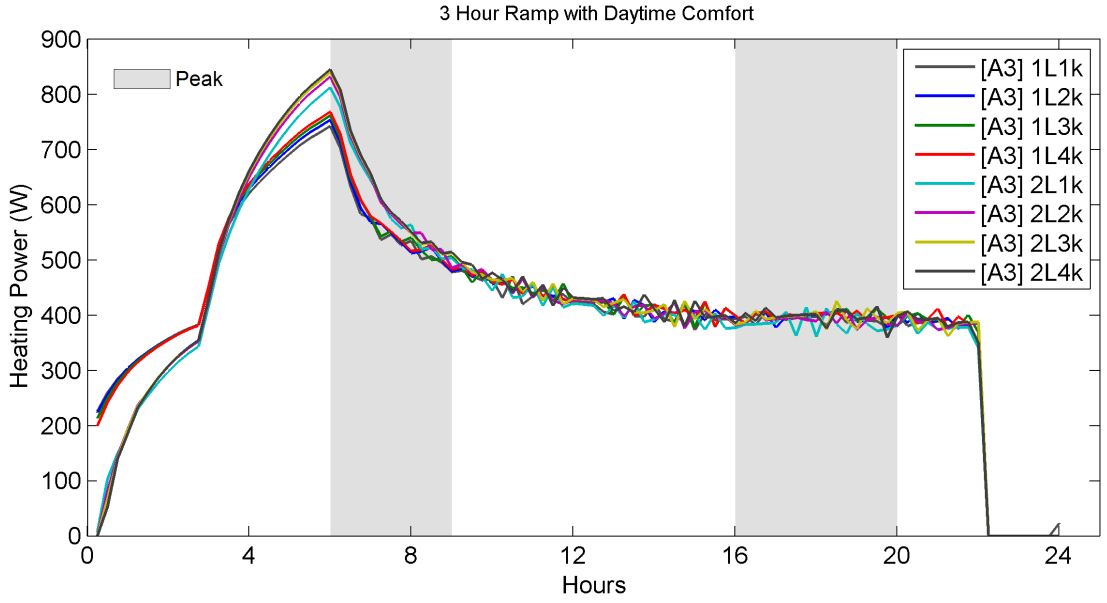

Figure 5.36: 3 hour ramp with acceptable daytime comfort power results- 13 capacitance model with temperature dependent HT coefficients

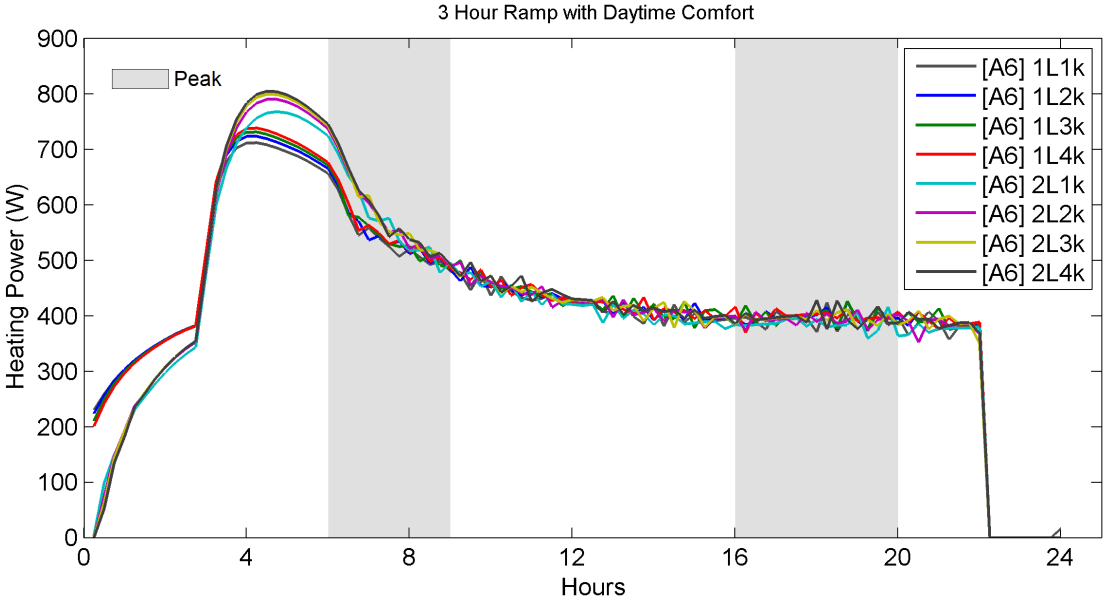

Figure 5.37: 3 hour transition curve with acceptable daytime comfort power results - 13 capacitance model with temperature dependent HT coefficients

Table 5.22: Response due to 3 hour ramp and mass alterations - wood floors

	3 Hour Ramp					
	1*L, 1k	**1L, 2*k**	**1*L, 4*k**	**2*L, 1*k**	**2*L, 2*k**	**2*L, 4*k**
C (J/K)	4.62×10^5	4.62×10^5	4.62×10^5	9.25×10^5	9.25×10^5	9.25×10^5
R (m^2K/W)	0.08	0.04	0.02	0.16	0.08	0.04
	Impact [%]	**Impact [%]**	**Impact [%]**	**Impact [%]**	**Impact [%]**	**Impact [%]**
q_{am}^{max}	-41%	-40%	-39%	-34%	-33%	-32%
Consumption [kWh]	1%	1%	3%	0%	2%	3%
Temperature Decay Time [Hours]	2	2.25	2.25	3	3	3

Table 5.23: Response due to 3 hour transition curve and mass alterations - wood floors

	3 Hour Transition Curve					
	1*L, 1k	**1L, 2*k**	**1*L, 4*k**	**2*L, 1*k**	**2*L, 2*k**	**2*L, 4*k**
C (J/K)	4.62×10^5	4.62×10^5	4.62×10^5	9.25×10^5	9.25×10^5	9.25×10^5
R (m^2K/W)	0.08	0.04	0.02	0.16	0.08	0.04
	Impact [%]	**Impact [%]**	**Impact [%]**	**Impact [%]**	**Impact [%]**	**Impact [%]**
q_{am}^{max}	-47%	-46%	-46%	-42%	-41%	-40%
Consumption [kWh]	1%	2%	3%	0%	2%	3%
Temperature Decay Time [Hours]	2	2.25	2.25	3	3	3

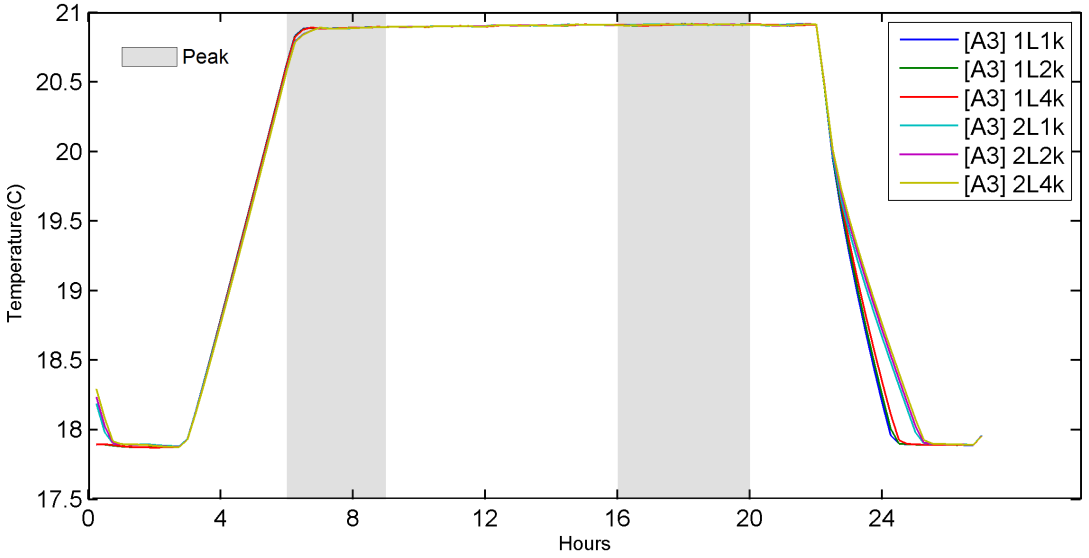

Figure 5.38: 3 hour ramp with acceptable daytime comfort air temperature results - 13 capacitance model with temperature dependent HT coefficients

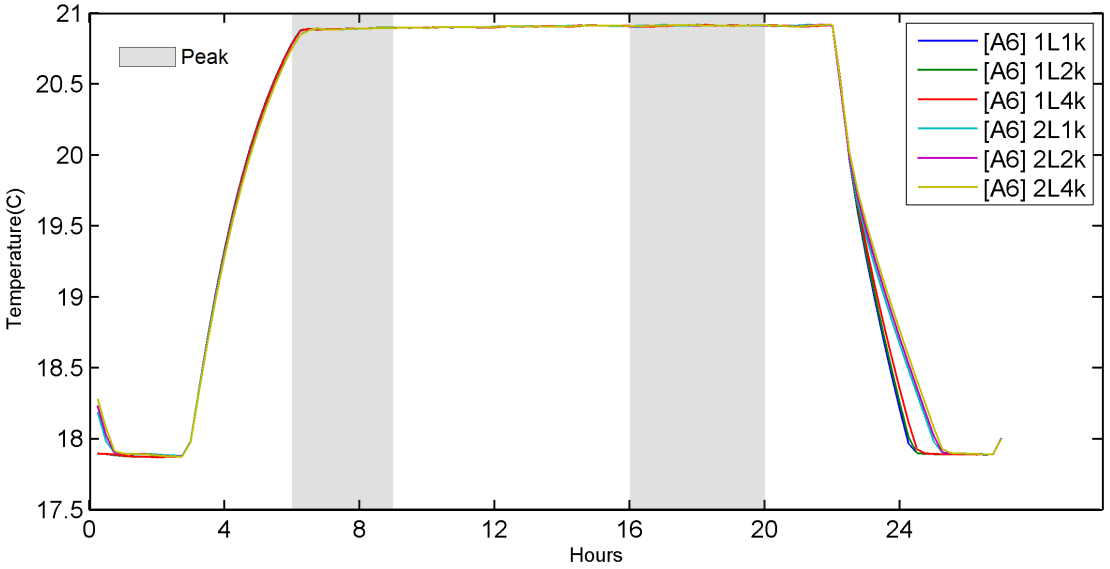

Figure 5.39: 3 hour transition curve with acceptable daytime comfort air temperature results - 13 capacitance model with temperature dependent HT coefficients

When comparing zones with different levels of thermal mass, thickness and conductivity plan an important role in the room thermal dynamics and behavior. As thickness and conductivity increase, the peak reduction is reduced, however, the temperature decay time is increased. From the study it can be generally concluded that increasing the thickness, while maintaining the conductivity level gives the best compromise between peak reduction and temperature decay time. A longer temperature decay time means that there is a delay in when the heater will turn on again to maintain the night time set back temperature set point.

5.4 Case Study: Commercial Bank Building

Commercial and institutional buildings using electricity as their only energy source are common in Québec and they contribute to a significant portion of the winter grid peak. This section presents an alternative method of building simulation to a detailed simulation software. A simple explicit finite difference model of a

building used as a bank was created and compared to a calibrated EnergyPlus model (Lavigne et al., 2014). Using the previously determined demand response strategy optimized through "NSGA-II" (Deb et al., 2002), a multi-objective genetic algorithm, the two models were compared.

Commercial buildings in Quebec often have a total building peak power cap, and if this is exceeded, higher charges may be applied by the utility company to the customer for this increased peak demand. As an example, if the customer has a minimum billing demand under 65kW, they are charged at Rate G (Hydro-Québec, 2015a). Rate G has the following energy costs: \$9.65/kWh for the first 15,090 kWh and \$6.13/kWh for the remaining consumption. The price of power above 50kW for rate G is \$17.19/kW. Therefore, even though peak demand for a customer may only occur for 15 minutes (as an example), they can still face significant charges for this peak demand above 50kW. In order to avoid these additional fees caused by peak power demands, demand response strategies become attractive solutions for commercial customers.

5.4.1 Building Description

The building used to create an explicit finite difference model is a 427 square meter (4,600sqft) single storey commercial building used as a bank. A 3D rendering of the building can be seen in Figure 5.40. A model in energy plus was created of the building with 21 thermal zones, shown in Figure 5.41. The location of the building is in Trois Riviere, Québec. The wall insulation is 3 RSI, while the roof insulation is 3.45 RSI. The windows are assumed as double glazing low-e type with 12.7mm air gap.

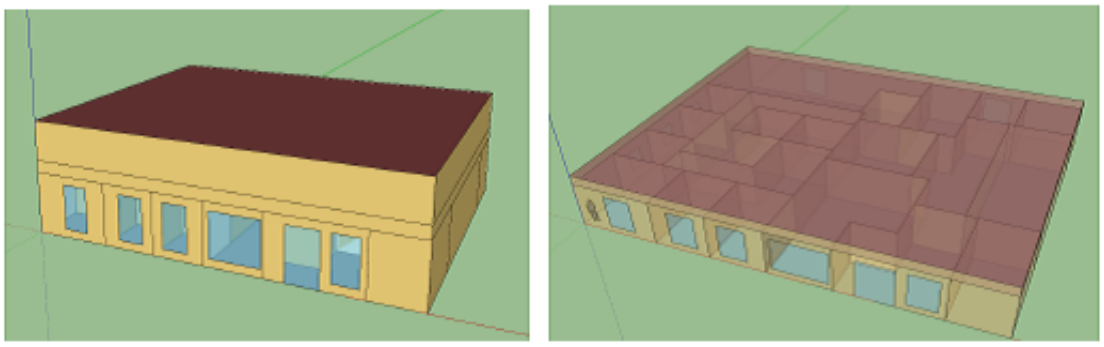

Figure 5.40: Rendering of the building showing thermal zones (Lavigne et al., 2014)

Figure 5.41: Thermal zones of the building (Lavigne et al., 2014)

5.4.2 EnergyPlus Model

In order to analyze and predict the impact of different DR strategies applied to the building, a detailed calibrated model was needed developed (Lavigne et al., 2014). The model had to be able to capture the daily power profile behavior

during peak days. The total electric power demand on 15-minute intervals metered between 2011 and 2013 was provided, but no sub-metering or operation data from the BAS were available. It was decided to use data of one summer week, one winter week and one shoulder season week for the calibration process. Measured profiles during these weeks should follow a predictable pattern and cover different weather conditions. The selection of relatively short calibrating periods also has the advantage of reducing running time and the amount of data generated when launching parametric runs.

An "Initial" EnergyPlus model was created for the building and a manually adjusted model was created from this initial model to better match the measured electricity data. Figure 5.42 shows the results for three days in winter (Sunday, Monday and Tuesday). The load shown is for the entire building, including heating, cooling, plug loads, lighting etc. The days are Sunday January 23 to Tuesday January 25 in the year 2011. The first ("Initial") building simulation model was completed in the SIMEB (Hydro-Québec, 2015b) software to which the geometry was imported. SIMEB is a user interface for the building simulation softwares DOE and EnergyPlus. The mechanical and electrical drawings provided comprehensive imformationinformation about light density, maximum and minimum airflow rates, terminal reheat and baseboard rated capacities. SIMEB default values were used for plug loads and infiltration rates. Those values are based on the default assumptions in the performance compliance method of MNECB (1997). The SIMEB simulation results were compared with 15-min. interval metered data from January 1st, 2011 to October 10th, 2013. Some of the differences observed can be attributed to limitations of the SIMEB interface. For example, the SIMEB schedules are built on a one-hour timestep basis, smaller time increments cannot be implemented. In addition, all zones served by the same HVAC system must have the same zone heating equipment, etc. These differences were correctedly manually in the EnergyPlus input file (.idf). The Initial EnergyPlus model of the

building underestimates the building demand, therefore an optimization model was necessary. First, the assisted calibration module in the SIMEB software aided in identifying influential parameters. The module has a pre-calibration routine that identifies potential problematic parameters based on monthly bill differences. Combining this information with the level of uncertainty on certain simulation parameters, the following parameters were identified for calibration: minimum outside air of two rooftop units, static pressure rise of two rooftop units, infiltration airflow of perimeter zones, plug load density of three major zones and insulation thickness of exterior walls and roof. After parametric runs were performed to evaluate the influence of these parameters, it was found that the minimum outside air had the most important impact on the results during the heated occupied periods. However, each of the parameters had a different impact on the results depending on weather conditions and occupancy periods. An optimized "calibrated" EnergyPlus model was then created using the optimization tool GenOpt (Wetter, 2010)an optimization package developed by the LBNL DOE laboratory. The objective function to be minimized was defined as the coefficient of variation of the root mean square error (CV-RMSE) between the 15-minute time interval metered data and the model results for the whole year of 2011. Since all parameters were influential at one point, they were selected for the optimization processes and constrained with physically feasible minimum and maximum values. Two different algorithms were used, a genetic algorithm and generalized pattern search and gave relatively the same results for each parameter value. Figure 5.43 shows results of the calibrated model. Further information regarding the building, the Energy Plus model and optimization procedure refer to (Lavigne et al., 2014).

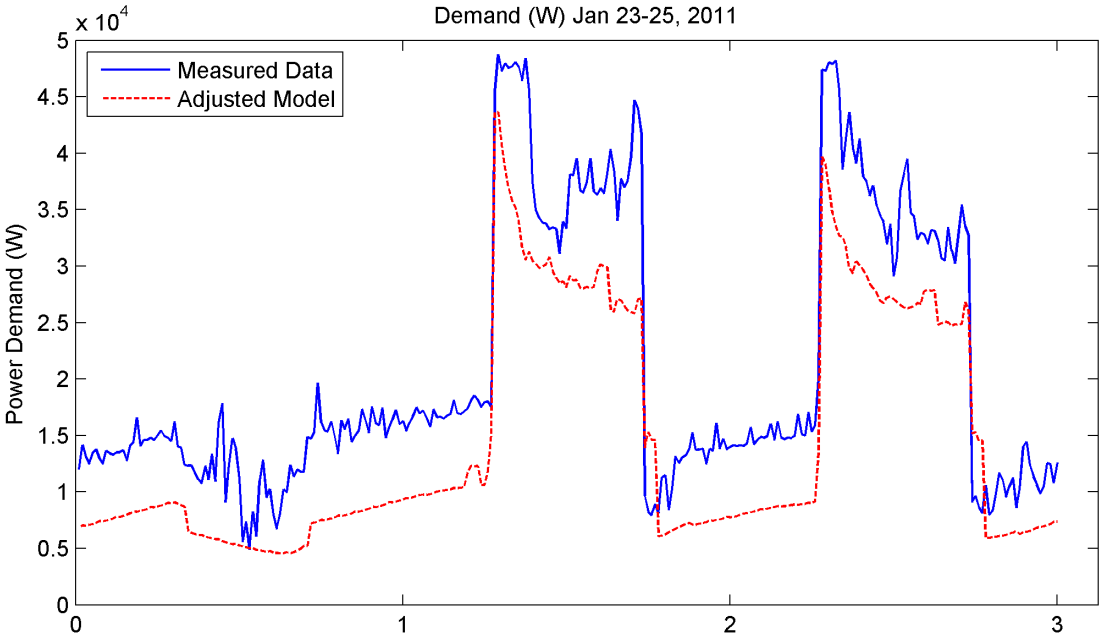

Figure 5.42: Measured data and adjusted energy plus model

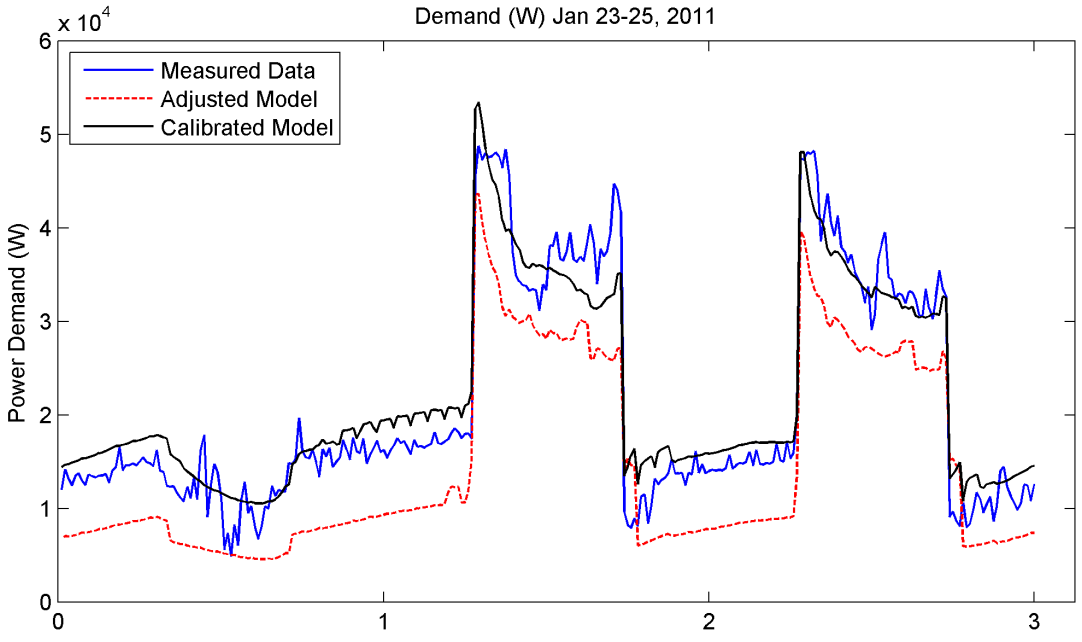

Figure 5.43: Measured data vs. adjusted and calibrated energy plus model

The model was calibrated with the measurement of total power consumption of the building at 15 minute intervals for the year 2011. The normal error (NMBE) and the regression coefficient of the squared error (CVRMSE) of the calibrated

model are below the limits specified by the ASHRAE 14-2002 guideline for a time interval, as shown in Table 5.24.

Table 5.24: Statistical indices of the calibrated model

	CV-RSME	**NMBE**
Initial E+ Model	34.6%	-7.6%
Adjusted E+ Model	30.9%	-11.1%
Calibrated E+ Model	17.3%	-1%
Guideline 14-2002 Limit	30%	10%

5.4.3 Thermal Network of Building for Finite Difference Model

Figure 5.44 shows the thermal network used for an explicit finite difference analysis of the building. The building consists of four exterior walls, a roof and a slab on grade flooring, as well as many interior wall partitions creating 21 zones within the building. For the explicit finite difference model, the building is initially modelled as a single zone with four capacitances (one for the air, one for the exterior walls and roof and two for the concrete floor slab). The effect of solar radiation on the behaviour of the building was also incorporated into the model and it is assumed that 50% of solar radiation transmitted through the windows hits the floor while the other 50% hit the other 5 interior surfaces. It is also assumed there is a carpet over the concrete floor slab.

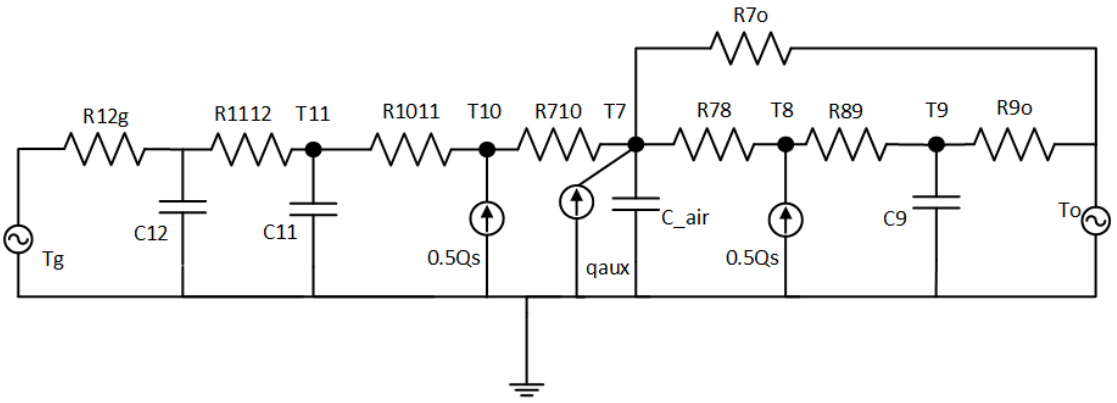

T7 – Indoor air temperature
T8 – Walls, ceiling surfaces
T9 – ½ into gypsum board
T10 – Floor surface (assume carpeted)
T11 – ½ into gypsum board
R7o – Window and infiltration
Ti – Adjacent room temperature
To – Outdoor temperature

C_air – Air thermal capacitance
C9 – Capacitance of walls and ceiling
C11 – Capacitance of ½ concrete floor
C12 – Capacitance of ½ concrete floor

Figure 5.44: Thermal network of the building

Table 5.25 shows the building properties and Table 5.26 depicts model parameters, which can be adjusted for further calibration. Table 5.27 shows the building operating schedules provided by the building owner as a reference for the heating schedule for the building.

Table 5.25: Building component R-values

Building Component	**R-value** $(m^2K/watt)$	**Area** (m^2)
Walls	3.0	231.5
Roof	3.45	425.5
Floor	0.59	425.5
Windows	0.33	21.6

Table 5.26: Initial model parameters

Parameter	Value
Ground temperature	13°C
infiltration	0.35 ach
C_air	62,293,200 J/K (40x)
C9 (walls & roof)	6,286,376 J/K
C11 (concrete floor)	74,888,000 J/K
C12 (concrete floor)	74,888,000 J/K
qaux	50 kW
Kp	25,000 W/K
Time step	15 sec

Table 5.27: Typical building operating schedules

Day	Occupancy	HVAC operation	Lighting operation
Mon-Tue	8:30 to 17:00	7:00 to 17:30	8:00 to 17:30
Wed-Thur	8:30 to 20:00	7:00 to 20:30	8:00 to 20:30
Friday	8:30 to 16:00	7:00 to 20:30	8:00 to 16:30
Saturday	8:30 to 15:00	7:00 to 15:30	8:00 to 15:30
Sunday	Unoccupied	Off	Off

Results of Initial Finite Difference Model

Simulations with the explicit finite difference method were done for 14 days starting on January 23, 2011. The set point during occupied times was set at 23°C and unoccupied times it was set at 18°C. Figure 5.45 shows four days (one unoccupied Sunday and three weekdays) from January 23 to 26, 2011. The model shows some correlation between the model and measured data during unoccupied times (Sunday and nights), but the daytime demand from the finite difference model

does not match the measured data. One possible reason for this discrepancy is assuming a constant value for air infiltration from outside. In the next step a variable infiltration will be implemented with different values for occupied and unoccupied times.

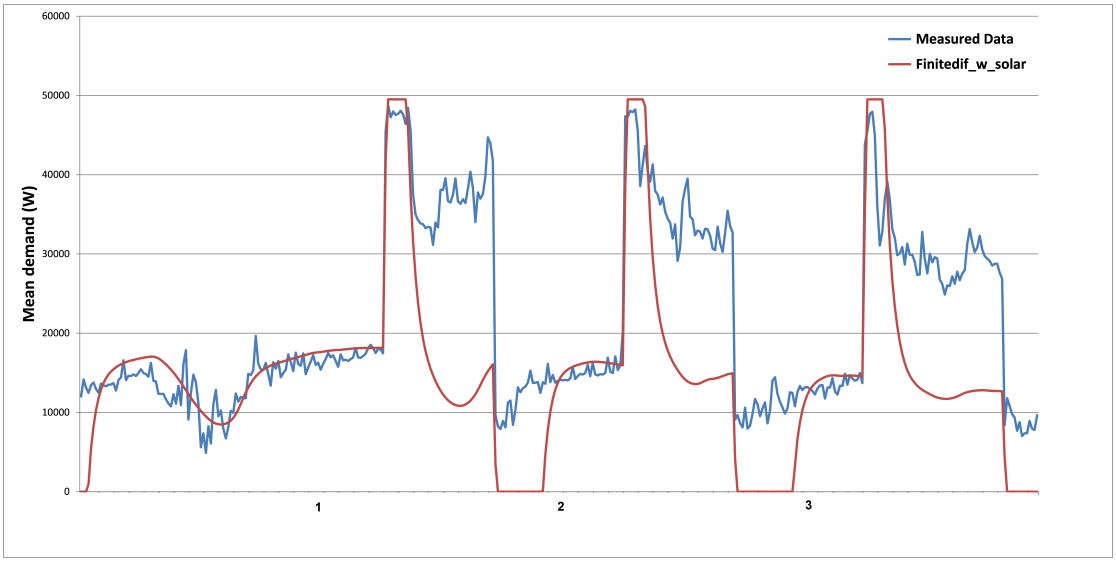

Figure 5.45: January 23-26, 2011 - whole building consumption initial results

Results of Model with Variable Infiltration

A second model was created that has different values of infiltration for occupied and unoccupied times, shown in Table 5.28. The model parameters suggest that there is more infiltration during occupied times compared to unoccupied times. Possible reasons for higher infiltration values during occupied times are that the entrance doors are being opened and closed more often, fresh air intake to maintain proper CO_2 levels, or more infiltration through the heating system ducting in order to maintain the higher set point.

Table 5.28: Variable model parameters

Winter Season	**Occupied**	**Unoccupied**
Parameter	**Value**	**Value**
Temperature set point	23°C	18°C
Ground temperature	20°C	20°C
infiltration	1.5 ach	0.4 ach
C_air	10,901,000 J/K (7x)	10,901,000 J/K (7x)
C9 (walls and roof)	6,286,376 J/K	6,286,376 J/K
C11 (concrete floor)	74,888,000 J/K	74,888,000 J/K
C12 (concrete floor)	74,888,000 J/K	74,888,000 J/K
qaux	50 kW	50 kW
Kp	50,000 W/K	50,000 W/K
Time step	15 seconds	15 seconds

Figure 5.46 shows the results of the finite difference model with variable infiltration. There are still some areas to improve, such as when the temperature set point drops from 23°C to 18°C at the end of the day. However, when looking at the NMBE and the CVRMSE of the finite difference model, in Table 5.29, the results satisfy the ASHRAE 14-2002 guideline for the one week winter period.

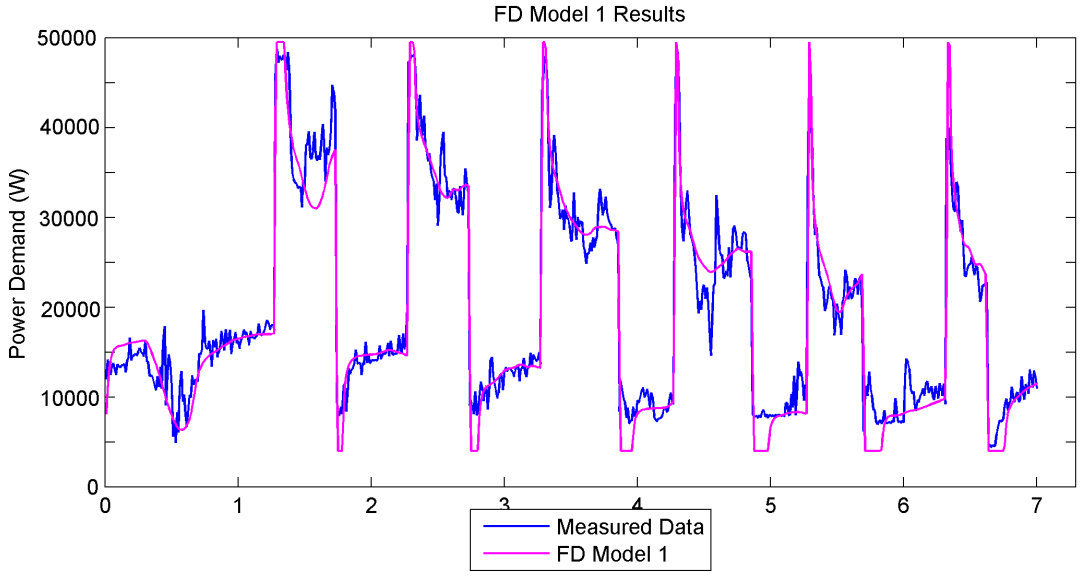

Figure 5.46: Variable finite difference model results

Table 5.29: Statistical indices of variable finite difference model - W-06 only (winter week)

	CV-RSME	NMBE
Adjusted E+ Model	30.5%	-26.6%
FD Variable Infiltration	13.3%	-2.9%
Calibrated E+ Model	13.6%	-1.2%
Guideline 14-2002 Limit	30%	10%

Table 5.30: Thermal network parameters

Parameter	Value
R78	0.000174 °C/W
R89	0.0000618 °C/W
R9o	0.0047 °C/W
R7o	0.0042 / 0.0014 °C/W
R710	0.0010 °C/W
R1011	0.0000618 °C/W
R1112	0.000124 °C/W
R12g	0.0000618 °C/W
C_air	10,901,000 J/K (7x)
C9	6,286,376 J/K
C11	78,888,000 J/K
C12	78,888,000 J/K
qaux	50 kW
Kp	25 kW/K

As can be seen, the variable finite difference model performed for the two weeks of January 23 to February 6, 2011 satisfies the ASHRAE 14-2002 calibration guideline. The values of the thermal network parameters are shown in Table 5.30. Further improvements can be done by optimizing the thermal network parameters, improving the accuracy of the heater control etc, but this demonstrates well that a simple RC thermal network model can adequately predict thermal behaviour for this type of building in these weather conditions.

5.4.4 Finite Difference Model with Variable Infiltration and Interior Partitions Included

The finite difference model presented in section 5.4.3 neglected to incorporate the thermal mass present in the interior partition walls, in the form of gypsum board, making an assumption that these partitions do will not significantly affect the model behaviour and accuracy. There is a significant area of interior walls (360 m^2), so it was decided to create another model incorporating this mass for comparison. Figure 5.47 depicts the adjusted thermal network to include the interior walls and Table 5.31 lists the thermal network parameter values.

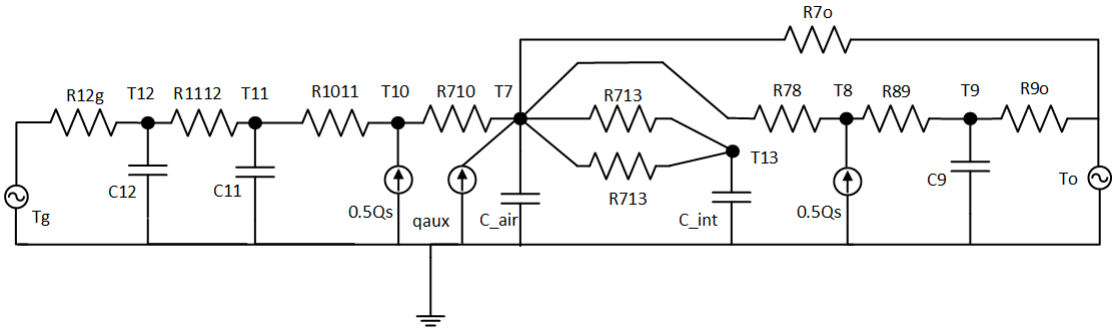

T7 – Indoor air temperature
T8 – Walls, ceiling surfaces
T9 – ½ into gypsum board
T10 – Floor surface (assume carpeted)
T11 – ½ into gypsum board
T11 – ½ into interior partitions
R7o – Window and infiltration
Ti – Adjacent room temperature
To – Outdoor temperature

C_air – Air thermal capacitance
C9 – Capacitance of walls and ceiling
C11 – Capacitance of ½ concrete floor
C12 – Capacitance of ½ concrete floor
C_int – Interior partitions (gypsum board in walls)

Figure 5.47: Thermal network representing the bank building incorporating interior partitions

Table 5.31: Revised thermal network parameters

Parameter	Value
R78	0.000174 °C/W
R89	0.0000618 °C/W
R9o	0.0047 °C/W
R7o	0.0042 / 0.0014 °C/W
R710	0.0010 °C/W
R1011	0.0000618 °C/W
R1112	0.000124 °C/W
R12g	0.0000618 °C/W
C_air	10,901,000 J/K (7x)
C9	6,286,376 J/K
C11	78,888,000 J/K
C12	78,888,000 J/K
qaux	50 kW
Kp	25 kW/K
Cint	0.000135 J/K
R713	0.000135 °C/W

Figure 5.48 shows one day results for the two finite difference models. As is expected, the model with interior partitions has a lag as it takes longer to reach the set point when there is more thermal mass in a zone. Figure 5.49 shows several days of model results, and again, this model also satisfies ASHREA Guideline 14-2002, as seen in Table 5.32.

Now that a model exists with the interior partitions included, retrofit feasibility studies can be done (such as incorporating phase change materials as thermal mass into the walls).

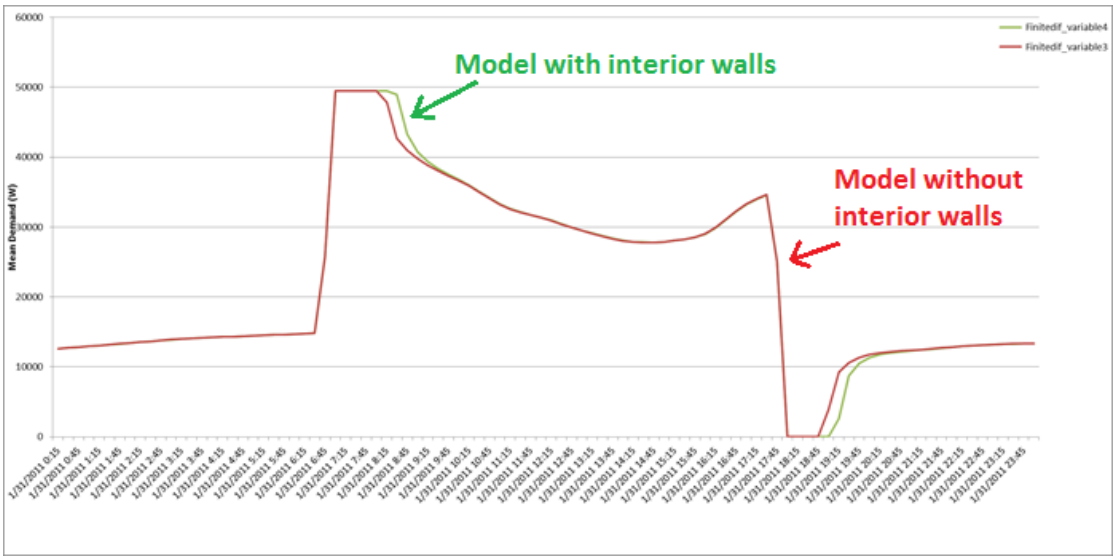

Figure 5.48: Comparison of model without interior partitions to model incorporating interior partitions

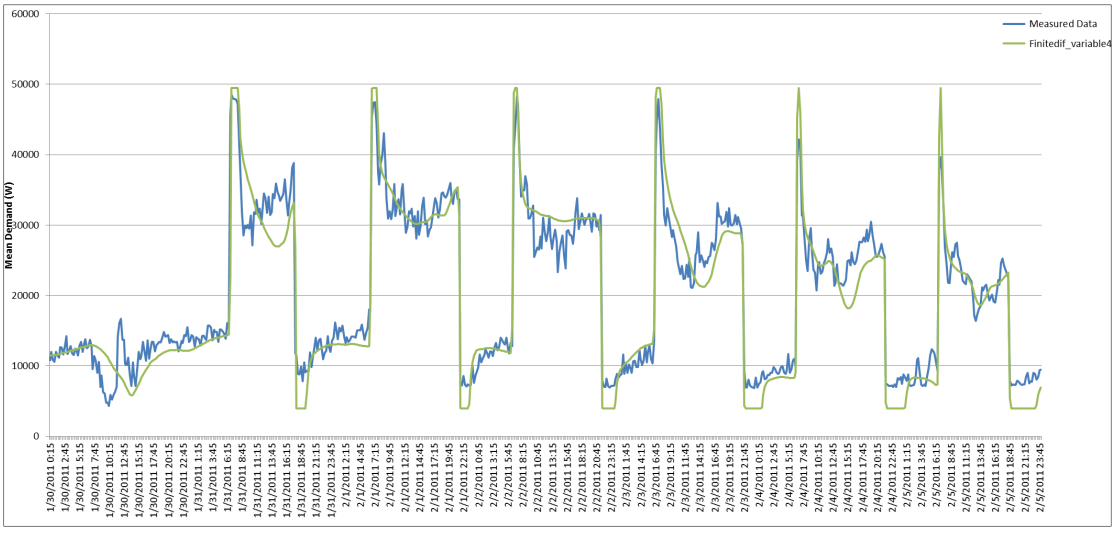

Figure 5.49: model with interior partitions and measured data

Table 5.32: Statistical indices of model with interior partitions

	CV-RSME	NMBE
FD Variable Infiltration with Interior Partitions	14.1%	-2.8%
FD Variable Infiltration	13.3%	-2.9%
Calibrated E+ Model	13.6	-1.2%
Guideline 14-2002 Limit	30%	10%

5.4.5 Demand Response: Ramping Set Point Strategies

Preliminary "demand response" strategies have been investigated and results are shown in this section. The strategies studied are applying different types of temperature set point schedules to the building, with the purpose of reducing energy consumption and electrical peaks during peak hours, and at the same time maintaining adequate thermal comfort conditions for the building occupants. Peak hours happen in the weekday mornings between 6-9am and at night between 4-8pm. The day of January 24, 2011 was taken for the analysis as outdoor temperatures reached below -25°C, shown in Figure 5.50 (Lavigne et al., 2014). Figure 5.51 shows the standard set point schedule along with the optimized temperature set point previously determined in (Lavigne et al., 2014). The strategy is similar to the one implemented by Hydro Québec which was found using multi objective function optimization. In the previous, more detailed DR investigation using the EnergyPlus model, (Lavigne et al., 2014), along with global temperature adjustment, modifications were also done to the performance of the rooftop units and the fresh air intake. Due to the simple nature of the finite difference model presented here, only global temperature adjustment strategies have been looked into at this time.

Demand Reduction Indicators

Demand reduction indicators were computed to quantitatively compare the resulting demand profiles over peak periods with the reference scenario. The possible demand rebound at the end of the set point strategies could also create new peaks, but at a different time. The demand impact of the few hours following the peak period was thus of interest. Results were first averaged of 15 minute interval, the timebase used for demand metering.

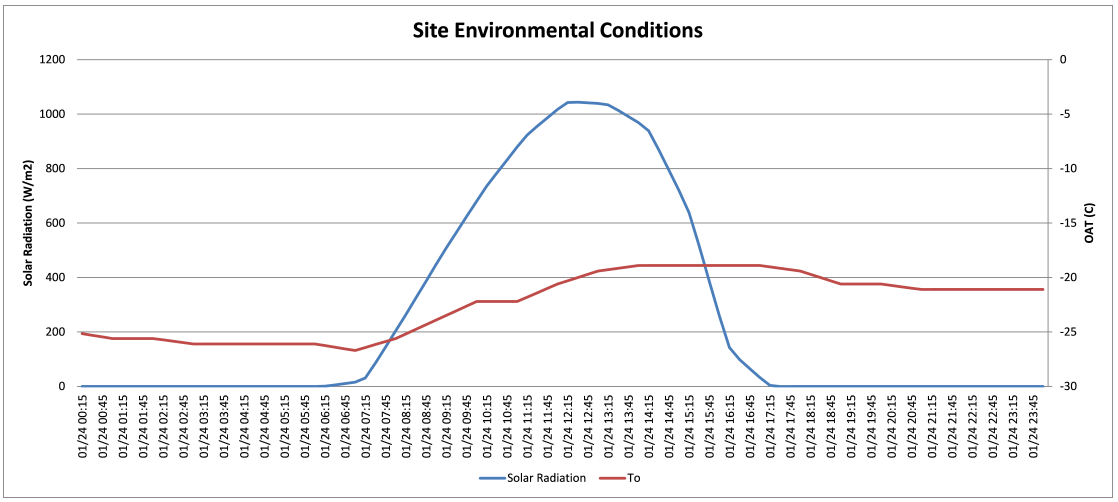

Figure 5.50: January 24, 2011 environmental conditions

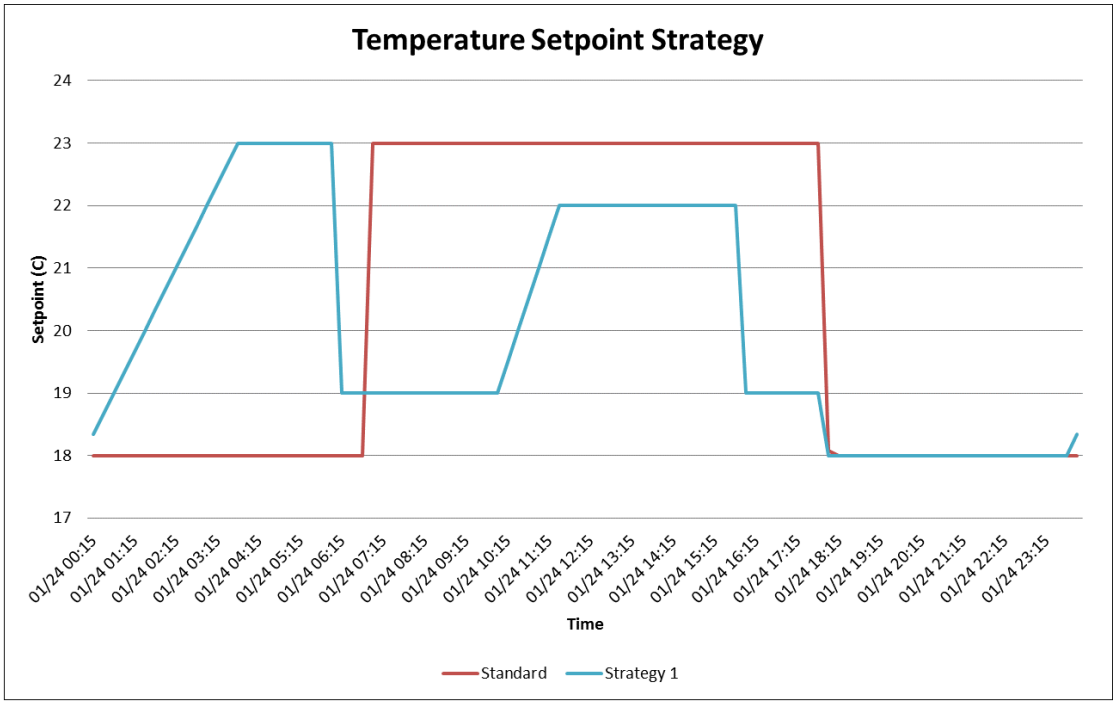

Figure 5.51: Thermostat ramp set point strategy

Figure 5.52 shows the daily power demand profile for the demand response strategy using the two finite difference models presented in sections 5.4.3 and 5.4.4. As can be seen, the strategy is successful in reducing the morning peak by up to 28%. The rebound time after the peak hours is also not negatively affected.

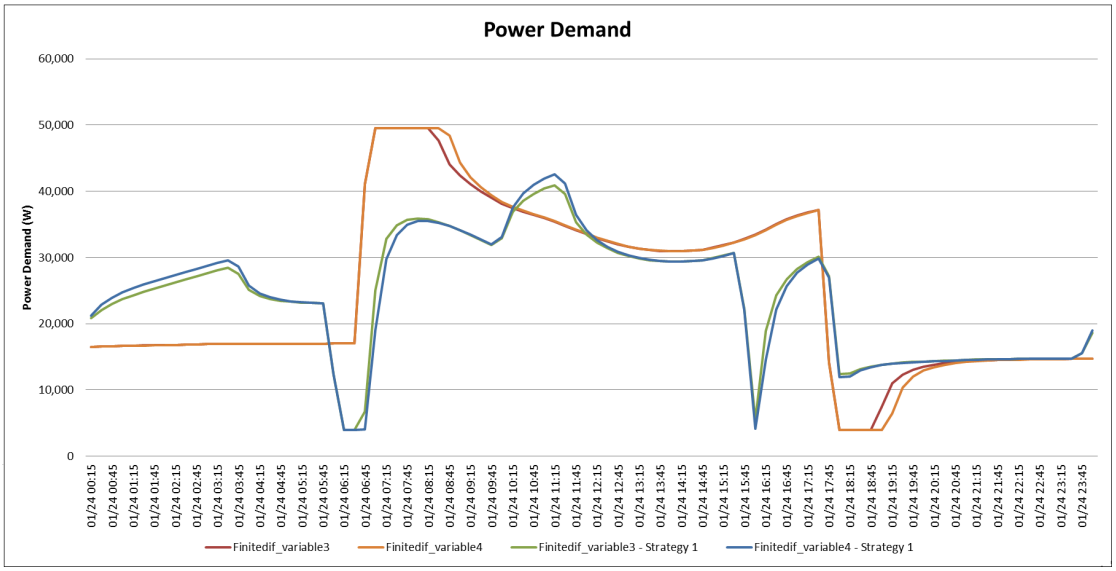

Figure 5.52: Power demand of the DR ramping strategies

Table 5.33 lists the demand reduction impacts of strategy 1 when compared to the standard operating temperature set point schedule. By implementing an alternative temperature profile over the 24 hour period, the building electricity peak was reduced by 14%, while overall consumption was reduced by 3%, morning peak was reduced by 28% and the afternoon peak was reduced by 20%. Rebound times were also not greatly affected. This shows that a simple strategy can have positive results for demand response on extreme climatic winter days.

Table 5.33: Impact of ramping strategies on power demand

		Model without interior walls			Model with interior walls		
		Baseline	Strategy 1		Baseline	Strategy 1	
		[W]	Demand [W]	Impact [%]	[W]	Demand [W]	Impact [%]
Building peak		49,500	40,925	**-17%**	49,500	42,550	**-14%**
AM	q_{am}^{max}	49,500	35,925	**-27%**	49,500	35,530	**-28%**
	$\overline{q}_{am}$	42,190	26,586	**-37%**	42,868	25,357	**-41%**
	$rebound_{am}$	38,123	35,805	**-6%**	38,508	36,450	**-5%**
PM	q_{pm}^{max}	37,207	30,117	**-19%**	37,141	29,870	**-20%**
	$\overline{q}_{pm}$	42,190	26,586	**-37%**	18,166	18,534	**2%**
	$rebound_{pm}$	14,301	14,541	**2%**	14,177	14,531	**2%**
Building daily consumption [kWh]		599	583	**-3%**	599	584	**-2%**

Chapter 6

Conclusions

In this thesis, modelling resolution for the purpose of space heating load predictions in a residential and commercial building has been investigated. There was a focus on simple and physically meaningful building thermal models. Experiments were conducted at two highly instrumented houses and equivalent RC network thermal models for the purpose of model based control were developed for a north zone in the houses. Through experimentation and simulation, peak power (due to space heating) reduction strategies were investigated. Conclusions are that the simple three capacitance model is effective in capturing the heat transfer phenomena in the low mass zone, while the detailed 13 capacitance model shows slightly better results, making the three capacitance model suitable for use in model based control.

For the different set point profiles incorporating ramping strategies, it was found that the relative impact is that doubling the ramp duration from 1 to 2 hours approximately doubles the peak reduction. Optimal transition curves do not significantly out perform ramps due to the low mass of the zone. Optimal transition curves are better suited for higher mass buildings.

When comparing zones with different levels of thermal mass, thickness and conductivity plan an important role in the room thermal dynamics and behavior.

As thickness and conductivity increase, the peak reduction is reduced, however, the temperature decay time is increased. From the study it can be generally concluded that increasing the thickness, while maintaining the conductivity level gives the best compromise between peak reduction and temperature decay time. A longer temperature decay time means that there is a delay in when the heater will turn on again to maintain the night time set back temperature set point.

A low order model was then used on a case study of a small commercial building and the model was able to meet calibration standards for the current operating conditions of the building. The current model may not be suitable if changes occurred to the amount and schedule of fresh air intake. Two low order RC thermal network configurations were compared when modelling an occupied commercial building used as a bank. The first model did not include the mass of the interior partitions, making an assumption that the interior partitions do not significantly affect the results of the model. The second model incorporated the interior partitions and it was seen that both the models sufficiently capture the thermal behaviour of the building and meet calibration standards. An advantage of the model with interior partitions is that it can be used in future retrofit feasibility studies (such as incorporating phase change material as thermal mass into the interior partitions).

6.1 Summary of Contributions

1. Several RC thermal network models of varying detail have been created for a zone in the EHBE facility. Low order thermal network models developed are shown to be suitable for control-oriented modelling.

2. Investigation of simple peak power reduction strategies that could be implemented into real residential buildings or other convectively heated buildings.

3. Investigation of a commercial building and viability of using simplified RC thermal network models.

6.2 Recommendations for Future Work

1. Create further models of the EHBE, including a whole building model, a south zone and a basement zone, to be used in further studies.

2. Continue studies on simplified models for building control applications. Develop adequate MPC models for buildings to optimize energy efficiency, thermal comfort, demand reduction etc.

3. Further experimental research using real life scenario of winter peak environmental conditions and realistic thermostat set points using different building types.

4. Continue modelling studies using different heating sources such as forced air, radiant floor heating etc., and also for cooling season. Continue modelling studies for zones of different levels of thermal mass (low mass, medium mass and heavy mass).

5. Study the integration and control of active solar energy systems in buildings by using model based control. Optimized operation of active solar systems and low energy buildings can be highly beneficial in reducing energy consumption, peak loads and increasing thermal comfort for the occupants.

6. Statistical analysis of large scale databases of building simulation models may allow the identification of archetypal thermal networks, and determine correlations between the building geometry and material properties and the corresponding RC parameters.

7. A systematic approach should be developed for the identification of simplified building models, possibly in conjunction with a frequency domain approach. The frequency domain approach may help to systematically select model resolution and also possibly the ramping rates for a given building construction.

8. Further Bank Building studies including summer peak demand reduction and load shifting.

List of References

Abadie, M., de Camargo, M., Mendonça, K., & Blondeau, P. (2012). Improving the prediction of zonal modeling for forced convection airflows in rooms. *Building and Environment*, *48*(0), 173 – 182.

Ali, M., Jokisalo, J., Siren, K., & Lehtonen, M. (2014). Combining the demand response of direct electric space heating and partial thermal storage using {LP} optimization. *Electric Power Systems Research*, *106*(0), 160 – 167.

ASHRAE (2005). *ASHRAE Handbook of fundamentals*. American Society of Heating Refrigerating and Air-Conditioning Engineers Inc.

Athienitis, A., Chandrashekar, M., & Sullivan, H. (1985). Modelling and analysis of thermal networks through subnetworks for multizone passive solar buildings. *Applied Mathematical Modelling*, *9*(2), 109 – 116.

Athienitis, A., & O'Brien, W. (2015). *Modelling, Design, and Optimization of Net-Zero Energy Buildings*. Wiley.

Athienitis, A., Stylianou, M., & Shou, J. (1990). Methodology for building thermal dynamics studies and control applications. *ASHRAE Transactions*, (pt 2), 839 – 848.

Athienitis, A., Sullivan, H., & Hollands, K. (1986). Analytical model, sensitivity analysis, and algorithm for temperature swings in direct gain rooms. *Solar Energy*, *36*(4), 303 – 312.

Athienitis, A., Sullivan, H., & Hollands, K. (1987). Discrete fourier series models for building auxiliary energy loads based on network formulation techniques. *Solar Energy*, *39*(3), 203 – 210.

Athienitis, A. K. (1994). *Building thermal analysis*. Boston,MA: MathSoft Inc.

Athienitis, A. K., & Santamouris, M. (2002). *Thermal Analysis and Design of Passive Solar Buildings*. London, UK: James & James.

B. Lachal, O. G., W. U. Weber (1992). *Simplified methods for the thermal analysis of multifamily and administrative buildings*. GA (USA): .

Bacher, P., & Madsen, H. (2011). Identifying suitable models for the heat dynamics of buildings. *Energy and Buildings*, *43*(7), 1511 – 1522.

Bekey, G. A. (1970). System identification- an introduction and a survey. *SIMULATION*, *15*(4), 151–166.

Bonneau, D., Rongere, F., Covalet, D., & Gauthier, B. (1993). Clim2000: modular software for energy simulation in buildings. In *Proceedings of IBPSA 1993*. Adelaide, Australia.

Bouia, H., & Dalicieux, P. (1991). Simplified modelling of air movements inside dwelling room. In *Proceedings of building simulation 91 conference, IBPSA (The International Building Performance Simulation Association)*. Nice, France.

Braun, J. E. (1990). Reducing energy costs and peak electrical demand through optimal control of building thermal storage. *ASHRAE Transactions*, (pt 2), 876 – 888.

Braun, J. E., & Lee, K.-H. (2006). Assessment of demand limiting using building thermal mass in small commercial buildings. *ASHRAE Transactions*, *112 PART 1*, 547 – 558.

BuildOpt-VIE (2015). Buildopt-vie. Available at `www.bph.tuwien.ac.at`.

Callaway, D., & Hiskens, I. (2011). Achieving controllability of electric loads. *Proceedings of the IEEE*, *99*(1), 184–199.

Camacho, E., & Bordons, C. (2004). *Model Predictive Control*. London, UK: Springer.

Candanedo, J., & Athienitis, A. (2010). Simplified linear models for predictive control of advanced solar homes with passive and active thermal storage. In *Proceedings of Internationl High Performance Building Conference*.

Candanedo, J. A., Allard, A., & Athienitis, A. K. (2010). Predictive Control of Radiant Floor Heating and Transmitted Irradiance in a Room with High Solar Gains.

Candanedo, J. A., Dehkordi, V. R., & Lopez, P. (2013). A control-oriented simplified building modelling strategy. In *Proceedings of BS 2013- 13th Conference of International Building Performance Simulation Association*, (pp. 3682 – 3689). Chambery, France.

Candanedo, J. A., Dehkordi, V. R., Saberi-Derakhtenjani, A., & Athienitis, A. K. (2015). Near-optimal transition between temperature setpoints for peak load reduction in small buildings. *Energy and Buildings*, *87*(0), 123 – 133.

Chen, Y., Athienitis, A. K., & Galal, K. E. (2013). Frequency domain and finite difference modeling of ventilated concrete slabs and comparison with field measurements: Part 1, modeling methodology. *International Journal of Heat and Mass Transfer*, *66*(0), 948 – 956.

Cigler, J., Tomasko, P., & Siroky, J. (2013). BuildingLAB: A tool to analyze performance of model predictive controllers for buildings. *Energy and Buildings*, *57*, 34–41.

COMSOL (2015). COMSOL Multiphysics. Available at `/http://www.comsol.com/`.

CRA (2005). Impact evaluation of the california statewide pricing pilot, prepared for the california energy commission. Available at `http://sites.energetics.com/madri/toolbox/pdfs/pricing/cra_2005_impact_eval_ca_pricing_pilot.pdf`.

Deb, K., Pratap, A., Agarwal, S., & Meyarivan, T. (2002). A fast and elitist multiobjective genetic algorithm: NSGA-II. *IEEE Transactions on Evolutionary Computation*, *6*(2), 182–197.

Deng, K., Goyal, S., Barooah, P., & Mehta, P. G. (2014). Structure-preserving model reduction of nonlinear building thermal models. *Automatica*, *50*(4), 1188 – 1195.

DOE (2013). EnergyPlus engineering reference - the reference to EnergyPlus calculations (in case you want or need to know). US Department of Energy.

EIA (2005). Residential energy consumption survey: preliminary housing characteristics tables. Available at `http://www.eia.gov/consumption/residential/`.

EnergyPlus (2015). U.S. Department of Energy (DOE). Available at `/http://www.eere.energy.gov/buildings/energyplus`.

ESP-r (2015). Available at `http://www.esru.strath.ac.uk/Programs/ESP-r.htm`.

FLUENT (2015). Available at `/http://www.ansys.com`.

Foucquier, A., Robert, S., Suard, F., Stéphan, L., & Jay, A. (2013). State of the art in building modelling and energy performances prediction: A review. *Renewable and Sustainable Energy Reviews*, *23*(0), 272 – 288.

Fournier, M., & Leduc, M.-A. (2014). Study of electrical heating setpoint modulation strategies for residential demand response. In *Proceedings of eSim Conference 2014*. Ottawa, Ontario.

Fraisse, G., Viardot, C., Lafabrie, O., & Achard, G. (2002). Development of a simplified and accurate building model based on electrical analogy. *Energy and Buildings*, *34*(10), 1017 – 1031.

Gillespie, K. L., Cowan, J. D., Frazell, C. W., Haberl, J. S., Heinemeier, K. H., Kummer, J. P., Culp, C. H., Watson, T. E., Arnold, C. G., Baxter, V. D., Evans, R. a., Hogan, J. F., Kohloss, F. H., & Montgomery, R. D. (2002). Measurement of Energy and Demand Savings. *8400*, 170.

Goyal, S., & Barooah, P. (2012). A method for model-reduction of non-linear thermal dynamics of multi-zone buildings. *Energy and Buildings*, *47*(0), 332 – 340.

Goyal, S., Ingley, H. A., & Barooah, P. (2013). Occupancy-based zone-climate control for energy-efficient buildings: Complexity vs. performance. *Applied Energy*, *106*(0), 209 – 221.

Gunay, H. B., O'Brien, W., Beausoleil-Morrison, I., & Perna, A. (2014). On the behavioral effects of residential electricity submetering in a heating season. *Building and Environment*, *81*(0), 396 – 403.

Haghighat, F., & Athienitis, A. (1988). Comparison between time domain and frequency domain computer program for building energy analysis. *Computer-Aided Design*, *20*(9), 525 – 532.

Hazyuk, I., Ghiaus, C., & Penhouet, D. (2012). Optimal temperature control of intermittently heated buildings using model predictive control: Part {II} – control algorithm. *Building and Environment*, *51*(0), 388 – 394.

Hendron, B., & Engebrecht, C. (2010). Building america house simulation protocols. Available at `http://www.nrel.gov/docs/fy11osti/49246.pdf`.

Henze, G., Dodier, R., & Krarti, M. (1997). Development of a Predictive Optimal Controller for Thermal Energy Storage Systems. *HVAC&R Research*, *3*(3), 233–264.

Henze, G., Kalz, D., Liu, S., & Felsmann, C. (2005a). Experimental Analysis of Model-Based Predictive Optimal Control for Active and Passive Building Thermal Storage Inventory. *HVAC&R Research*, *11*(2), 189–213.

Henze, G. P., Kalz, D. E., Liu, S., & Felsmann, C. (2005b). Experimental analysis of model-based predictive optimal control for active and passive building thermal storage inventory. *HVAC&R Research*, *11*(2), 189–213.

Herter, K., McAuliffe, P., & Rosenfeld, A. (2007). An exploratory analysis of california residential customer response to critical peak pricing of electricity. *Energy*, *32*(1), 25 – 34.

Huebner, G. M., Cooper, J., & Jones, K. (2013). Domestic energy consumption—what role do comfort, habit, and knowledge about the heating system play? *Energy and Buildings*, *66*(0), 626 – 636.

Hydro-Québec (2013). Rapport annual (annual report) 2013. Available at `/http://www.hydroquebec.com/publications/fr/index.html`.

Hydro-Québec (2015a). Rates for Business Customers. Accessed June 2015, Available at `/http://www.hydroquebec.com/business/rates-and-billing/rates/electricity-rates-business-customers/`.

Hydro-Québec (2015b). SIMEB Software. Available at `/https://www.simeb.ca/`.

ICER (2012). Experiences on the regulatory approaches to the implementations of smart meters: annex4 – case study. smart meters in italy. Available at `http://www.icer-regulators.net/portal/page/portal/ICER_HOME/publications_press/ICER_Reports_2009_2012/Reports_Annexes/Annex%204%20-%20Case%20study%20from%20Italy`.

IDA (2015). Accessed January 2015. Available at `http://www.equa.se`.

Ingersoll, J., & Huang, J. (1985). Heating energy use management in residential buildings by temperature control. *Energy and Buildings*, *8*(1), 27 – 35.

International Code Council (2009). International energy conservation code. Accessed January 2015. Available at `http://publicecodes.cyberregs.com/icod/iecc/2009/index.htm`.

IPMVP-Committee (2002). International Performance Measurement & Verification Protocol International Performance Measurement & Verification Protocol. Accessed January 2015. Available at `http://www.nrel.gov/docs/fy02osti/31505.pdf`.

Jazayeri, P., Schellenberg, A., Rosehart, W., Doudna, J., Widergren, S., Lawrence, D., Mickey, J., & Jones, S. (2005). A survey of load control programs for price and system stability. *Power Systems, IEEE Transactions on*, *20*(3), 1504–1509.

Katipamula, S., & Lu, N. (2006). valuation of residential hvac control strategies for demand response programs (symposium papers - ch-06-7 demand response strategies for building systems). *ASHRAE Transactions*, (112(1):535), 1–12.

Keane, D., & Goett, A. (1988). Voluntary residential time-of-use rates: lessons learned from pacific gas and electric company's experiment. *Power Systems, IEEE Transactions on*, *3*(4), 1764–1768.

Kintner-Meyer, M., & a.F. Emery (1995). Optimal control of an HVAC system using cold storage and building thermal capacitance. *Energy and Buildings*, *23*(1), 19–31.

Kummert, M., André, P., & Nicolas, J. (2001). Optimal heating control in a passive solar commercial building. *Solar Energy*, *69, Supplement 6*(0), 103 – 116. {EUROSUN} 2000 Selected Proceedings.

Kummert, M., Andre, P., & Argiriou, A. A. (2006). Comparing control strategies using experimental and simulation results: Methodology and application to heating control of passive solar buildings. *HVAC and R Research*, *12*(3 A), 553 – 575.

Langner, M. R., Henze, G. P., Corbin, C. D., & Brandemuehl, M. J. (2012). An investigation of design parameters that affect commercial high-rise office building energy consumption and demand. *Journal of Building Performance Simulation*, *5*(5), 313–328.

Lavigne, K., Daoud, A., Sansregret, S., & Leduc, M.-A. (2014). Demand response strategies in a small all-electric commercial building in quebec. In *Proceedings of eSim Conference 2014*. Ottawa, Ontario.

LBNL (2006). Demand shifting with thermal mass in large commercial buildings: field tests, simulations and audit. Accessed January 2015. Available at `http://www.smartgridinformation.info/pdf/1873_doc_1.pdf`.

Le Bel, C., & Gelinas, S. (2012). All-electric experimental twin housss: The ultimate demand mangement testing tool. In *Proceedings of The IASTED International Symposium on Power and Energy (PE 2013)*. Marina Del Rey, California.

Le Bel, C., & Handfield, L. (2008). Cold load pick-up algorithms for line-voltage thermostats in a winter climate. (pp. 199 – 203). Baltimore, MD, United states.

Leduc, M.-A., Daoud, A., & LeBel, C. (2011). Developing winter residential demand response strategies for electric space heating. In *Proceedings of 12th Conference of International Building Performance Simulation Association*, (pp. 1111 – 1118). Sydney, NSW, Australia.

Lee, K. H., & Braun, J. E. (2008). Development of methods for determining demand-limiting setpoint trajectories in buildings using short-term measurements. *Building and Environment*, *43*(10), 1755 – 1768.

Lettvin, J., Maturana, H. R., McCulloch, W. S., & Pitts, W. H. (1959). What the frog's eye tells the frog's brain. In *In Proceedings of the Institute of Radio Engineers*, vol. 47, (pp. 1940 – 1951).

Lindén, A.-L., Carlsson-Kanyama, A., & Eriksson, B. (2006). Efficient and inefficient aspects of residential energy behaviour: What are the policy instruments for change? *Energy Policy*, *34*(14), 1918 – 1927.

Ljung, L. (2010). Perspectives on system identification. *Annual Reviews in Control*, *34*(1), 1 – 12.

Lu, N., & Katipamula, S. (2005). Control strategies of thermostatically controlled appliances in a competitive electricity market. In *Power Engineering Society General Meeting, 2005. IEEE*, (pp. 202–207 Vol. 1).

Manning, M. M., Swinton, M. C., Szadkowski, F., Gusdorf, J., & Ruest, K. (2007). The effects of thermostat setback and setup on seasonal energy consumption, surface temperatures, and recovery times at the ccht twin house research facility. *ASHRAE Transactions*, *113 PART 1*, 630 – 641.

McAdams (1959). *Heat Transmission, 3rd ed.*. McGraw-Hill.

Meier, A., Aragon, C., Peffer, T., Perry, D., & Pritoni, M. (2011). Usability of residential thermostats: Preliminary investigations. *Building and Environment*, *46*(10), 1891 – 1898.

MNECB (1997). Canadian commission on building and fire codes, performance compliance for buildings.

Moon, J. W., & Han, S.-H. (2011a). Thermostat strategies impact on energy consumption in residential buildings. *Energy and Buildings*, *43*(2–3), 338 – 346.

Moon, J. W., & Han, S.-H. (2011b). Thermostat strategies impact on energy consumption in residential buildings. *Energy and Buildings*, *43*(2–3), 338 – 346.

NREL (2013). Variability in measured space temperatures in 60 homes. Accessed January 2015. Available at `http://www.nrel.gov/docs/fy13osti/58059.pdf`.

Paris, B., Eynard, J., Grieu, S., & Polit, M. (2011). Hybrid pid-fuzzy control scheme for managing energy resources in buildings. *Applied Soft Computing*, *11*(8), 5068 – 5080.

Paris, B., Eynard, J., Grieu, S., Talbert, T., & Polit, M. (2010). Heating control schemes for energy management in buildings. *Energy and Buildings*, *42*(10), 1908 – 1917.

Peffer, T., Pritoni, M., Meier, A., Aragon, C., & Perry, D. (2011). How people use thermostats in homes: A review. *Building and Environment*, *46*(12), 2529 – 2541.

Persson, T., Nordlander, S., & Rönnelid, M. (2005). Electrical savings by use of wood pellet stoves and solar heating systems in electrically heated single-family houses. *Energy and Buildings*, *37*(9), 920 – 929.

PGE (2004). Direct load control pilot for electric space heat – pilot evaluation and impact measurement. Available at `http://www.nwcouncil.org/media/4499/dlf_waterheat.pdf`.

Pietila, A., Beausoleil-Morrison, I., & Newsham, G. R. (2012). Zero peak housing: Exploring the possibility of eliminating electrical draws from houses during periods of high demand on the electrical grid. *Building and Environment*, *58*(0), 103 – 113.

PNNL (2007). Pacific northwest gridwisetm testbed demonstration projects, part i. Available at `http://www2.econ.iastate.edu/tesfatsi/OlympicPeninsulaProject.FinalReport_pnnl17167.pdf`.

Polly, B., Kruis, N., & Roberts, D. (2011). Assessing and improving the accuracy of energy analysis for residential building.

Pérez-Lombard, L., Ortiz, J., & Pout, C. (2008). A review on buildings energy consumption information. *Energy and Buildings*, *40*(3), 394 – 398.

Reddy, T., Norford, L., & Kempton, W. (1991). Shaving residential air-conditioner electricity peaks by intelligent use of the building thermal mass. *Energy*, *16*(7), 1001 – 1010.

Reddy, T. A. (2006). Literature Review on Calibration of Building Energy Simulation Programs. *ASHRAE Transactions*, *112*(1), 226–240.

RESNET (2006). 2006 mortgage industry national home energy rating systems standards. Accessed January 2015. Available at `http://www.resnet.us/standards/RESNET_Mortgage_Industry_National_HERS_Standards.pdf`.

Reynders, G., Nuytten, T., & Saelens, D. (2013). Potential of structural thermal mass for demand-side management in dwellings. *Building and Environment*, *64*(0), 187 – 199.

Rode, C., & Grau, K. (2011). Whole building hygrothermal simulation model solar house. *ASHRAE Transactions*, *109*, 572 – 582.

Shou, J. (1991). *A computer technique for heating control analysis and application to radiant heating*. Ph.D. thesis, Concordia University, Montreal, Canada.

Statistics Canada (2011a). Households and the environment: Energy use. Accessed January 2015. Available at `http://www.statcan.gc.ca/pub/11-526-s/11-526-s2013002-eng.htm`.

Statistics Canada (2011b). Report of energy supply and demand in canada. Accessed January 2015. Available at `http://www5.statcan.gc.ca/olc-cel/olc.action?objId=57-003-X&objType=2&lang=en&limit=0`.

Åström, K., & Eykhoff, P. (1971). System identification—a survey. *Automatica*, *7*(2), 123 – 162.

Tan, G., & Glicksman, L. R. (2005). Application of integrating multi-zone model with {CFD} simulation to natural ventilation prediction. *Energy and Buildings*, *37*(10), 1049 – 1057.

Tariku, F., Kumaran, M., & Fazio, P. (2008). Thermostat setback effect in whole building performance. In *Building Physics Symposium*. Lueven, Belgium.

Teeter, J., & Chow, M.-Y. (1998). Application of functional link neural network to hvac thermal dynamic system identification. *Industrial Electronics, IEEE Transactions on*, *45*(1), 170–176.

TRNSYS (2015). Available at `/http://www.trnsys.com/`.

Troncoso, R. (1997). A hybrid monitoring-modeling procedure for analyzing the performance of large central chilling plants. vol. 97, (pp. 421–428).

Urban, B., & Gomez, C. (2013). A case for thermostat user models. In *Proceedings of 13th Conference of International Building Performance Simulation Association*. Chambery, France.

Webster, L., & Bradford, J. (2008). M & V Guidelines: Measurement and Verification for Federal Energy. (pp. 1–306).

Wetter, M. (2010). GenOpt: Generic optimization program. Available at `/http://simulationresearch.lbl.gov/GO/index.html`.

Wilhite, H., Nakagami, H., Masuda, T., Yamaga, Y., & Haneda, H. (1996). A cross-cultural analysis of household energy use behaviour in japan and norway. *Energy Policy*, *24*(9), 795 – 803.

Winn, R. C., & Wins, C. B. (1985). Optimal control of auxiliary heating of passive-solar-heated buildings. *Solar Energy*, *35*(5), 419–427.

World Business Council for Sustainable Development (2007). Energy efficiency in buildings: Business realities and opportunities: Summary report. Accessed January 2015. Available at `http://www.c2es.org/docUploads/EEBSummaryReportFINAL.pdf`.

Wurtz, E. (1995). *Three-dimensional modeling of thermal and airflow trans- fers in building using an object-oriented simulation environment [in French]*. Ph.D. thesis, Ecole Nationale des Ponts et Chaussees, France.

Wurtz, E., Mora, L., & Inard, C. (2006). An equation-based simulation environment to investigate fast building simulation. *Building and Environment*, *41*(11), 1571 – 1583.

Yin, R., Xu, P., Piette, M. A., & Kiliccote, S. (2010). Study on auto-dr and pre-cooling of commercial buildings with thermal mass in california. *Energy and Buildings*, *42*(7), 967 – 975.

Appendix A: Monitored Data from Twin Houses

Experiment 1

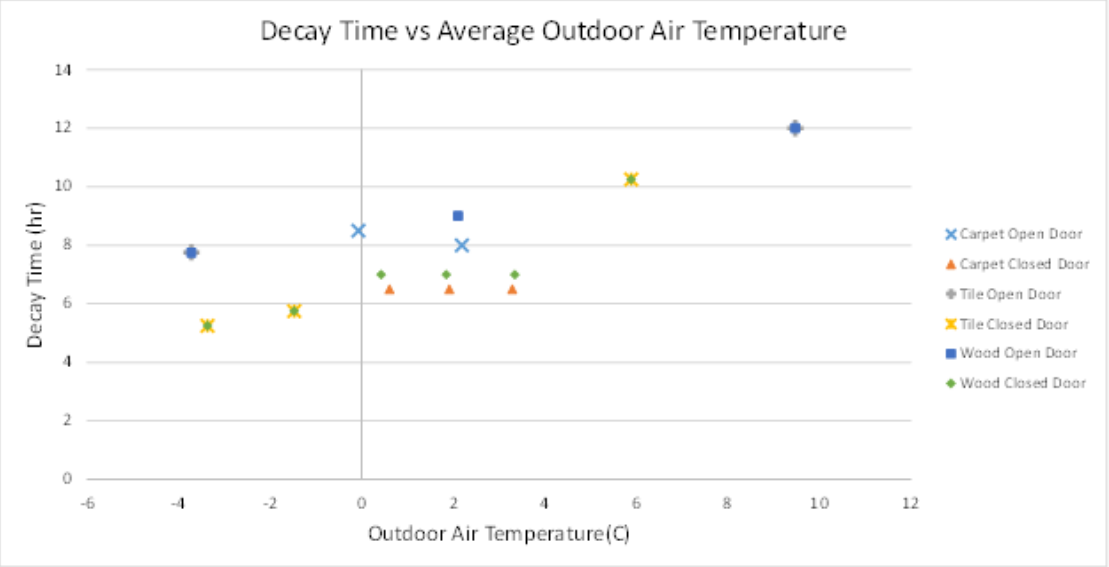

Figure 1: Indoor Temperature Decay Time vs. Average Outdoor Air Temperature

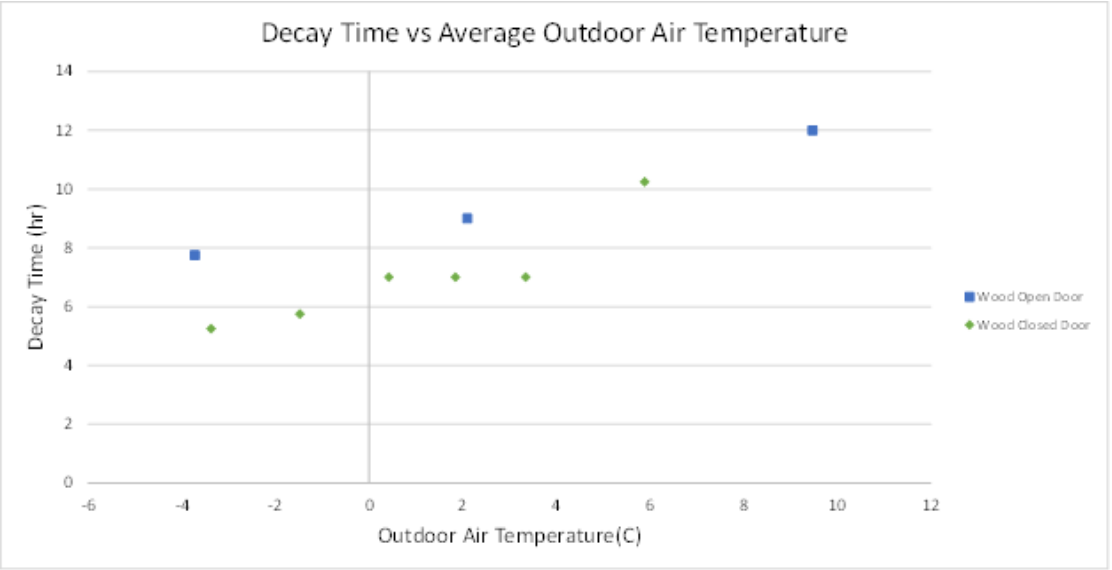

Figure 2: Decay Time vs. Average Outdoor Air Temperature - Wood Floor

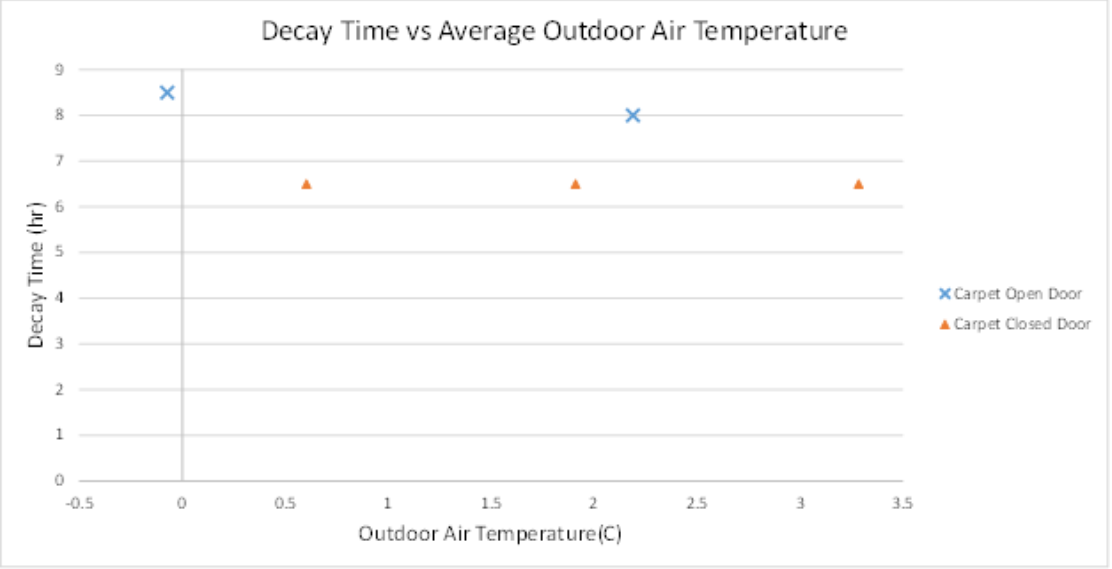

Figure 3: Decay Time vs. Average Outdoor Air Temperature - Carpet Floor

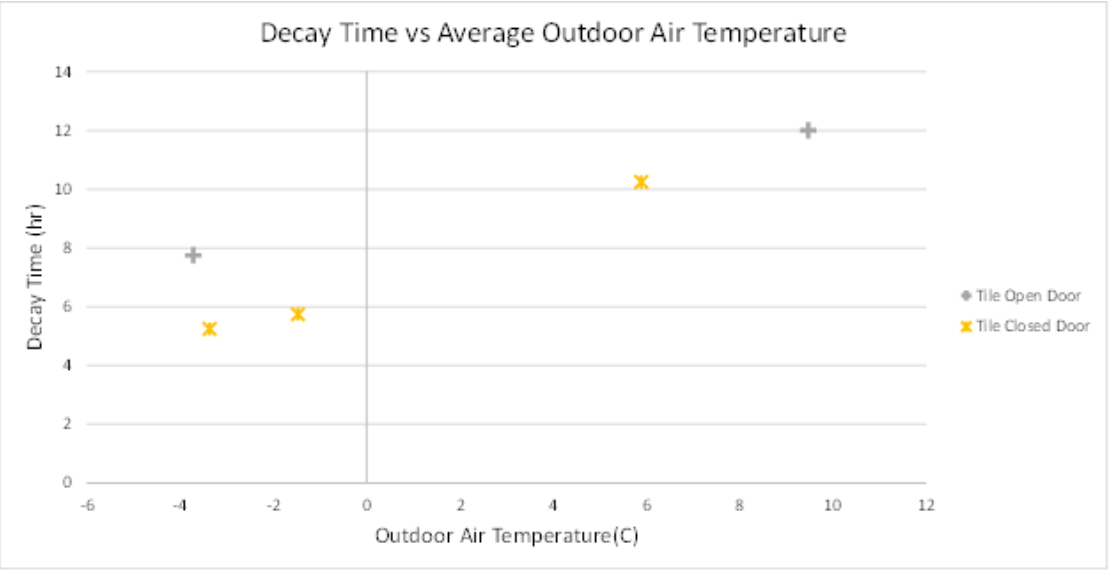

Figure 4: Decay Time vs. Average Outdoor Air Temperature - Tile Floor

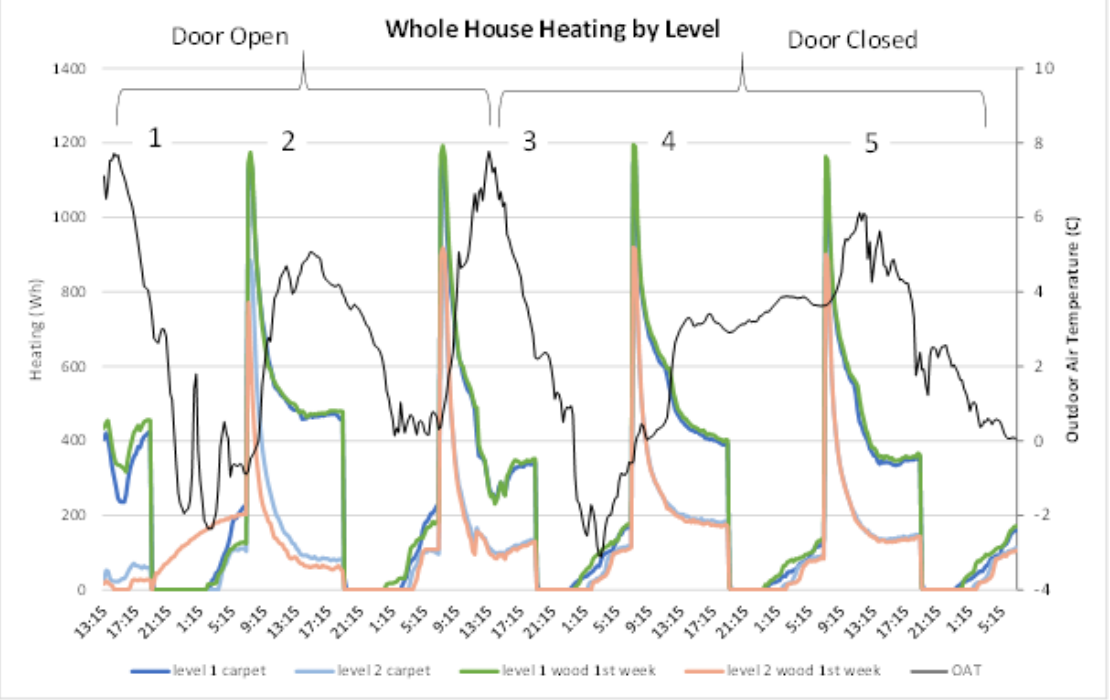

Figure 5: House Heating Demand by Level – Week 1

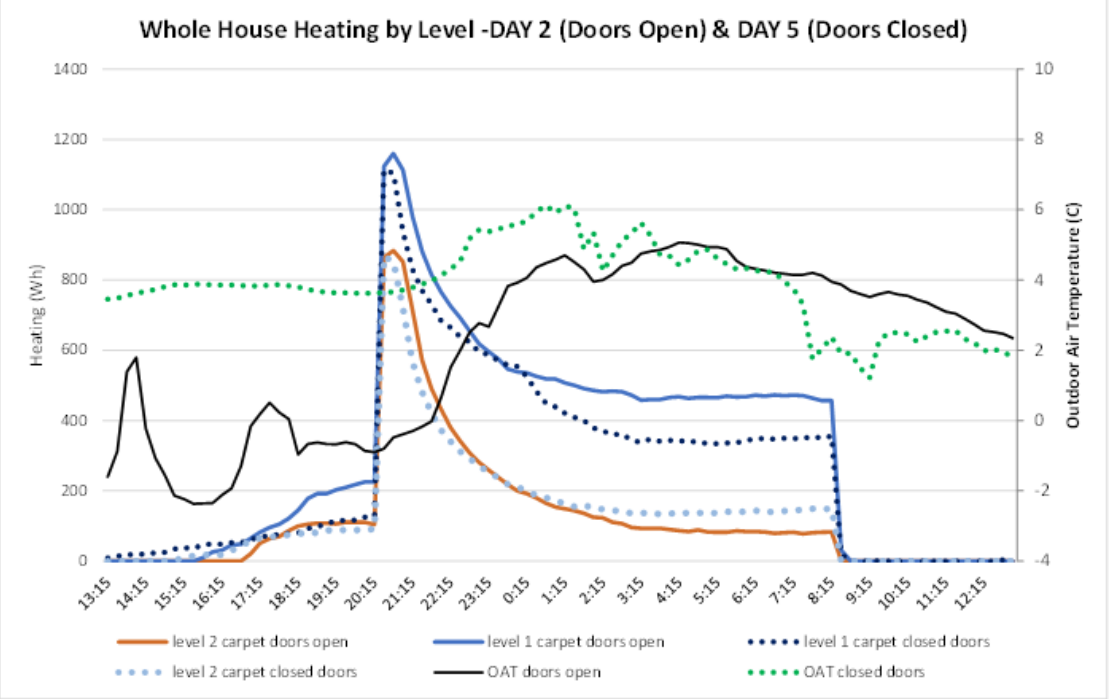

Figure 6: Whole House Heating by Level - Open vs. Closed Door Day Week 1

	Total House kWh		Level 1 (RC)kWh / Percent of Total				Level 2 (Etage)kWh / Percent of Total				Garage and SSkWh / Percent of Total			
	Carpet	Wood	Carpet		Wood		Carpet		Wood		Carpet		Wood	
Day 2 (Doors Open)	69	68	30	43%	29	43%	12	17%	12	18%	27	39%	26	39%
Day 5 (Doors Closed)	63	64	25	40%	26	41%	13	20%	12	19%	25	40%	25	39%

Figure 7: Heating Demand by House Level Comparison - Carpet Floor Week 1

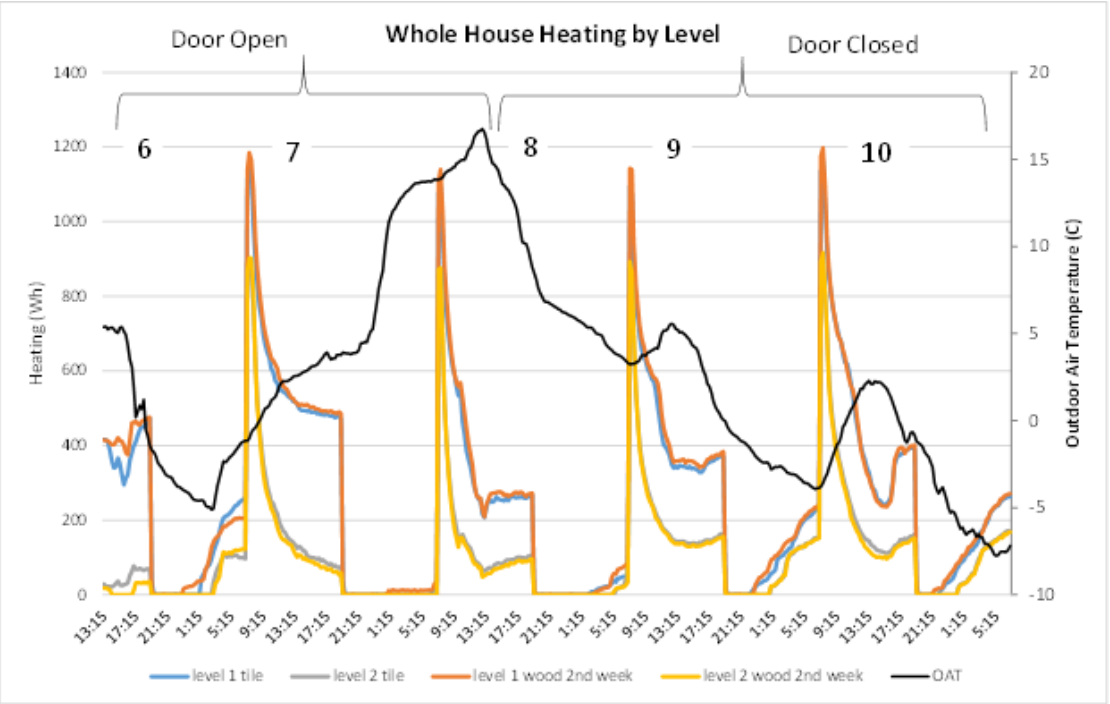

Figure 8: House Heating Demand by Level - Week 2

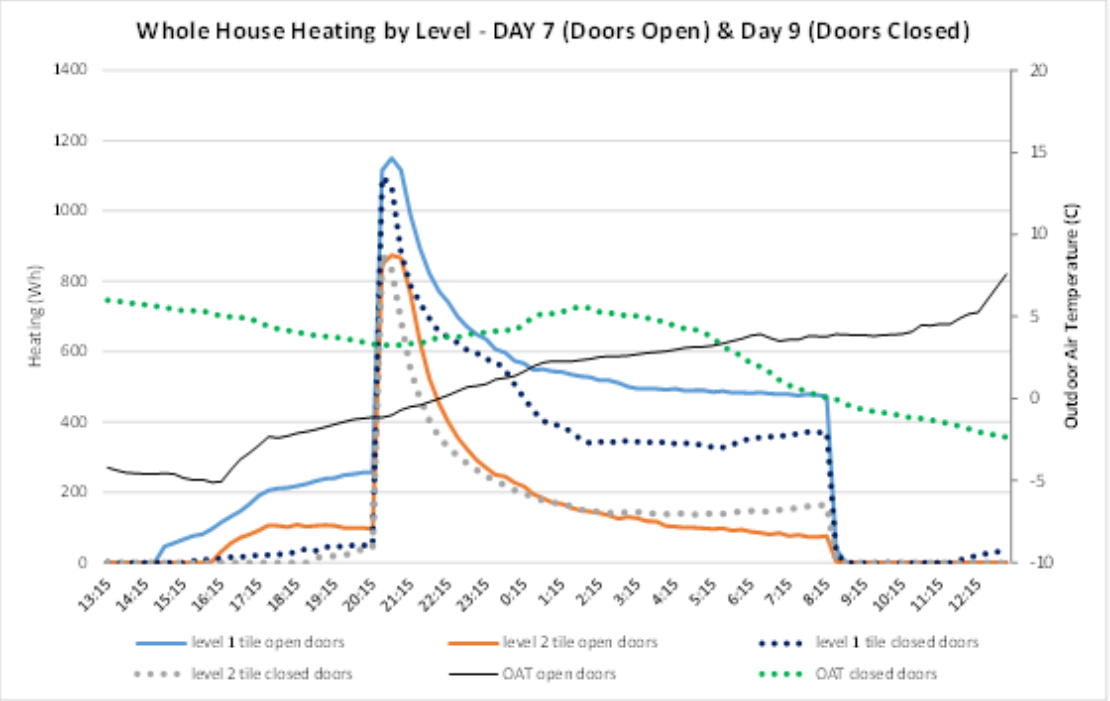

Figure 9: Whole House Heating by Level - Open vs. Closed Door Day Week 2

	Total House kWh		Level 1(RC) kWh / Percent of Total				Level 2 kWh (Etage)/ Percent of Total				Garage and SS kWh / Percent of Total			
	Tile	Wood	Tile		Wood		Tile		Wood		Tile		Wood	
Day 7 (Doors Open)	76	76	33	43%	33	44%	13	17%	12	16%	31	41%	31	40%
Day 9 (Doors Closed)	60	60	23	39%	24	41%	11	19%	11	19%	25	42%	24	41%

Figure 10: Heating Demand by House Level Comparison - Tile Floor Week 2

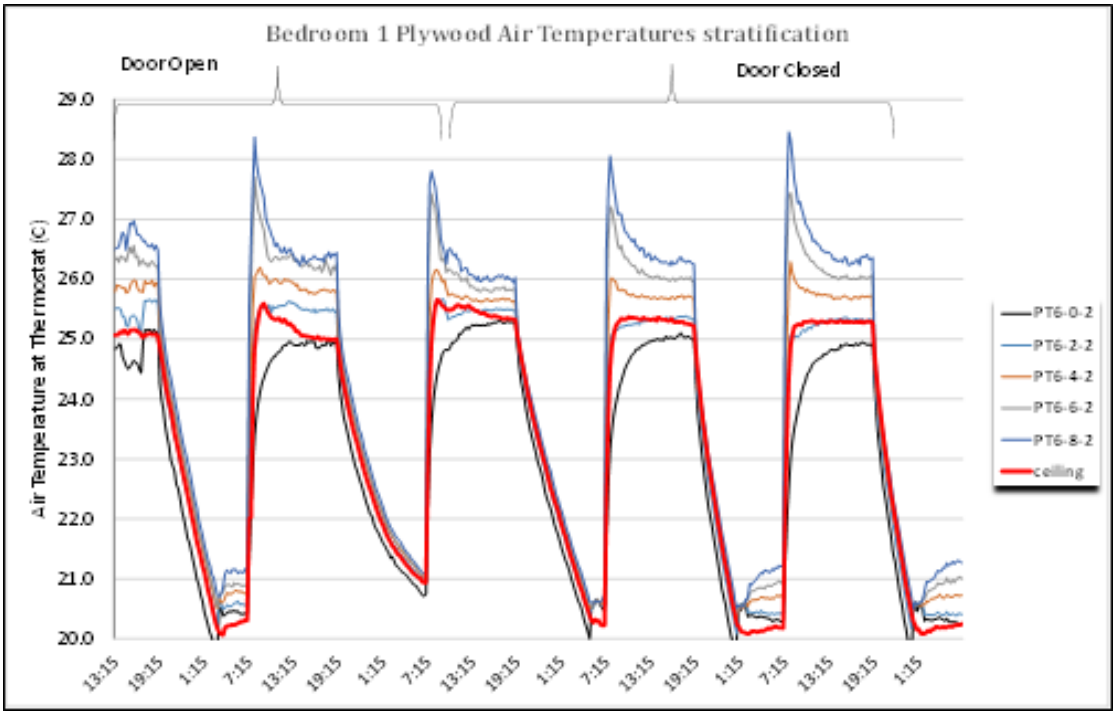

Figure 11: Bedroom 1 Air Temperature Stratification Wood Floor

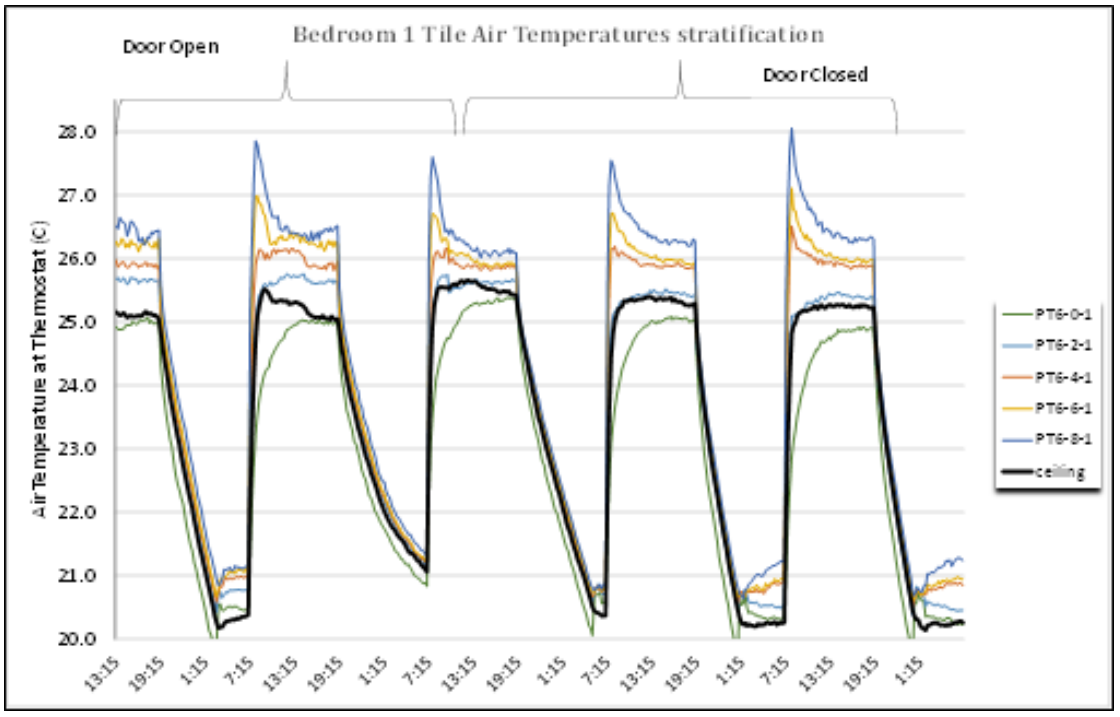

Figure 12: Bedroom 1 Air Temperature Stratification Tile Floor

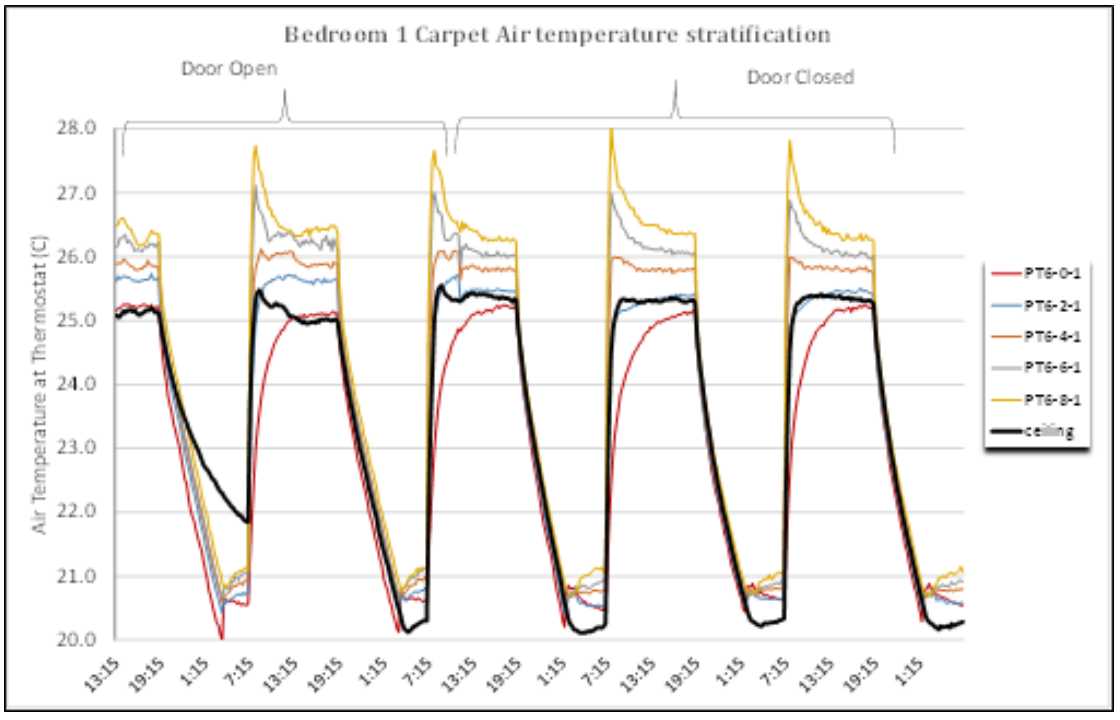

Figure 13: Bedroom 1 Air Temperature Stratification Carpet Floor

Appendix B: MATLAB Code - Sample of Detailed Model

```
a=1;

% a=1;
L=1;
k=1;
cap=1;
% for L=1:2;
%     for k = 1:4;
%         for cap = 1:2;

    clearvars -except k L a cap

    %Height of room

deltaT=15; %seconds

T_low=18; %step down night time temperature USER INPUT
T_high=21; %step up day time temperature USER INPUT
T_out=-23;

ramp_start = 3; % am hour start of ramp USER INPUT
ramp = 3; %ramp length in hours USER INPUT

ramp_start2 = 13; % pm hour start of ramp USER INPUT

o=(ramp*3600/deltaT)+2; % For ramp function
x=T_high-T_low; % For ramp function
y=x/o; % For ramp function

%Number of days
No=1;
NT=No*86400/deltaT; %number of time steps in a day
p=1:1:NT;
t=p.*deltaT;
%qmax in watts of baseboard heater.  Heater is pulse width
modulated with 15
%second cyles
% qmax=1240; %watt
% qmax=1190;
if cap == 1
    qmax=1184;
elseif cap == 2
    qmax = 1184*0.75;
else
    qmax=1180*4.5;
end
%proportional control constand of baseboard heater
```

```
Kp=2000; %watt/degC
Ki=0.1;
i=1;
%create step change for thermostat setpoint

% TO HAVE 2 STEP CHANGE
% %BEFORE FIRST RAMP
while i < (ramp_start)*3601/deltaT
    Tsp1(i)=T_low; %degC
    i=i+1;
end
%FIRST RAMP
while i < (ramp_start+ramp)*3601/deltaT
    Tsp1(i)=Tsp1(i-1)+y; % Create Ramp function
    i=i+1;
end
%BETWEEN RAMPS = Stay at T_high for X hours
while i<=(ramp_start+3+ramp)*3601/deltaT
    Tsp1(i)=T_high; %degC
    i=i+1;
end
% BETWEEN RAMPS = Go back to T_low (OR NOT)
while i<=(ramp_start2)*3601/deltaT
    Tsp1(i)=T_low; %degC
    i=i+1;
end
%SECOND RAMP
while i<=(ramp_start2+ramp)*3601/deltaT
    Tsp1(i)=Tsp1(i-1)+y; % Create Ramp function
    %Tsp1(i)=T_high;
    i=i+1;
end
%AFTER SECOND RAMP
while i<=(ramp_start2+6+ramp)*3601/deltaT
    Tsp1(i)=T_high; %degC
    i=i+1;
end
% AFTER SECOND RAMP
while i<=NT;
    Tsp1(i)=T_low; %degC
    i=i+1;
end


% WHOLE YEAR SIMULATION
load=importdata('Tyear.mat');
Tyear=load;
```

```
t_new=linspace(1,numel(Tyear),240*numel(Tyear));
Tyear_15sec = interp1(Tyear, t_new);
days=365;
Tsp=repmat(Tsp1,1,days);
To=Tyear_15sec;

%Import "near-optimal" temperature profile OR RAMP
load2=importdata('Ramp3hOCTD5.mat');
t_new2=linspace(1,numel(load2),240/4*numel(load2));
Tsp2=interp1(load2, t_new2);
Tsp=repmat(Tsp2,1,days);

%    [ ]            [ ]                [ ]                 [X]
%------------ %------------ % --------------------% ------------
--------%
% One comfort % Two Comfort % Preheating with day % Preheating
withOUT day
% time [OCT]  % times [TCT] % time comfort [POCT] % time comfort
[PTCT]
%------------ %------------ % --------------------% ------------
--------%
% StepOCT     % StepTCT     % StepPOCT            % StepPTCT
% Ramp1hOCT   % Ramp1hTCT   % Ramp1hPOCT          % Ramp1hPTCT
% Ramp2hOCT   % Ramp2hTCT   % Ramp2hPOCT          % Ramp2hPTCT
% Ramp3hOCT   % Ramp3hTCT   % Ramp3hPOCT          % Ramp3hPTCT
% Trans1hOCT  % Trans1hTCT  % Trans1hPOCT         % Trans1hPTCT
% Trans2hOCT  % Trans2hTCT  % Trans2hPOCT         % Trans2hPTCT
% Trans3hOCT  % Trans3hTCT  % Trans3hPOCT         % Trans3hPTCT

%SPECIFIC DAYS SIMULATION IE NOT WHOLE YEAR
% load=importdata('To2014-2.mat'); %12 days experiment 2
%
% % % load=importdata('Tout_3.mat');
%
% Tout_data=load;
% t_new=linspace(1,numel(Tout_data),240/4*numel(Tout_data));
% Tout_15sec = interp1(Tout_data, t_new);
% To=Tout_15sec;
% days=12;
% %days=numel(Tout_data)/96;
% load2=importdata('Tsp2014-2.mat');
% Tsp1=interp1(load2,t_new);
% Tsp=repmat(Tsp1,1,days);
% %
% qload=importdata('P2014.mat');
% qaux_mes = interp1(qload, t_new);
```

```
%
% %Load Solar Radiation
% load2=importdata('SR_greendays.mat');
% % load2=importdata('SR_3.mat');
% SR_data=load2;
% t_new=linspace(1,numel(SR_data),240/4*numel(SR_data));
% SR_15sec = interp1(SR_data, t_new);
% SR=SR_15sec;


Nfinal=NT*58; %second
dT=1; %second
u=0;
j=1;
qaux=zeros(Nfinal,1);
T7=zeros(Nfinal,1);
T8=zeros(Nfinal,1);
T9=zeros(Nfinal,1);
T10=zeros(Nfinal,1);
T11=zeros(Nfinal,1);
T12=zeros(Nfinal,1);
T13=zeros(Nfinal,1);
T14=zeros(Nfinal,1);
T15=zeros(Nfinal,1);
T16=zeros(Nfinal,1);
T17=zeros(Nfinal,1);
T18=zeros(Nfinal,1);
T19=zeros(Nfinal,1);
T20=zeros(Nfinal,1);
T21=zeros(Nfinal,1);
T22=zeros(Nfinal,1);
T23=zeros(Nfinal,1);
T24=zeros(Nfinal,1);
T25=zeros(Nfinal,1);
qaux(1)=0.5*qmax; %watt
T7(1)=T_low; %degC
T8(1)=T_low; %degC
T9(1)=T_low; %degC
T10(1)=T_low; %degC
T11(1)=T_low; %degC
T12(1)=T_low; %degC
T13(1)=T_low; %degC
T14(1)=T_low; %degC
T15(1)=T_low; %degC
T16(1)=T_low; %degC
T17(1)=T_low; %degC
T18(1)=T_low; %degC
```

```
T19(1)=T_low; %degC
T20(1)=T_low; %degC
T21(1)=T_low; %degC
T22(1)=T_low; %degC
T23(1)=T_low; %degC
T24(1)=T_low; %degC
T25(1)=T_low; %degC

%Height of room
Hh=2.489; %m
%Length of room (South/North Wall)
Lh=3.3; %m
%Width of room (West/East Wall)
Wh=4.2; %m
%Exterior Surfaces:
    %Surface 1 = South Wall (Interior)
    %Surface 2 = East Wall (Exterior)
    %Surface 3 = North Wall (Exterior)
    %Surface 4 = West Wall (Interior)
    %Surface 5 = Ceiling (Exterior)
    %Surface 6 = Floor (Interior)
%Internal Height
Hi=2.4; %m
%Window Areas
Aw=[0;0;1.7324;0]; %m^2
%Net Wall areas
A=[Lh*Hh-Aw(1); Wh*Hh-Aw(2); Lh*Hh-Aw(3); Wh*Hh-Aw(4); Wh*Lh;
Wh*Lh]; %m^2
%room volume
Vol=A(5)*Hi; %m^3
%Window Resistance (U=3)
Rw=0.5; %m^2*degC/watt
%interior film coefficient of surfaces walls
h=6; %watt/(m^2*degC)
%interior film coeffients
hc=[h; h; h; h; 6; 6];%watt/(m^2*degC)

hc1 = zeros(Nfinal,1); %Surface 1 = South Wall (Interior)
hc2 = zeros(Nfinal,1); %Surface 2 = East Wall (Exterior)
hc3 = zeros(Nfinal,1); %Surface 3 = North Wall (Exterior)
hc4 = zeros(Nfinal,1); %Surface 4 = West Wall (Interior)
hc5 = zeros(Nfinal,1); %Surface 5 = Ceiling (Exterior)
hc6 = zeros(Nfinal,1); %Surface 6 = Floor (Interior)

hc1(1) = 1.31*(abs((T10(1)-T7(1)))^(1/3)); %Vertical Surface
hc2(1) = 1.31*(abs((T8(1)-T7(1)))^(1/3)); %Vertical Surface
hc3(1) = 1.31*(abs((T8(1)-T7(1)))^(1/3)); %Vertical Surface
```

```
hc4(1) = 1.31*(abs((T10(1)-T7(1)))^(1/3)); %Vertical Surface
hc5(1) = 0.59*(abs(((T8(1)-T7(1)))/2)^0.25); %Ceiling Surface
hc6(1) = 1.52*(abs(((T10(1)-T7(1)))/2)^(1/3)); %Floor Surface

hr1 = zeros(Nfinal,1);
hr2 = zeros(Nfinal,1);
hr3 = zeros(Nfinal,1);
hr4 = zeros(Nfinal,1);
hr5 = zeros(Nfinal,1);
hr6 = zeros(Nfinal,1);

eps = 0.9; %emmisivity of walls
sig = 5.6703*(10^-8); %stefan boltzman constant

hr1(1)= eps*sig*4*(((T10(1)+273+T7(1)+273)/2)^3);
hr2(1)= eps*sig*4*(((T8(1)+273+T7(1)+273)/2)^3);
hr3(1)= eps*sig*4*(((T8(1)+273+T7(1)+273)/2)^3);
hr4(1)= eps*sig*4*(((T10(1)+273+T7(1)+273)/2)^3);
hr5(1)= eps*sig*4*(((T8(1)+273+T7(1)+273)/2)^3);
hr6(1)= eps*sig*4*(((T10(1)+273+T7(1)+273)/2)^3);

h1 = zeros(Nfinal,1);
h2 = zeros(Nfinal,1);
h3 = zeros(Nfinal,1);
h4 = zeros(Nfinal,1);
h5 = zeros(Nfinal,1);
h6 = zeros(Nfinal,1);

h1(1) = hc1(1) + hr1(1);
h2(1) = hc2(1) + hr2(1);
h3(1) = hc3(1) + hr3(1);
h4(1) = hc4(1) + hr4(1);
h5(1) = hc5(1) + hr5(1);
h6(1) = hc6(1) + hr6(1);

% air change per hour for infiltration/exfiltration
ach=0.019;
achi=18;
%ach=0.019; %air changes per hour
%specific heat of air
cp=1000; %joule/(kg*degC)
%density of air
rho=1.2; %kg/m^3

% For air flow calculation
beta_air = 0.00343; % coefficient of thermal expansion 1/K
mu_air = 0.00001827; % dynamic viscosity kg/m s
```

```
Pr_air = 0.71; %Prandtl number
k_air = 0.0251; %conductivity of air kW/m K
g = 9.807; %acceleration due to gravity m/s2

%U of infiltration exterior
Uinf=ach*Vol*cp*rho/3600; %watt/degC
%U of infilation interior
Uinfi=achi*Vol*cp*rho/3600;  %watt/degC
%Wall azimuth
%azimuth=[35; -55; 215; 125]; %degree

%%%%%%%%%%%%%%%%%%%%%%%%%%%%%%%%%%%%%%%%%%%%%%%%%%%%%%%%
%THERMAL RESISTANCES OF WALLS (incl air films)
%%%%%%%%%%%%%%%%%%%%%%%%%%%%%%%%%%%%%%%%%%%%%%%%%%%%%%%%

%Vertical Exterior Walls
%Gypsum board layer
Lgyp=0.0127*L; %m
rhogyp=640; %kg/m^3
kgyp=0.16*k; %watt/(m*degC)
cgyp=1150; %joule/(kg*degC)
%Airgap and enermax
Rener=0.708; %(m^2*degC)/watt
%Insulation layer
Rins=3.89; %(m^2*degC)/watt
%Air gap, Fiberboard, plywood, vinyl
Rsid=0.48; %(m^2*degC)/watt
%Exterior film
ho=20; %watt/(m^2*degC)
%15% framing area
ff=0.25; %percentage
%Wood stud
Rf=1.1667; %(m^2*degC)/watt

R1 = zeros(Nfinal,1);
R2 = zeros(Nfinal,1);
R3 = zeros(Nfinal,1);
R4 = zeros(Nfinal,1);
R5 = zeros(Nfinal,1);
R6 = zeros(Nfinal,1);
Rc = zeros(Nfinal,1);

%Exterior wall resistance
R2(1)=1/(((1-
ff)/((Lgyp/kgyp)+Rener+Rins+Rsid+(1/ho)+(1/h2(1))))+(((ff)/((Lgy
p/kgyp)+Rener+Rf+Rsid+(1/ho)+(1/h2(1)))))); %(m^2*degC)/watt
R3(1)=R2(1); %(m^2*degC)/watt
```

```
%Vertical Interior Walls resistance
Rair=0.18;
R1(1)=1/(((1-
ff)/((2*Lgyp/kgyp)+Rair+(2/h1(1))))+(((ff)/((2*Lgyp/kgyp)+Rf+(2/
h1(1))))));%(m^2*degC)/watt
R4(1)=R1(1);%(m^2*degC)/watt
%R(1)=R(2);
%R(4)=R(2);

%Ceiling
Rinsc=5.28;%(m^2*degC)/watt
%attic air film
ha=12; %watt/(m^2*degC)
%Ceiling resistance
Rc(1)=1/(((1-
ff)/((Lgyp/kgyp)+Rener+Rinsc+(1/ha)+(1/h5(1))))+(((ff)/((Lgyp/kg
yp)+Rener+Rf+(1/ha)+(1/h5(1))))));%(m^2*degC)/watt

%Roof
%shingle backer board
Rb=0.14;%(m^2*degC)/watt
%Wood shingles
Rsh=0.078;%(m^2*degC)/watt
%Roof resistance
Rr=1/(((1-
ff)/(Rb+Rsh+(1/ho)+(1/ha)))+(((ff)/(Rb+Rf+Rsh+(1/ha)+(1/ho)))));
%(m^2*degC)/watt

%Assume 30 degree roof slope, calculate ceiling-roff combined
resistance
%per unit ceiling area (Assuming no attic ventilation)

Ar=A(5)/cos(30*3.14/180); %m^2
%Combined Celining-roof resistance
R5(1)=((Rc(1)/A(5))+(Rr/Ar))*A(5); %(m^2*degC)/watt

%Floor
%insulation and plywood and truss
rhoply=650;
cply=2200;
Lply=0.0347;
Rfl=0.34;%(m^2*degC)/watt
Rjoi=2.5;
kply=0.12;
%=============
% rhoply=450;
```

```
% cply=1880;
% Lply=0.0347;
% Rfl=0.34;%(m^2*degC)/watt
% Rjoi=2.5;
% kply=0.12;
%Floor resistance
R6(1)=1/(((1-
ff)/((Lply/kply)+Rair+(1/h6(1))+(1/h5(1))))+(((ff)/((Lply/kply)+
Rjoi+(1/h6(1))+(1/h5(1))))));%(m^2*degC)

%WALL CAPACITANCES
c=rhogyp*cgyp*Lgyp; %Joule/m^2 GYPSUM
cply=cply*rhoply*Lply;
C=[c*A(1); c*A(2); c*A(3); c*A(4); c*A(5); cply*A(6)]; %Joule
Cair=8*cp*rho*Vol; %Joule



%Thermal Network - 13 capacitance

    %Surface 1 = South Wall  (Interior)
    %Surface 2 = East Wall   (Exterior)
    %Surface 3 = North Wall  (Exterior)
    %Surface 4 = West Wall   (Interior)
    %Surface 5 = Ceiling     (Exterior)
    %Surface 6 = Floor       (Interior)

%thermal capacitance of interior layer of the exterior walls

C9  = C(2)/2;
C20 = C9;
C13 = C(3)/2;
C22 = C13;
C11 = C(4)/2;
C21 = C11;
C15 = C(1)/2;
C23 = C15;
C19 = C(6)/2;
C25 = C19;
C17 = C(5)/2;
C24 = C17;

R78 = zeros(Nfinal,1);
R710 = zeros(Nfinal,1);
R712 = zeros(Nfinal,1);
R716 = zeros(Nfinal,1);
R714 = zeros(Nfinal,1);
```

```
R718 = zeros(Nfinal,1);
R23i = zeros(Nfinal,1);
R21i = zeros(Nfinal,1);
R25i = zeros(Nfinal,1);
R22o = zeros(Nfinal,1);
R20o = zeros(Nfinal,1);
R24o = zeros(Nfinal,1);

% C9=C(2)+C(3)+C(5); %C9 in Mathcad %Joule/degC
% C11=C(1)+C(4)+C(6); %C11 in Mathcad %Joule
%Convective thermal resistance form air node to exterior wall
surfaces
R78(1)  = 1/((A(2)*h2(1))); %Surface 2 = East Wall %degC/watt
R712(1) = 1/((A(3)*h3(1))); %Surface 3 = North Wall
R716(1) = 1/((A(5)*h5(1))); %Surface 5 = Ceiling
%Convectiv thermal resistance from air node to ineterior wall
surfaces
R710(1) = 1/((A(4)*h4(1))); %Surface 4 = West Wall %degC/watt
R714(1) = 1/((A(1)*h1(1))); %Surface 1 = South Wall %degC/watt
R718(1) = 1/((A(6)*h6(1))); %Surface 6 = Floor %degC/watt
%Infiltration and window thermal resistance
R7o=1/(Uinf+(Aw(3)/Rw));%degC/watt
%Infiltration from interior
R7i=1/(Uinfi);
%SPLIT GYPSUM BOARD INTO 3 LAYERS WITH 2 CAPACITANCES
R89= 1/((kgyp*A(2)*3/Lgyp));%degC/watt
R920 = R89;
R1213 = 1/((kgyp*A(3)*3/Lgyp));%degC/watt
R1322 = R1213;
R1617 = 1/((kgyp*A(5)*3/Lgyp));%degC/watt
R1724 = R1617;

R20o(1) = R89+(1/((A(2)/R2(1))));%degC/watt
R22o(1) = R1213+(1/((A(3)/R3(1))));%degC/watt
R24o(1) = R1617+(1/((A(5)/R5(1))));%degC/watt

R1011 = 1/((kgyp*A(4)*3/Lgyp));%degC/watt
R1121 = R1011;
R1415 = 1/((kgyp*A(1)*3/Lgyp));%degC/watt
R1523 = R1415;
R1819 = 1/((kply*A(6)*3/Lply));%degC/watt
R1925 = R1819;

R21i(1) = R1011+(1/((A(4)/R4(1))));%degC/watt
R23i(1) = R1415+(1/((A(1)/R1(1))));%degC/watt
R25i(1) = R1819+(1/((A(6)/R6(1))));%degC/watt
```

```
% TS=[(C9/((1/R89)+(1/R9o))); (C11/((1/R1011)+(1/R11i)))];
%seconds
% detlaTcrit=min(TS); %seconds

%grashof number
Gr=zeros(Nfinal,1);
Gr(1)=g*beta_air*0.5*(Hi^3)/(mu_air^2);
%inter-zonal convection
Uzn=zeros(Nfinal,1);
Uzn(1)=0.3*(Gr(1)^0.5)*Pr_air*k_air*2/Hi;

%Controller parameters
Prop=zeros(Nfinal,1);
Int=zeros(Nfinal,1);
I=zeros(Nfinal,1);
PID=zeros(Nfinal,1);
Error=zeros(Nfinal,1);
Tsperr=zeros(Nfinal,1);

u=0;
%while dT>0.1
   dd=1;
   ddd=1;
   Int=zeros(Nfinal,1);
   I=zeros(Nfinal,1);
   for j=1:Nfinal-1
       if j>1
           if Tsp(j)==26
               Tsp(j)=26;
           end
           if Tsp(j)==21;
               Tsp(j)=21;
           else
               Tsp(j)=Tsp(j);
           end
           if abs(Tsp(j)- Tsp(j-1)) > 0.01 %if setpoint is
changed - reset the integral portion of controller
               Tsperr(j) = abs(Tsp(j)- Tsp(j-1)); %check to see
when setpoint is changed
               Int=zeros(Nfinal,1);
               I=zeros(Nfinal,1);
               ddd=ddd+1;
           else
               dd=dd+1;
           end
       end
       if Tsp(j)>T7(j)
```

```
            Error(j+1)=Tsp(j)-T7(j); % set Error parameter to
temperature error
        else
            Error(j+1)=0;
        end
        Prop(j+1)=Error(j+1); % set Prop parameter to Error
        %if Error(j+1) > 0 %if temperature error is greater than
zero (elimenates any Error when air is higher than setpoint
value)
            Int(j+1)=(Error(j+1)+Error(j))*deltaT/2; %set Int
parameter to average error multiplied by time step
        %else
        %    Int(j+1)=0; % if no Error - Int is set to zero
        %end
        I(j+1)=sum(Int);   % sum of Int terms
        PID(j+1)=Kp*Prop(j)+Ki*I(j+1); %value of actuator
(auxiliary heater)
        if PID(j+1)>qmax && Error(j+1)>0.1 %threshold of 0.01
degree C
            qaux(j+1)=qmax;%watt
        elseif Error(j+1)>0.1
            qaux(j+1)=PID(j+1);%watt
        else
            qaux(j+1)=0;%watt
        end
        T7(j+1)  = (deltaT/(Cair))*(qaux(j)+((((T8(j)-
T7(j))/R78(j))+((T18(j)-T7(j))/R718(j))+((T14(j)-
T7(j))/R714(j))+((T16(j)-T7(j))/R716(j))+((T12(j)-
T7(j))/R712(j))+((To(j)-T7(j))/R7o)+((T10(j)-
T7(j))/R710(j))))))+T7(j);
        T8(j+1)  =
((T7(j)/R78(j))+(T9(j)/R89))/((1/R78(j))+(1/R89));%degC
        T10(j+1) =
((T7(j)/R710(j))+(T11(j)/R1011))/((1/R710(j))+(1/R1011));%degC
        T9(j+1)  = (deltaT/C9)*(((T8(j)-T9(j))/R89)+((T20(j)-
T9(j))/R920))+T9(j);%degC
        T11(j+1) = (deltaT/C11)*(((T21(j)-
T11(j))/R1121)+((T10(j)-T11(j))/R1011))+T11(j);%degC
        T12(j+1) =
((T7(j)/R712(j))+(T13(j)/R1213))/((1/R712(j))+(1/R1213));%degC
        T13(j+1) = (deltaT/C13)*(((T12(j)-
T13(j))/R1213)+((T22(j)-T13(j))/R1322))+T13(j);%degC
        T14(j+1) =
((T7(j)/R714(j))+(T15(j)/R1415))/((1/R714(j))+(1/R1415));%degC
        T15(j+1) = (deltaT/C15)*(((T23(j)-
T15(j))/R1523)+((T14(j)-T15(j))/R1415))+T15(j);%degC
```

```
       T16(j+1) =
((T7(j)/R716(j))+(T17(j)/R1617))/((1/R716(j))+(1/R1617));%degC
       T17(j+1) = (deltaT/C17)*(((T16(j)-
T17(j))/R1617)+((T24(j)-T17(j))/R1724))+T17(j);%degC
       T18(j+1) =
((T7(j)/R718(j))+(T19(j)/R1819))/((1/R718(j))+(1/R1819));%degC
       T19(j+1) = (deltaT/C19)*(((T25(j)-
T19(j))/R1925)+((T18(j)-T19(j))/R1819))+T19(j);%degC
       T20(j+1) = (deltaT/C20)*(((To(j)-
T20(j))/R20o(j))+((T9(j)-T20(j))/R920))+T20(j);%degC
       T21(j+1) = (deltaT/C21)*(((T11(j)-T21(j))/R1121)+((21-
T21(j))/R21i(j)))+T21(j);%degC
       T22(j+1) = (deltaT/C22)*(((To(j)-
T22(j))/R22o(j))+((T13(j)-T22(j))/R1322))+T22(j);%degC
       T23(j+1) = (deltaT/C23)*(((T15(j)-
T23(j))/R1523)+((T7(j+1)-T23(j))/R23i(j)))+T23(j);%degC
       T24(j+1) = (deltaT/C24)*(((To(j)-
T24(j))/R24o(j))+((T17(j)-T24(j))/R1724))+T24(j);%degC
       T25(j+1) = (deltaT/C25)*(((T19(j)-
T25(j))/R1925)+((T7(j+1)-T25(j))/R25i(j)))+T25(j);%degC
       q12(j+1) = (T12(j)-To(j))/(R3(j)/A(3));
       q8(j+1)  = (T8(j)-To(j))/(R3(j)/A(2));
       q16(j+1) = (T16(j)-To(j))/(R5(j)/A(5));
       q14(j+1) = (T14(j)- T7(j))/(R1(j)/A(1));
       q10(j+1) = (T10(j)-T7(j))/(R4(j)/A(4));
       q18(j+1) = (T18(j)-T7(j))/(R6(j)/A(6));
       Gr(j+1)=g*beta_air*1*(Hi^3)/(mu_air^2);
       Uzn(j+1)=0.4*(Gr(j+1)^0.5)*Pr_air*k_air*1/Hi;
       hc1(j+1) = 1.26*(abs(T14(j+1)-T7(j+1))^(1/3)); %Vertical
Surface
       hc2(j+1) = 1.26*(abs(T8(j+1)-T7(j+1))^(1/3)); %Vertical
Surface
       hc3(j+1) = 1.26*(abs(T12(j+1)-T7(j+1))^(1/3)); %Vertical
Surface
       hc4(j+1) = 1.26*(abs(T10(j+1)-T7(j+1))^(1/3)); %Vertical
Surface
       if T16(j+1) > T7(j+1)
           hc5(j+1) = 0.59*(abs((T16(j+1)-T7(j+1))/0.9)^0.25);
       else
           hc5(j+1) = 1.52*(abs(T16(j+1)-T7(j+1))^(1/3));
       end
       %hc5(j+1) = 0.59*(abs((T16(j+1)-T7(j+1))/2)^0.25);
%Ceiling Surface
       if T18(j+1) > T7(j+1)
           hc6(j+1) = 1.52*(abs(T18(j+1)-T7(j+1))^(1/3));
       else
```

```
            hc6(j+1) = 0.59*(abs((T18(j+1)-T7(j+1))/0.9)^0.25);
%Floor Surface
        end
        hc62(j+1) = 0.59*(abs((T18(j+1)-T7(j+1))/2)^0.25)';
        hr1(j+1)= eps*sig*4*(((T14(j+1)+273+T7(j+1)+273)/2)^3);
        hr2(j+1)= eps*sig*4*(((T8(j+1)+273+T7(j+1)+273)/2)^3);
        hr3(j+1)= eps*sig*4*(((T12(j+1)+273+T7(j+1)+273)/2)^3);
        hr4(j+1)= eps*sig*4*(((T10(j+1)+273+T7(j+1)+273)/2)^3);
        hr5(j+1)= eps*sig*4*(((T16(j+1)+273+T7(j+1)+273)/2)^3);
        hr6(j+1)= eps*sig*4*(((T18(j+1)+273+T7(j+1)+273)/2)^3);
        h1(j+1) = hc1(j+1) + hr1(j+1);
        h2(j+1) = hc2(j+1) + hr2(j+1);
        h3(j+1) = hc3(j+1) + hr3(j+1);
        h4(j+1) = hc4(j+1) + hr4(j+1);
        h5(j+1) = hc5(j+1) + hr5(j+1);
        h6(j+1) = hc6(j+1) + hr6(j+1);
        R1(j+1)=1/(((1-
ff)/((2*Lgyp/kgyp)+Rair+(2/h1(j+1))))+(((ff)/((2*Lgyp/kgyp)+Rf+(
2/h1(j+1))))));%(m^2*degC)/watt
        R2(j+1)=1/(((1-
ff)/((Lgyp/kgyp)+Rener+Rins+Rsid+(1/ho)+(1/h2(j+1))))+(((ff)/((L
gyp/kgyp)+Rener+Rf+Rsid+(1/ho)+(1/h2(j+1)))))); %(m^2*degC)/watt
        R3(j+1)=R2(j+1); %(m^2*degC)/watt
        R4(j+1)=R1(j+1);%(m^2*degC)/watt
        Rc(j+1)=1/(((1-
ff)/((Lgyp/kgyp)+Rener+Rinsc+(1/ha)+(1/h5(j+1))))+(((ff)/((Lgyp/
kgyp)+Rener+Rf+(1/ha)+(1/h5(j+1))))));%(m^2*degC)/watt
        R5(j+1)=((Rc(j+1)/A(5))+(Rr/Ar))*A(5); %(m^2*degC)/watt
        R6(j+1)=1/(((1-
ff)/((Lply/kply)+Rair+(1/h6(j+1))+(1/h5(j+1))))+(((ff)/((Lply/kp
ly)+Rjoi+(1/h6(j+1))+(1/h5(j+1))))));%(m^2*degC)
        R78(j+1)  = 1/((A(2)*h2(j+1))); %Surface 2 = East Wall
%degC/watt
        R712(j+1) = 1/((A(3)*h3(j+1))); %Surface 3 = North Wall
        R716(j+1) = 1/((A(5)*h5(j+1))); %Surface 5 = Ceiling
        R710(j+1) = 1/((A(4)*h4(j+1))); %Surface 4 = West Wall
%degC/watt
        R714(j+1) = 1/((A(1)*h1(j+1))); %Surface 1 = South Wall
%degC/watt
        R718(j+1) = 1/((A(6)*h6(j+1))); %Surface 6 = Floor
%degC/watt
        R20o(j+1) = R89+(1/((A(2)/R2(j+1))));%degC/watt
        R22o(j+1) = R1213+(1/((A(3)/R3(j+1))));%degC/watt
        R24o(j+1) = R1617+(1/((A(5)/R5(j+1))));%degC/watt
        R21i(j+1) = R1011+(1/((A(4)/R4(j+1))));%degC/watt
        R23i(j+1) = R1415+(1/((A(1)/R1(j+1))));%degC/watt
        R25i(j+1) = R1819+(1/((A(6)/R6(j+1))));%degC/watt
```

```
       j=j+1;
    end
    dT=abs(T7(Nfinal)-T7(1));
    T7(1)=T7(Nfinal);%degC
    u=u+1;
%end
xx=reshape(T7,60,[]);
%Averages every 60 values to get 15 minute average value
TT7=sum(xx,1)./size(xx,1); %watt
xx=reshape(qaux,60,[]);
%Averages every 60 values to get 15 minute average value
qqaux=sum(xx,1)./size(xx,1); %watt
Q=qqaux*0.25; %Watthour
%Set point temperature
xx=reshape(Tsp,60,[]);
Tssp=sum(xx,1)./size(xx,1);
%outdoor temperature
xx=reshape(To,60,[]);
Too=sum(xx,1)./size(xx,1);

xx=reshape(Tsp1,60,[]);
Tsp11=sum(xx,1)./size(xx,1);


Tair=transpose(TT7); %degC
Energy=transpose(Q); %Wh
Power=transpose(qqaux); %W
intPower=int64(Power); % Power values rounded to whole numbers
T_P=[TT7;qqaux];
TT_PP=transpose(T_P);

peak = max(Power);
peak_red= (qmax-peak)/qmax*100;
TotalE = sum(Energy); % Wh
```

Appendix C: Temperature Set Point Strategy Results

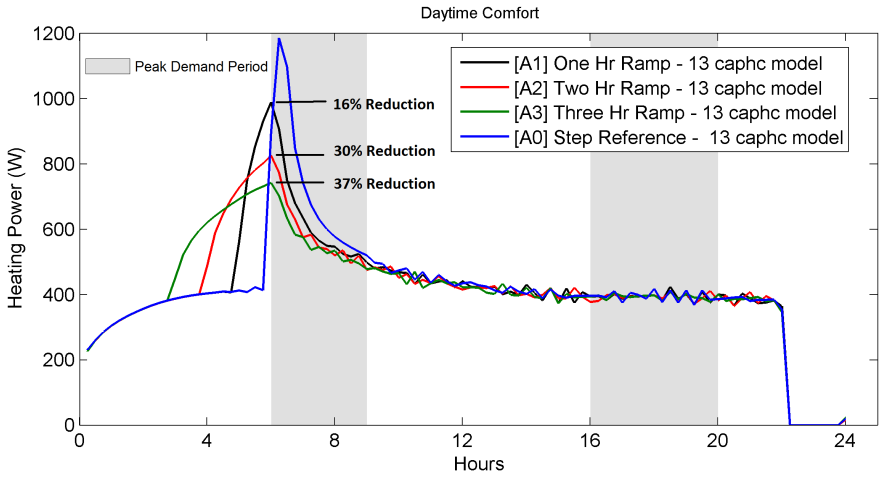

Figure 14: Ramping strategies power results - daytime comfort - 13 capacitance model with temperature dependent HT coefficients

Table 1: Demand response indicators for daytime comfort ramping strategies (13 capacitance model)

		[A0] Step Reference	[A1] 1 Hr Ramp		[A2] 2 Hr Ramp		[A3] 3 Hr Ramp	
		[W]	Demand [W]	Impact [%]	Demand [W]	Impact [%]	Demand [W]	Impact [%]
Building peak		1184	988	**-17%**	825	**-30%**	742	**-37%**
AM	q_{am}^{max}	1184	906	**-23%**	773	**-35%**	702	**-41%**
	$\bar{q}_{am}$	709	607	**-14%**	572	**-19%**	551	**-22%**
	$rebound_{am}$	470	462	**-2%**	458	**-2%**	454	**-3%**
PM	q_{pm}^{max}	418	424	**2%**	411	**-1%**	407	**-3%**
	$\bar{q}_{pm}$	390	389	**0%**	389	**0%**	389	**0%**
	$rebound_{pm}$	3	2	**-16%**	2	**-17%**	3	**17%**
Building daily consumption [kWh]		9.81	9.86	**0%**	9.83	**0%**	9.91	**1%**

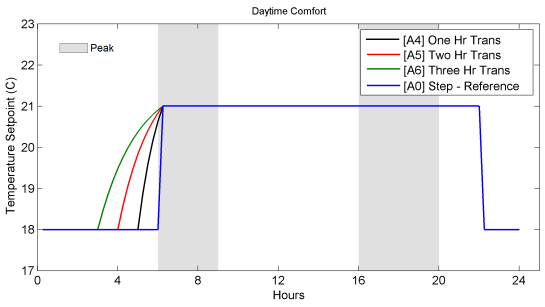

Figure 15: Optimal transition curves - daytime comfort

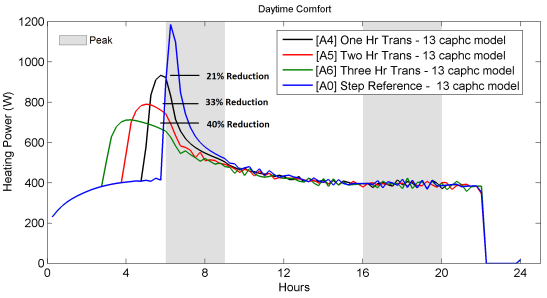

Figure 16: Optimal transition curves - daytime comfort - 13 capacitance model with temperature dependent HT coefficients

Table 2: Demand response indicators for daytime comfort transition curve strategies (13 capacitance model)

		[A0] Step Reference	[A4] 1 Hr Transition		[A5] 2 Hr Transition		[A6] 3 Hr Transition	
		[W]	Demand [W]	Impact [%]	Demand [W]	Impact [%]	Demand [W]	Impact [%]
Building peak		1184	932	**-21%**	789	**-33%**	711	**-40%**
AM	q_{am}^{max}	1184	831	**-30%**	693	**-41%**	626	**-47%**
	$\overline{q}_{am}$	709	598	**-16%**	553	**-22%**	531	**-25%**
	$rebound_{am}$	470	462	**-2%**	457	**-3%**	451	**-4%**
PM	q_{pm}^{max}	418	415	**-1%**	407	**-2%**	424	**2%**
	$\overline{q}_{pm}$	390	389	**0%**	389	**0%**	389	**0%**
	$rebound_{pm}$	3	3	**2%**	3	**-1%**	2	**-16%**
Building daily consumption [kWh]		9.81	9.85	**0%**	9.84	**0%**	9.94	

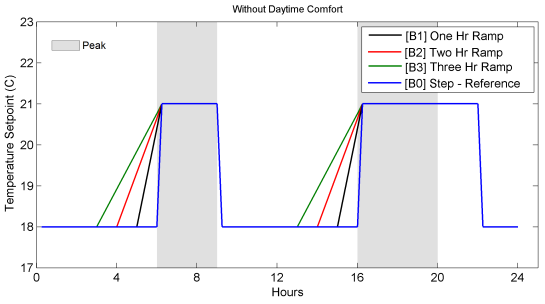

Figure 17: Ramping strategies - without daytime comfort

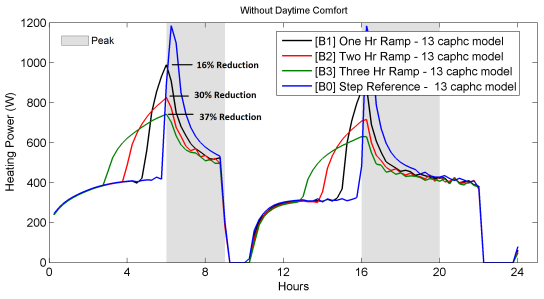

Figure 18: Ramping strategies power results - without daytime comfort - 13 capacitance model with temperature dependent HT coefficients

Table 3: Demand response indicators for ramping strategies without daytime comfort (13 Capacitance Model)

		[B0] Step Reference	[B1] 1 Hr Ramp		[B2] 2 Hr Ramp		[B3] 3 Hr Ramp	
		[W]	Demand [W]	Impact [%]	Demand [W]	Impact [%]	Demand [W]	Impact [%]
Building peak		1184	990	**-16%**	826	**-30%**	743	**-37%**
AM	q_{am}^{max}	1184	907	**-23%**	774	**-35%**	702	**-41%**
	$\overline{q}_{am}$	683	581	**-15%**	547	**-20%**	528	**-23%**
	$rebound_{am}$	81	73	**-10%**	69	**-15%**	64	**-21%**
PM	q_{pm}^{max}	1184	878	**-26%**	716	**-40%**	630	**-47%**
	$\overline{q}_{pm}$	533	474	**-11%**	453	**-15%**	439	**-18%**
	$rebound_{pm}$	10	8	**-22%**	7	**-31%**	6	**-40%**
Building daily consumption [kWh]		9.38	9.46	**1%**	9.46	**1%**	9.58	**2%**

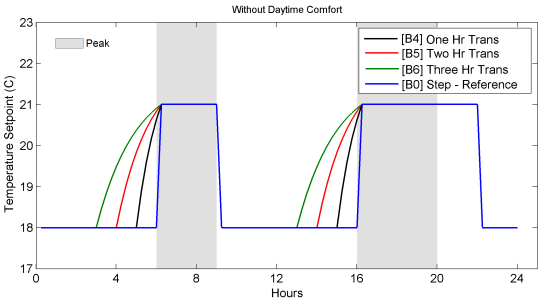

Figure 19: Optimal transition curves - without daytime comfort

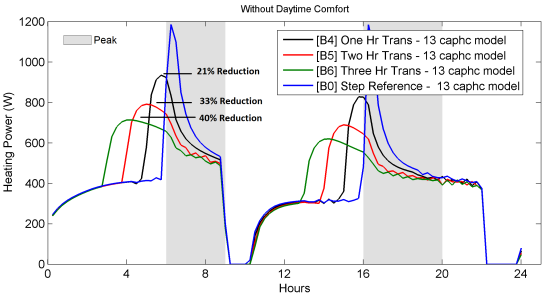

Figure 20: Optimal transition curves power results - without daytime comfort - 13 capacitance model with temperature dependent HT coefficients

Table 4: Demand response indicators for transition curve strategies without daytime comfort (13 capacitance model)

		[B0] Step Reference	[B4] 1 Hr Transition		[B5] 2 Hr Transition		[B6] 3 Hr Transition	
		[W]	Demand [W]	Impact [%]	Demand [W]	Impact [%]	Demand [W]	Impact [%]
Building peak		1184	934	**-21%**	791	**-33%**	713	**-40%**
AM	q_{am}^{max}	1184	832	**-30%**	694	**-41%**	627	**-47%**
	$\overline{q}_{am}$	683	573	**-16%**	528	**-23%**	506	**-26%**
	$rebound_{am}$	81	73	**-10%**	67	**-18%**	62	**-23%**
PM	q_{pm}^{max}	1184	788	**-33%**	619	**-48%**	527	**-56%**
	$\overline{q}_{pm}$	533	468	**-12%**	440	**-17%**	425	**-20%**
	$rebound_{pm}$	10	8	**-18%**	7	**-31%**	6	**-40%**
Building daily consumption [kWh]		9.38	9.46	**1%**	9.49	**1%**	9.64	**3%**

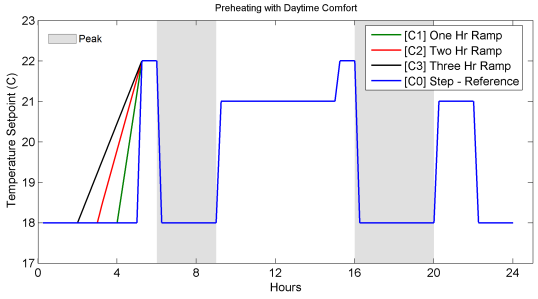

Figure 21: Ramping strategies - preheating with daytime comfort

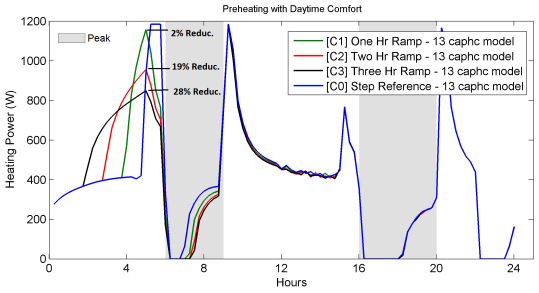

Figure 22: Ramping strategies power results - preheating with daytime comfort

Table 5: Demand response indicators for ramping strategies with preheating and daytime comfort (13 capacitance model)

		[A0] Step Reference	[C1] 1 Hr Ramp		[C2] 2 Hr Ramp		[C3] 3 Hr Ramp	
		[W]	Demand [W]	Impact [%]	Demand [W]	Impact [%]	Demand [W]	Impact [%]
Building peak		1184	1184	**0%**	1184	**0%**	1184	**0%**
AM	q_{am}^{max}	1184	762	**-36%**	754	**-36%**	750	**-37%**
	$\overline{q}_{am}$	709	211	**-70%**	188	**-73%**	178	**-75%**
	$rebound_{am}$	470	735	**56%**	727	**55%**	722	**54%**
PM	q_{pm}^{max}	418	1165	**179%**	1165	**179%**	1165	**179%**
	$\overline{q}_{pm}$	390	303	**-22%**	303	**-22%**	302	**-23%**
	$rebound_{pm}$	3	28	**1002%**	28	**1013%**	28	**1014%**
Building daily consumption [kWh]		9.81	9.55	**-3%**	9.54	**-3%**	9.65	**-2%**

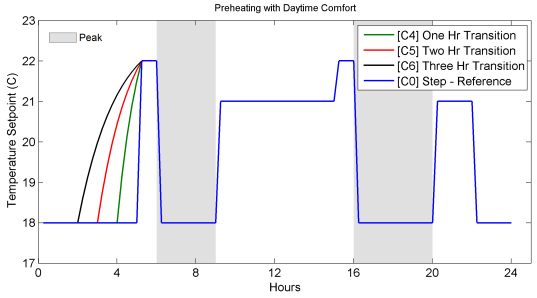

Figure 23: Optimal transition curves - preheating with daytime comfort

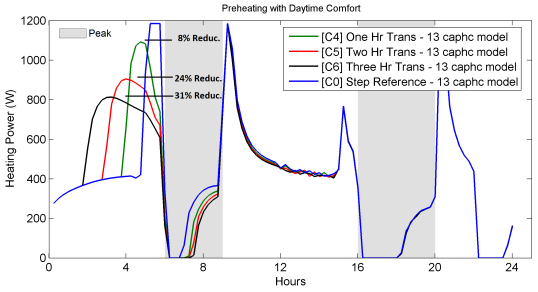

Figure 24: Optimal transition curves power results - preheating with daytime comfort

Table 6: Demand response indicators for transition curves with preheating and daytime comfort (13 capacitance model)

		[A0] Step Reference	[C4] 1 Hr Transition		[C5] 2 Hr Transition		[C6] 3 Hr Transition	
		[W]	Demand [W]	Impact [%]	Demand [W]	Impact [%]	Demand [W]	Impact [%]
Building peak		1184	1184	**0%**	1184	**0%**	1184	**0%**
AM	q_{am}^{max}	1184	760	**-36%**	753	**-36%**	746	**-37%**
	$\overline{q}_{am}$	709	206	**-70%**	185	**-73%**	169	**-75%**
	$rebound_{am}$	470	733	**56%**	725	**55%**	718	**54%**
PM	q_{pm}^{max}	418	1165	**179%**	1165	**179%**	1165	**179%**
	$\overline{q}_{pm}$	390	303	**-22%**	302	**-22%**	302	**-23%**
	$rebound_{pm}$	3	28	**1002%**	28	**1013%**	28	**1014%**
Building daily consumption [kWh]		9.81	9.56	**-3%**	9.55	**-3%**	9.68	**-2%**

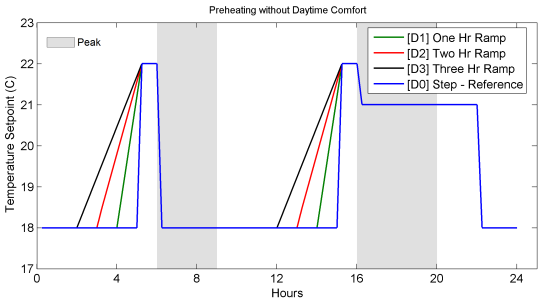

Figure 25: Ramping strategies - preheating without daytime comfort

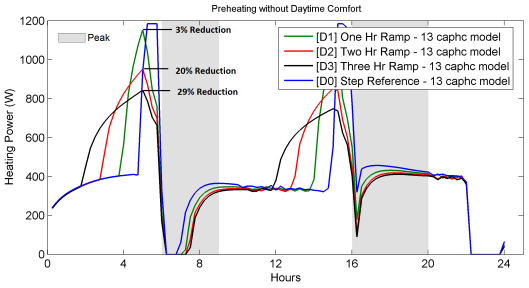

Figure 26: Ramping power results - preheating without daytime comfort

Table 7: Demand response indicators for ramping strategies without preheating and daytime comfort (13 capacitance model)

		[B0] Step Reference	[D1] 1 Hr Ramp		[D2] 2 Hr Ramp		[D3] 3 Hr Ramp	
		[W]	Demand [W]	Impact [%]	Demand [W]	Impact [%]	Demand [W]	Impact [%]
Building peak		1184	1152	**-3%**	950	**-20%**	843	**-29%**
AM	q_{am}^{max}	1184	345	**-71%**	331	**-72%**	323	**-73%**
	$\overline{q}_{am}$	683	175	**-74%**	151	**-78%**	140	**-79%**
	$rebound_{am}$	81	343	**323**	336	**314%**	330	**307%**
PM	q_{pm}^{max}	1184	432	**-64%**	419	**-65%**	412	**-65%**
	$\overline{q}_{pm}$	533	399	**-25%**	384	**-28%**	378	**-29%**
	$rebound_{pm}$	10	6	**-36%**	5	**-48%**	5	**-48%**
Building daily consumption [kWh]		9.38	9.45	**1%**	9.49	**1%**	9.63	

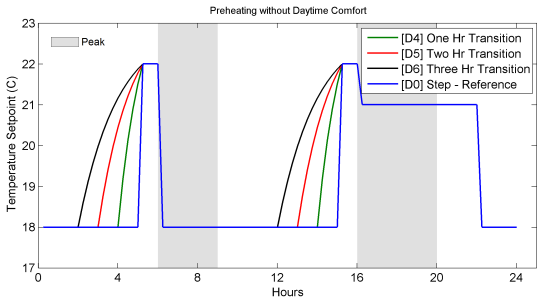

Figure 27: Optimal transition curves - preheating without daytime comfort

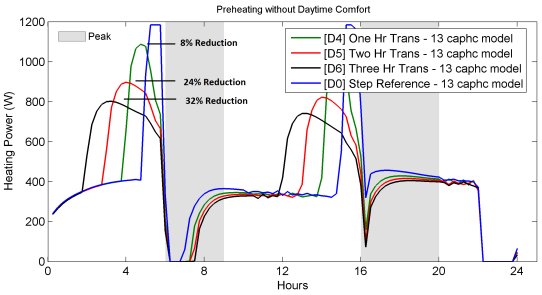

Figure 28: Optimal transition curves power results - preheating without daytime comfort

Table 8: Demand response indicators for transition curves without preheating and daytime comfort (13 capacitance model)

		[B0] Step Reference	[D4] 1 Hr Transition		[D5] 2 Hr Transition		[D6] 3 Hr Transition	
		[W]	Demand [W]	Impact [%]	Demand [W]	Impact [%]	Demand [W]	Impact [%]
Building peak		1184	1087	**-8%**	897	**-24%**	802	**-32%**
AM	q_{am}^{max}	1184	342	**-71%**	328	**-72%**	316	**-73%**
	$\overline{q}_{am}$	683	169	**-75%**	148	**-78%**	131	**-81%**
	$rebound_{am}$	81	342	**322%**	334	**312%**	327	**303%**
PM	q_{pm}^{max}	1184	429	**-64%**	416	**-65%**	405	**-66%**
	$\overline{q}_{pm}$	533	396	**-26%**	382	**-28%**	371	**-30%**
	$rebound_{pm}$	10	6	**-40%**	5	**-48%**	4	**-58%**
Building daily consumption [kWh]		9.38	9.47	**1%**	9.52	**2%**	9.71	**4%**

Appendix D: Thermal Network with Second Air Node Near Temperature Sensor

In the experiment at each temperature change increase, the air temperature reading would also measure higher than the actual set point. This could be due to the sensor being close to the point where the heat is released. There may be a sudden temperature rise in the vicinity of that point. A few minutes later, the heat starts to dissipate to the surrounding areas (remaining air in the room) until the temperature in the room evens out to a value closer to the set point. Table 29 displays this.

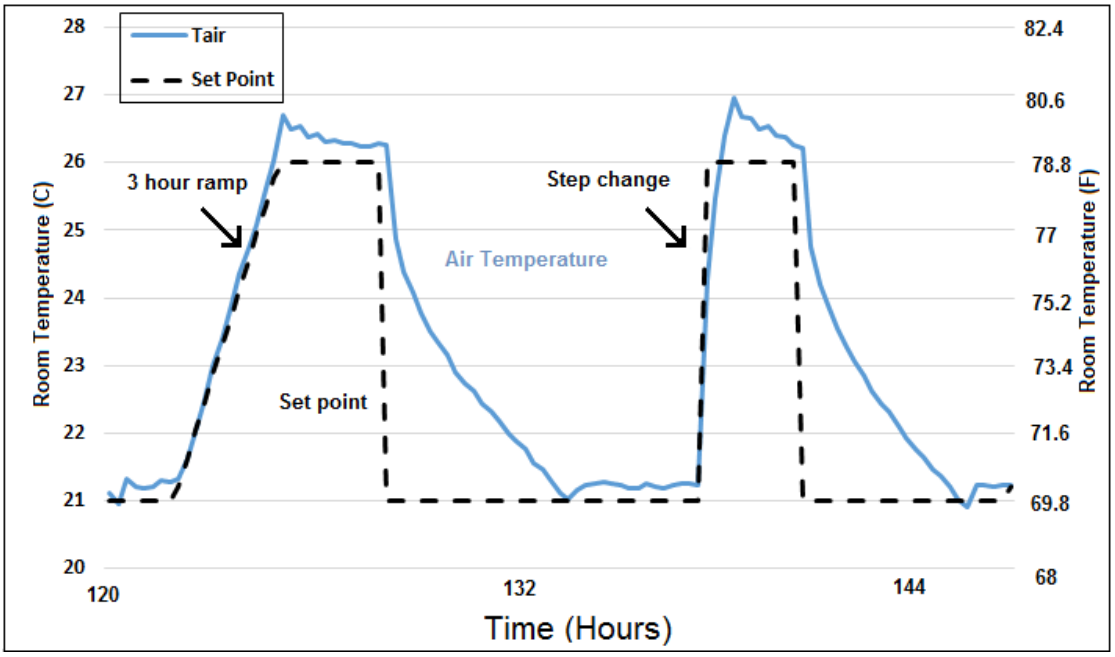

Figure 29: Experiment 2 air temperature - wood floors

Another approach to thermal network modelling is to model a small node with a capacitance to area in the vicinity of the temperature sensor, and connected with a resistance to the original air node in the network. This new small node becomes the air node (the temperature read by the sensor). This could help to capture the faster dynamics with a small capacitance, while still capturing the longer delays. Figures 30 and 31 have this new air node added are three capacitance and thirteen capacitance thermal networks, respectively.

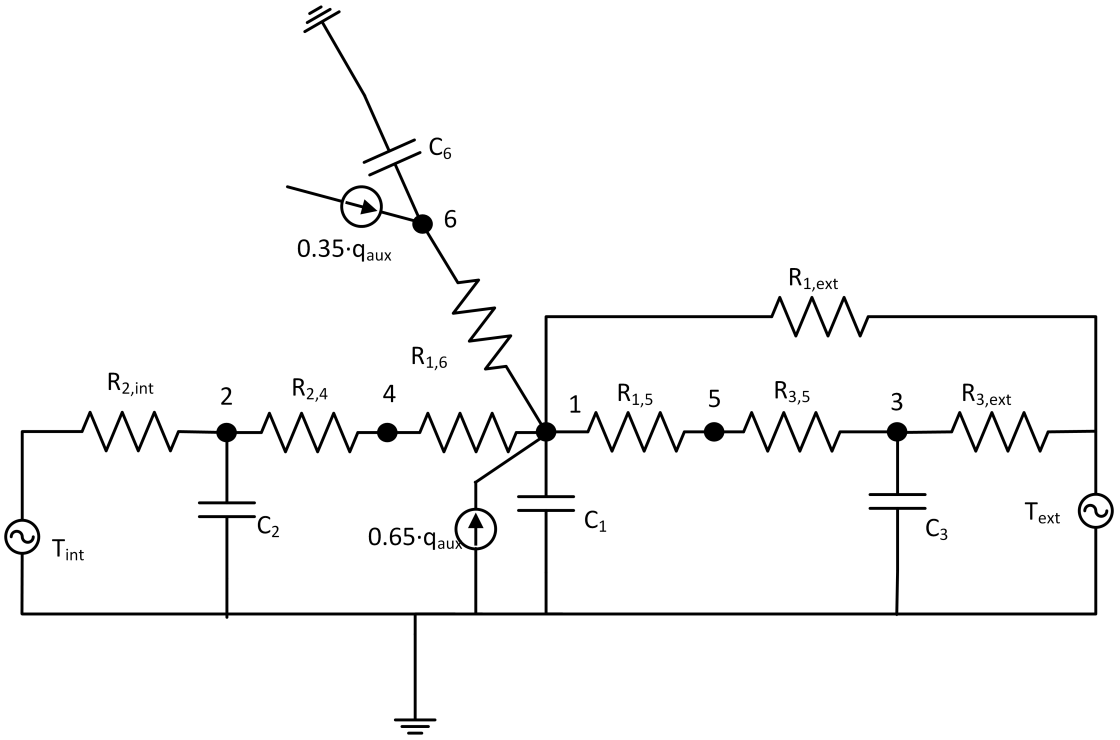

Figure 30: Fourth Order Equivalent RC Network

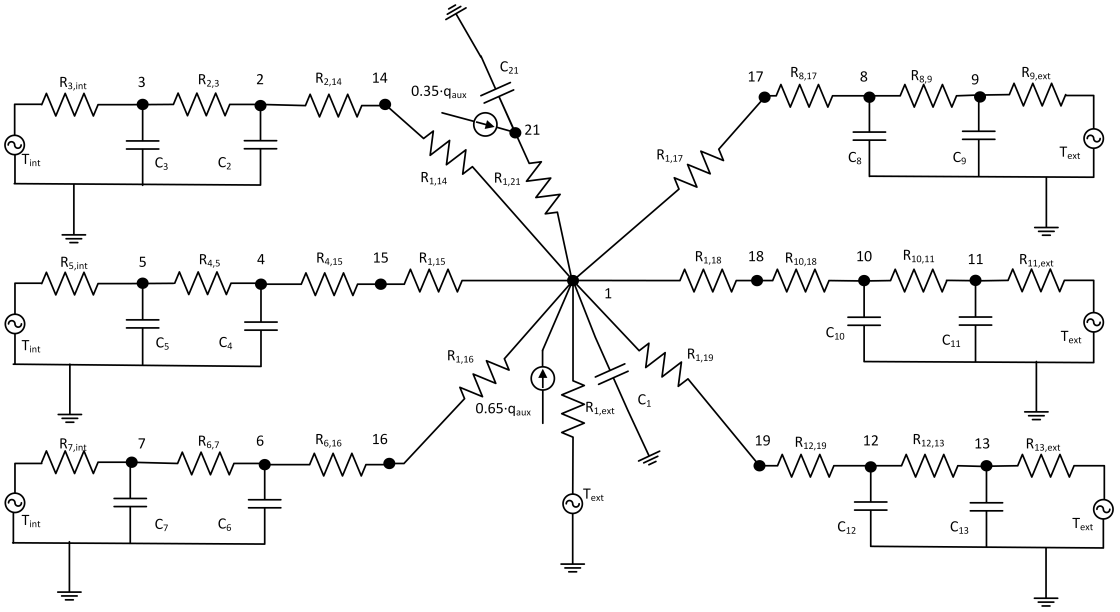

Figure 31: Fourteenth Order Equivalent RC Network, Separated Surfaces

Figure 32 shows the result of air temperature using the 14 capacitance thermal network. Further work should be done on better understanding and better

calibrating the values of the capacitance of the new air node, the resistance between the new and old air node, and how much heat is being directly supplied to each air node.

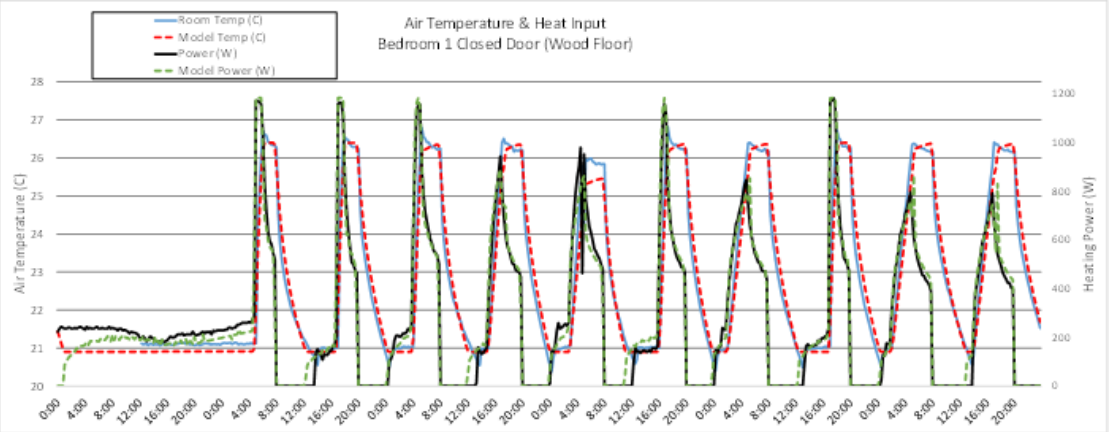

Figure 32: Modelling results of 14 capacitance thermal network